MONTHLY NOTICES

OF THE

ROYAL ASTRONOMICAL SOCIETY

Volume 117 No. 1 1957

Published and Sold by the

ROYAL ASTRONOMICAL SOCIETY
BURLINGTON HOUSE
LONDON, W.1

Price £1 0*s.* 0*d.*; *in U.S.A.* $3.20

(*Annual Subscription for volume of six numbers:* £5 5*s.* 0*d.*; *in U.S.A.* $16)

ROYAL ASTRONOMICAL SOCIETY

Founded 1820

NOW AVAILABLE

GEOPHYSICAL SUPPLEMENT

to the

MONTHLY NOTICES

Volume 7 No. 5

Price 15*s.* 0*d.*; *in U.S.A.* $2.30

CONTENTS

A. E. M. Geddes, Note on large microseisms recorded at Aberdeen on 1954 December 9.

A. H. Cook, Comparisons between relative gravity measurements with the Cambridge pendulum apparatus and Worden gravity meters in North America, South Africa, Australia, New Zealand, and Great Britain.

S. D. Chopra, The range of existence of Stoneley waves in an internal stratum. I. Symmetric vibrations.

K. E. Bullen, On the constitution of Mars (Second paper).

Robert Stoneley and Urs Hochstrasser, The attenuation of Rayleigh waves with depth in a medium with two surface layers.

Orders for the above should be addressed to:

THE ASSISTANT SECRETARY,
Royal Astronomical Society, Burlington House, London, W.1

MONTHLY NOTICES

OF THE

ROYAL ASTRONOMICAL SOCIETY

Vol. 117 No. 1

MEETING OF 1957 JANUARY 11

Professor Sir Harold Jeffreys, President, in the Chair

The President announced that the Council had awarded the Gold Medal of the Society to Professor Albrecht Unsöld for his work on the physics of stellar atmospheres.

The President announced that the Council had awarded the Jackson-Gwilt Medal and Gift to Mr R. P. de Kock for his systematic observations of variable stars over a period of more than twenty years.

The election by the Council of the following Fellows was duly confirmed:—

Colin Robert Edwards, c/o Engineering Division, Public Works Department, Perth, W. Australia (proposed by R. W. Boggis);

*Kenneth Hugh Fea, 4 Manor Drive, Hinchley Wood, Esher, Surrey (proposed by C. W. Allen);

Roger Francis Griffin, 12 Fir Tree Road, Banstead, Surrey (proposed by F. M. Holborn); and

*Philip James Message, Gonville and Caius College, Cambridge (proposed by H. Jeffreys).

The election by the Council of the following Junior Members was duly confirmed:—

David Francis Carter, 2 Peterborough Gardens, Ilford, Essex (proposed by G. W. Wakeford); and

Peter Calvin Kendall, 28 Grove Hill, South Woodford, London, E.18 (proposed by V. C. A. Ferraro).

Seventy-three presents were announced as having been received since the last meeting, including:—

Lund Observatory: (1) *Tables for the conversion of galactic into equatorial coordinates and for the direction cosines in the equatorial system*; and (2) *Table for the reduction of velocities to the local standard of rest* (presented by Lund Observatory).

* Transferred from Junior Membership.

INTERFEROMETRIC STUDY OF PROFILES OF FAINT FRAUNHOFER LINES

Z. Suemoto

(Communicated by the Director of the Cambridge Observatories)

(Received 1957 February 4)

Summary

Profiles of well isolated Fraunhofer lines in the red were measured interferometrically by crossing a Fabry–Perot interferometer (with dielectric coating) with the 9 m spectrograph of the Cambridge Observatories. The average effective resolving power was as high as 6×10^5. The wave-length distribution of the selective absorption coefficient was derived from the measured profiles, using Vitense's Model II. For every point of the disk faint lines give broader Doppler widths than do stronger lines. It is suggested that there is a circulation in the solar atmosphere, vertical upward motion in granules being converted into horizontal motion at about $\tau = 0{\cdot}4$, and finally changing into downward motions back to the convection layer.

---

1. *Introduction.*—From the measurement of profiles of faint Fraunhofer lines in the blue and violet regions Allen (1) found that the true widths of the faintest lines, as deduced from extrapolation of the measured widths, increase as we go from centre to limb on the Sun's disk. He interpreted this as due to an anisotropy of turbulence in the reversing layer, horizontal velocities being greater than vertical velocities. However, as is well known, even the faintest lines which can be measured with reasonable accuracy are not free from saturation, in the sense that the intensity absorbed at a given point of the line profile does not increase in proportion to the absorption coefficient. In other words, even the faintest lines are wider than true absorption coefficient widths by an appreciable amount which varies according to the position on the disk as well as from line to line. If we try to extrapolate from the measured widths to the widths of lines of infinitesimal intensity the results are therefore very uncertain.

In the present work the profiles of well-isolated faint lines in the red were measured at several positions on the disk, using a Fabry–Perot interferometer before the slit of the 9 m spectrograph. The profiles of the absorption coefficient were deduced from the measured profiles, using one of the modern models of the solar atmosphere. The results show that at any one point on the disk the Doppler widths decrease with increasing line intensity, suggesting that there is a decrease of turbulence upwards and that at about $\tau = 0{\cdot}4$ the horizontal velocities considerably exceed the vertical. From the velocity fields at various depths it seems that the vertical upward motions at about $\tau = 1$ are deflected to the horizontal near $\tau = 0{\cdot}4$, and are finally converted into downward motions back to the convection layer.

2. *Observations.*—Most faint lines, say of Rowland intensity less than 1, are blended appreciably, to such an extent as to make accurate measurement of their profiles difficult. Only in the red could numbers of well isolated lines be found.

Measurements were made in the solar tunnel of the Cambridge Observatories, by crossing a Fabry–Perot interferometer with the 9 m spectrograph. The optical arrangement is shown in Fig. 1. Since the interferometer was used before the spectrograph, we obtained parabolic channels similar to those of Shane (**2**), instead of circular channels. But the slit width was wider than Shane's and only a little narrower than inter-channel distances (Plate 1(*b*)). As was pointed out by Treanor (**3**), this arrangement has the disadvantage that the high resolving power of the interferometer can be lost by the finite resolving power of the spectrograph in the direction along the slit. It will be shown later, however, that in spite of some loss of resolution we still reached an average effective resolving power of 6×10^5.

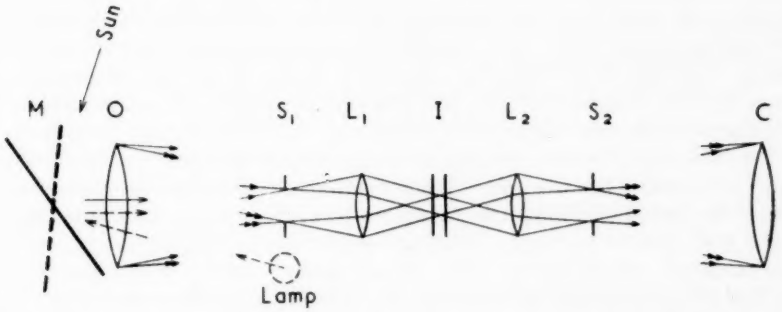

FIG. 1.—*Optical arrangement. Full lines: optical path for solar parabolic channels. Broken lines: path for Pointolite lamp used with 0·08 mm spacer.*

The solar image, of 16 cm diameter, was focused about 2 m before the spectrograph slit S_2 on another auxiliary slit S_1. The sunlight was then collimated and re-focused on to the spectrograph slit by two lenses L_1 and L_2, between which the Fabry–Perot interferometer I was situated. These two lenses, both of 50 cm focal length, were situated in such a way as to act as field lenses as well. The image of the telescope lens O is first focused on to the Fabry–Perot interferometer by L_1 and then the second lens L_2 projects this image on to the spectrograph collimator lens C. As the distance of the second lens L_2 from the slit S_2 is small compared with the spectrograph focal length, it acts approximately as a field lens, such as would normally be put just in front of the slit. This modified method worked quite satisfactorily and we were quite free of difficulties from dust or bubbles on the field lens. The lens L_2 also serves as a "ring lens" to project the interference fringes from infinity on to the spectrograph slit. The spectrograph is of the auto-collimation type, with an 18 cm collimator lens of 9 m focal length. A high quality grating, lent to the Cambridge Observatories by the Mount Wilson Observatory for eclipse work, was used in the second order.

Dr A. H. Jarrett kindly coated the interferometer plates especially for this investigation. They had a high efficiency 7-layer dielectric coating, giving a reflection coefficient of 94 per cent in the red, with very small absorption. A 7·5 mm quartz spacer was used and ideally, with perfect plate figures, the resolving power would have been about $1{\cdot}2 \times 10^6$. The light from ghost images of the first and second kind (**4**), was prevented from entering the slit by rotating each of the interferometer plates.

Because of the high efficiency of both grating and interferometer the exposure times were only about 40 sec at the centre of the disk. About thirty standardized photographs were obtained during the summer of 1953, covering five positions on the disk, in two spectral regions. For standardization, each plate (Ilford Rapid Process Panchromatic) was cut into halves, one of which was used for photographing the parabolic channels, the other for the standardization spectrum. The latter was obtained by replacing the interferometer by a neutral filter and putting a Hilger step wedge of rhodium over the slit, the exposure time varying by not more than a factor 2 between interferometer and wedge photographs. The two halves of the plate were brush developed together in Azol.

3. *Measurement.*—Most of the microphotometer tracings were made in the Tokyo Astronomical Observatory by the self-registering microphotometer described elsewhere (**5**). Each tracing was made along a parabolic channel with the microphotometer slit held parallel to the spectrograph dispersion. The tracing, therefore, is very similar to that of a normal spectrum, except that one has to steer on a slightly curved path, although holding the slit orientation fixed. The microphotometer magnification was 20×, and the projected dimensions of its slit 0·01 × 0·05 mm, the slit length being considerably less than the average width, 0·19 mm, of one channel. The slit was steered along this curved spectrum during the tracing, watching the plate through the microscope and adjusting the Y-axis slow motion by hand. Tracings were made in this way using three or four successive orders for each line on each plate. Since for each position on the disk there were three plates taken on different days, there were more than nine tracings for each line. The nine profiles were fitted together to give a final average profile.

The step wedge was calibrated at a sufficient number of wave-lengths by the National Physical Laboratory. In constructing characteristic curves, small corrections for light scattered in the spectrograph were applied to the wedge transmission. The measured intensity of this scattered light for 18 mm slit length was 2·1 per cent. The effective slit length for the calibration spectra was about 3·4 mm, after making allowance for the opacity of the steps, so that when viewed through this spectrograph the apparent transmission of each step exceeded the true transmission by 0·4 per cent. Although very small, this correction becomes comparatively important for the steps of small transmission: e.g. for the last step the real transmission was 6·4 per cent, the corrected transmission 6·8 per cent. Following this procedure, a more satisfactory fit was obtained between sections of the characteristic curve having different average densities.

4. *Corrections.*—There are three kinds of correction to be considered in spectra of this sort, arising respectively from uniform scattering, horizontal scattering from neighbouring parabolic channels, and the finite resolving power along the parabola.

The first of these was estimated as follows: The measured scattering in the red for 18 mm slit length was about 2·1 per cent, as already mentioned. The parabolic channels were photographed with the same slit length. But there are dark bands between the channels, and since the average channel width was 0·19 mm, with inter-channel distance 0·30 mm, the 2·1 per cent is reduced by a factor 0·19/0·30. The correction for uniform scattering is therefore on the average 1·3 per cent.

The horizontal scattering from neighbouring channels arises from the grating ghosts and from the outer wings of the instrumental profile. The ghost intensities were estimated by using the yellow mercury lines; the sum of the first four ghosts in the second order was 0·5 per cent. In the ghost spectrum there was always another image of the same colour as the primary line, in appearance like a ghost line but obliquely located. This image was attributed to double reflection at the two parallel interfaces of the components of the doublet spectrograph lens. The light going through the spectrograph passes twice through this layer so that the image should be the superposition of two, each having an intensity about $5{\cdot}10^{-2} \times 5{\cdot}10^{-2} = 2{\cdot}5 \times 10^{-3}$ of the primary line, in good agreement with observation. This false image is a little out of focus because of the lens action of the air between the two inner faces, and is slightly displaced because of the wedge shape of the air lens. It must be emphasized that the false image has nothing to do with the white light reflections at the outer surfaces of the lens. A spurious line of this sort can conveniently be included among the ghosts. The resulting ghost correction was finally estimated to be about 1 per cent.

The instrumental profile of the spectrograph was measured with special attention to the wings, by using λ4047 and λ5461 of a water-cooled Hg 198 isotope lamp for the core, and the red lines of an ordinary Ne discharge tube for the wings. All these measurements were consistent within the accuracy needed, so that only the Ne profile was used in the final estimate for the effect of the neighbouring parabolae.

The instrumental profile thus found was integrated numerically over the width of the channel, 0·19 mm, giving a kind of channel profile. Three of these were plotted side by side at the channel spacing, 0·30 mm. At the centre of the central channel the neighbouring channel on the violet side contributes an intensity 1·8 per cent, while that on the red side gives 0·8 per cent. This asymmetry is in the instrumental profile, and appears in all the Hg and Ne lines measured. Adding the two contributions we have 2·6 per cent false light at the channel centre. However, the amount varies a little across the channel and the average correction for the scattering from neighbouring channels, over the 0·05 mm width used for the microphotometry tracing, was estimated to be 2·7 per cent.

It is of interest to note that the minimum intensity between the channels can be understood in the same way. The superposed contributions from two channels, one from each side, give 25 per cent for the 0·19 mm channel width, whereas the measured minimum intensity was 27 per cent. Similarly, with the parabolic channels obtained with slit width 0·05 mm, the minimum intensity between channels was about 6 per cent, whereas the calculated intensity was 5 per cent.

The vertical instrumental profile can be divided into three parts: the vertical profile of the spectrograph, the resolving power of the Fabry–Perot interferometer, and the resolving power of the fringe imaging lens, including any de-focusing of the fringes on the slit.

The vertical profile of the spectrograph was measured by using a horizontal slit in place of the usual vertical slit. This was supplemented by another measurement, using a thin wire across the vertical slit. The measured vertical profile had a width 0·065 mm on the plate, agreeing with the theoretical value, 0·069 mm, for λ6300, with a square diaphragm 82 mm high over the 9 m spectrograph lens. Converted into wavelengths this width corresponds to 3 mA, 7 mA

and 11 mA respectively at the first, second and third of the interferometer fringes. We shall be dealing with solar line widths about 70 mA, and in comparison these widths should be negligible. However, as described later, they do affect the narrower iodine lines by which de-focusing of the fringe system on to the spectrograph slit was checked.

Various considerations show that the resolving power of the Fabry–Perot interferometer was near 10^6, but no reliable method could be devised to measure the actual resolving power given with the 7·5 mm spacer. It is well known, however, that the resolving power of a Fabry–Perot interferometer depends on the reflectivity of the coating, the surface quality of the two plates, and the adjustment. In this work the first two were measured together by using a 0·08 mm spacer in place of 7·5 mm, and the last factor was checked by an iodine absorption tube. Owing to the possibility of variations of reflectivity or plate quality, the same area of the interferometer had to be examined as was used for the solar spectrum. Thus the same set-up was used, changing only the spacer, and using a Pointolite lamp for source instead of the Sun, in order to avoid absorption lines. The lamp (Fig. 1), put near the focus of the condenser lens O, illuminated the secondary mirror M in just the same way as sunlight from the coelostat mirror. After reflection from the secondary mirror, the light was focused on the auxiliary slit S_1 and thence followed the same path as light from the Sun, so that exactly the same area of the interferometer was used. What one now gets on a spectrogram is parabolic channels, essentially similar to those from the thick spacer, but now with a very large inter-channel separation, 28 mm (Plate 1(*d*)). If one slowly narrows down the spectrogram slit the width of the channels at first decreases too, but finally one reaches a limit beyond which the channel width is more or less independent of slit width. The channel profile with the slit width below this limit is the profile of the interferometer, as seen through the spectrograph. The ratio of the inter-channel distance to the half-width of this profile equals the "effective number of reflections", which in turn is directly related to the reflectivity of the coating.

The measured interferometer profile was fitted to the formula

$$J/J_0 = 1 \Big/ \left\{ 1 + \frac{4R}{(1-R)^2} \sin^2 \frac{\phi}{2} \right\}$$

where ϕ is the phase angle, using two values for R, the reflectivity, 94 per cent and 92 per cent, the corresponding effective number of reflections being 49 and 36 respectively (6). In general the first value gives the better fit, but if one is concerned only with the core of the profile the lower reflectivity is better. This discrepancy is presumably associated with the surface quality, which does not appear in the formula. Were the coated surfaces not plane the fringe system formed by one part of the interferometer aperture would not be the same as that formed by other parts. The fringe system from the whole aperture would therefore be an aggregate of profiles whose centres are not exactly coincident. The lower reflectivity, 92 per cent, must therefore be interpreted as a kind of effective reflectivity, taking into account the surface quality, while the higher value, 94 per cent, more nearly represents the reflectivity of the coating itself. We are interested in the resolving power and should therefore use the 92 per cent.

With the 7·5 mm spacer a reflectivity of 92 per cent means a resolving power $8{\cdot}8 \times 10^5$. In wavelength units this is 7 mA, which is so small as not to affect

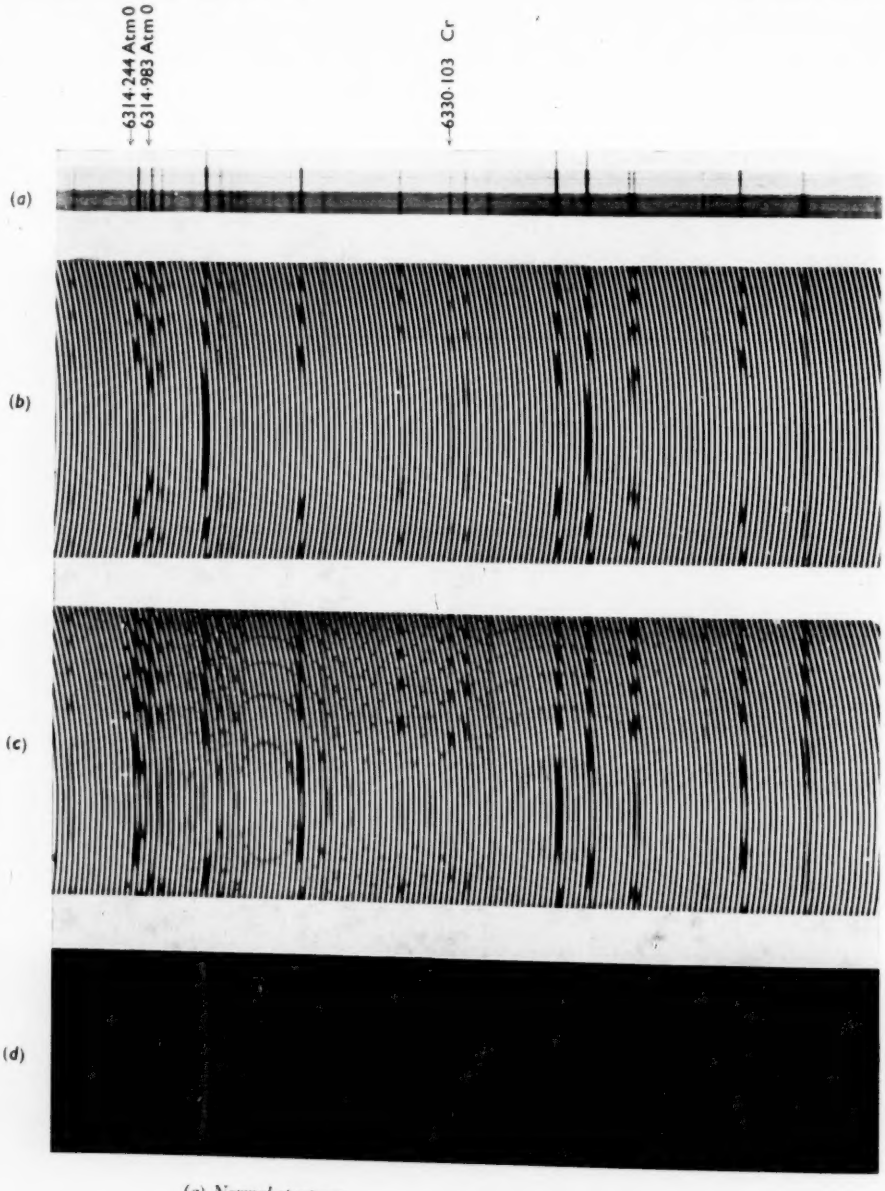

(*a*) *Normal spectrum.*
(*b*) *Parabolic channels with one of the measured lines, Cr.* 6330·103 *A.*
(*c*) *Parabolic channels using the iodine tube. Many of the fainter iodine lines have been lost in reproduction.*
(*d*) *Instrumental profile of the Fabry–Perot interferometer with* 0·08 *mm spacer.*

the profiles of the solar lines. It is to be noted in this connection that the intensity between orders was so low that it could be neglected altogether, especially since we are interested only in faint lines whose residual intensities are higher than 50 per cent.

The focusing of the fringe system on to the spectrograph slit was checked before or after the solar observations, using the same set-up to photograph through an iodine absorption tube (Plate 1 (*c*)). The iodine lines are supposed to be very sharp, and any broadening found from these photographs is to be attributed to the finite resolving power of the spectrograph along the slit. This effect is negligible near the centre of the fringe system, but becomes gradually more important as we go towards the outer fringes, for the dispersion diminishes outwards, from an infinite value at the centre. The measured iodine line profiles, expressed in wavelength units, are very narrow for the first fringe, but become shallower and wider as we go to the outer fringes, the first four fringes giving 17, 21, 22 and 23 mA respectively. The widths to be attributed to the finite vertical resolving power of the spectrograph are 3, 7 11 and 18 mA respectively, so that the corrected widths become 17, 20, 19 and 14 mA respectively. The tendency for the widths to increase outwards appears now to have been eliminated, and this has been taken to mean that the vertical instrumental profile of the spectrograph affects the definition of the fringe system more than de-focusing on to the spectrograph slit.

The iodine line width, after correction for the finite resolving power of the interferometer, was 14 mA. This seems a little too large, since iodine lines are frequently used to test resolving powers of the order of 500 000 (**7**). It is to be noted, however, that to get measurable absorption lines in the red the temperature of the iodine had to be raised as high as 40 deg. C. It is possible also that there may have been some maladjustment of the 7·5 mm spacer but, if so, we are certain that it was so small as to give a contribution to the solar line widths much less than, say, 10 mA.

Summarizing the discussion, the corrections to be applied are as follows: 1·3 per cent from uniformly scattered light, 1 per cent from grating ghosts plus reflection at the inner faces of the doublet spectrograph lens, and 2·6 per cent from light scattered from neighbouring channels. As these corrections are more or less uniform over a wide spectral range, they could be simply added together and regarded as the scattering. The sum, 4·9 per cent, was therefore applied to the measured profiles of nine Fraunhofer lines. Other corrections depending on resolving power were neglected altogether, since the average effective resolving power along the parabolic channels was as high as 6×10^5, i.e. gave a line width about 10 mA only.

5. *Profiles, equivalent widths and half half-widths.*—The corrected profiles are given in Table I. The lines are arranged and numbered in order of decreasing rate of diminution of η with depth (cf. Fig. 2). The table gives the profiles in terms of line depths in per cent, instead of residual intensities. Equivalent widths and observed half half-widths are in Table II, both in mA. Explanations of the last two columns in this table will be found in section 8. Line depths and equivalent widths at the disk centre are compared with mean values from Allen (**8**), in Table III. The agreement in equivalent widths appears to be very satisfactory. Allen's line depths, however, are systematically a little larger than ours, suggesting that his measures have been slightly over-corrected.

TABLE I

Line depths in per cent in the lines at five positions on the disk

cos θ	$\Delta\lambda=0$	10	20	40	60	80	100	120	140 mA
No. 1. 6252 V		**RI : −1**		**LEP : 0·29 eV**					
1·0	12·1	11·6	10·7	8·6	5·7	3·0	1·4	0·8	0·4
0·8	11·9	11·8	11·2	9·0	6·0	3·6	1·7	0·6	0·1
0·6	12·9	12·6	11·6	9·2	6·4	3·6	1·4	0·9	0·2
0·4	15·0	14·7	13·6	10·6	7·2	4·8	2·5	1·3	0·7
0·3	14·4	14·2	13·4	11·0	7·8	5·1	2·6	1·4	0·7
No. 2. 6330 Cr		**RI : 1**		**LEP : 0·94 eV**					
1·0	27·5	26·5	23·4	15·8	8·5	4·2	1·9	0·7	0·4
0·8	24·3	24·0	22·3	16·3	9·9	5·7	2·7	1·1	0·5
0·6	24·5	23·8	21·8	17·3	11·7	6·7	3·5	1·6	0·6
0·4	27·2	26·6	24·5	19·3	13·4	7·7	3·9	1·4	0·3
0·3	26·4	25·9	24·4	19·1	13·0	7·6	4·2	2·0	0·8
No. 3. 6393 Fe		**RI : 0**		**LEP : 2·27 eV**					
1·0	16·9	16·3	14·3	10·0	5·9	3·3	1·8	0·7	0·2
0·8	16·0	15·5	14·1	9·6	5·7	3·2	2·0	1·1	0·4
0·6	17·0	16·5	15·1	11·5	7·7	4·5	2·0	0·7	0·2
0·4	17·0	16·4	15·3	11·8	7·6	4·4	2·1	0·9	0·2
0·3	17·4	17·0	16·0	12·7	9·1	5·7	3·1	1·6	0·4
No. 4. 6229 Fe		**RI : 1**		**LEP : 2·83 eV**					
1·0	35·6	34·5	30·2	19·7	10·7	5·3	1·7	0·4	0·0
0·8	32·8	32·2	29·1	20·8	12·4	5·5	2·1	0·7	0·2
0·6	31·7	30·8	28·4	21·2	13·9	7·9	3·4	1·0	0·5
0·4	32·8	32·0	29·8	23·1	15·3	9·6	4·0	1·7	0·4
0·3	32 0	31·1	28·8	22·3	15·6	10·0	4·8	2·6	0·8
No. 5 6227 Fe		**RI : 1**		**LEP : 3·87 eV**					
1·0	25·5	24·7	21·4	14·8	8·4	3·5	1·5	0·6	0·2
0·8	25·0	24·2	22·0	15·4	8·9	4·6	1·6	0·7	0·2
0·6	24·5	24·0	22·2	16·8	11·0	6·1	2·9	0·9	0·0
0·4	24·6	24·0	22·4	17·6	11·9	7·0	3·6	1·8	0·6
0·3	23·5	23·3	21·7	16·8	11·5	6·9	3·8	1·8	0·6
No. 6. 6224 Ni		**RI : 1**		**LEP : 4·09 eV**					
1·0	25·5	24·5	21·7	15·1	8·8	4·4	1·9	0·9	0·2
0·8	24·6	24·1	21·7	15·8	9·5	5·3	1·6	0·2	0·0
0·6	23·3	22·5	20·9	16·1	10·9	5·6	2·4	1·1	0·5
0·4	23·8	23·5	21·9	17·4	12·3	7·3	3·8	1·8	0·3
0·3	22·4	21·6	20·0	15·5	10·3	5·7	2·6	0·9	0·0
No. 7. 6369 Fe^+		**RI : 0**		**LEP : 2·88 eV**					
1·0	17·2	16·7	14·8	10·5	5·7	2·9	1·3	0·4	0·1
0·8	15·2	14·9	13·9	11·0	6·6	3·7	1·5	0·3	0·0
0·6	14·8	14·6	13·6	10·2	6·3	3·4	1·1	0·3	0·1
0·4	14·0	13·6	12·8	10·2	6·5	3·4	1·7	0·7	0·3
0·3	14·0	13·6	12·5	9·8	6·7	4·3	2·2	1·1	0·4
No. 8. 6238 Fe^+		**RI : 2**		**LEP : 3·87 eV**					
1·0	35·3	34·1	30·6	23·0	14·9	8·7	4·5	2·4	1·1
0·8	33·5	32·4	29·5	22·4	15·7	9·7	4·8	2·2	0·9
0·6	30·7	29·9	27·8	22·1	15·8	10·0	5·8	3·1	0·4
0·4	28·9	28·4	26·9	21·8	16·1	9·6	5·5	2·6	1·5
0·3	24·3	23·9	22·9	18·6	13·7	8·0	3·9	1·2	0·5

TABLE I—*continued*

No. 9. 6248 Fe+		RI : 2			LEP : 3·87 eV				
cos θ	Δλ=0	10	20	40	60	80	100	120	140 mA
1·0	45·4	44·3	40·5	28·9	18·5	10·7	5·6	3·1	1·6
0·8	42·6	41·6	38·2	29·6	19·2	11·1	6·4	3·5	1·8
0·6	39·8	39·2	37·0	28·8	20·6	12·6	6·5	3·4	1·5
0·4	36·9	36·2	34·3	27·8	19·4	12·1	7·0	3·3	1·7
0·3	33·0	32·2	30·3	24·5	17·6	10·9	5·6	2·4	0·6

TABLE II

Centre limb variations of observed equivalent widths, observed and calculated half half-widths, and their effective optical depth for λ6310

W : *equivalent width in* **mA**. Δλ : *observed half half-width in* mA. $\Delta\lambda^c$: *corrected half half-width in* mA *derived from the profile of the absorption coefficient.* τ : *effective optical depth for* $\Delta\lambda^c$ *at* λ 6310

No. 1.	6252 V	RI : −1			No. 2.	6330 Cr	RI : 1	
cos θ	W	Δλ	$\Delta\lambda^c$		W	Δλ	$\Delta\lambda^c$	τ
1·0	14·7	59·0	55·8		27·8	44·6	40·3	0·70
0·8	15·3	64·5	58·8		28·4	53·8	48·0	0·58
0·6	16·0	62·6	55·8		30·1	58·0	52·2	0·41
0·4	19·3	60·6	54·2		33·6	60·0	50·3	0·25
0·3	19·8	65·6	59·6		33·6	59·5	51·5	0·17

No. 3.	6393 Fe		RI : 0		No. 4.	6229 Fe		RI : 1
cos θ	W	Δλ	$\Delta\lambda^c$	τ	W	Δλ	$\Delta\lambda^c$	τ
1·0	17·8	46·2	44·5	0·82	34·4	44·5	35·6	0·57
0·8	17·6	47·3	44·1	0·66	35·0	50·6	42·1	0·47
0·6	20·1	56·7	51·0	0·48	37·0	54·0	44·0	0·34
0·4	20·3	57·8	50·2	0·31	40·1	56·8	44·8	0·21
0·3	22·9	61·0	55·0	0·21	40·3	59·0	45·4	0·18

No. 5.	6227 Fe		RI : 1		No. 6.	6224 Ni		RI : 1
cos θ	W	Δλ	$\Delta\lambda^c$	τ	W	Δλ	$\Delta\lambda^c$	τ
1·0	25·4	46·9	40·2	0·71	26·4	47·2	41·1	0·71
0·8	26·4	49·6	43·1	0·56	26·2	52·5	43·9	0·56
0·6	28·9	57·2	48·0	0·41	27·6	58·0	48·6	0·42
0·4	31·0	59·4	48·8	0·26	30·6	60·4	51·3	0·27
0·3	30·0	59·6	46·7	0·18	26·5	60·0	45·6	0·18

No. 7.	6369 Fe+		RI : 0		No. 8.	6238 Fe+		RI : 2
cos θ	W	Δλ	$\Delta\lambda^c$	τ	W	Δλ	$\Delta\lambda^c$	τ
1·0	17·7	48·0	44·0	0·82	41·0	54·2	36·6	0·65
0·8	18·0	55·6	51·2	0·67	40·6	57·8	37·4	0·48
0·6	17·0	58·9	48·9	0·50	40·2	65·1	42·6	0·36
0·4	17·0	60·0	52·3	0·33	39·2	66·2	45·6	0·24
0·3	17·8	60·0	50·0	0·24	31·9	70·6	46·6	0·17

No. 9.	6248 Fe+		RI : 2	
cos θ	W	Δλ	$\Delta\lambda^c$	τ
1·0	52·5	51·5	30·9	0·44
0·8	52·2	55·9	33·7	0·36
0·6	52·2	60·9	36·6	0·26
0·4	49·6	63·4	38·8	0·18
0·3	43·1	64·5	37·7	0·11

TABLE III

Comparison with Allen at the disk centre

Wave-length	El.	RI	Line depths: Present work	Line depths: Allen	Equivalent widths: Present work	Equivalent widths: Allen
6223·996	Ni	1	25·5%	28%	26·4 mA	26 mA
6226·745	Fe	1	25·5	29	25·4	26
6229·240	Fe	1	35·6	37	34·4	34
6238·396	Fe^+	2	35·3	34	41·0	44
6247·569	Fe^+	2	45·4	50	52·5	53
6251·845	V	−1	12·1	13	14·7	13
6330·103	Cr	1	27·5	30	27·8	27
6369·479	Fe^+	0	17·2	14	17·7	17
6392·545	Fe	0	16·9	13	17·8	14

In Tables I and II most of the weaker lines show limb strengthening and the exceptions are lines from ionized atoms. Going from centre to limb, lines tend to become broader and shallower.

We shall now try to interpret the observed centre limb variation on the basis of one of the modern model solar atmospheres, and then will derive the true distribution of absorption coefficient with wave-length from the observed line profiles using the chosen model. In order to come to any conclusions about turbulence we shall need to derive the variation in the selective absorption coefficient over the line profile, because the measured profiles are all appreciably affected by saturation. In fact, a simple calculation on the Milne–Eddington model shows that, even for the faintest measured lines, with central line depths about 17 per cent, the correction for the half half-widths at the centre of the disk is of order of 10 per cent (cf. (**9**)).

6. *Equation of transfer and model solar atmosphere.*—Let us divide the equation of transfer into two parts, one for the line and the other for the continuum. The equation of transfer for the line can be written in the following form:

$$\frac{dI_\nu}{dx} = -\frac{1}{4\pi} p_\nu N_1 \left(B - \frac{N_2}{N_1} B' \right) h\nu I_\nu + \frac{1}{4\pi} p_\nu N_2 A h\nu,$$

where A, B' and B are respectively the Einstein probabilities of spontaneous and stimulated emissions and absorptions, and p_ν is the normalized function giving the form of the line. The equation can be brought into the conventional form

$$\cos\theta \frac{dI_\nu}{d\tau_\nu} = I_\nu - E_\nu$$

if we put

$$d\tau_\nu \cos\theta = -\kappa_\nu dx,$$

$$\kappa_\nu = \frac{1}{4\pi} p_\nu N_1 \left(B - \frac{N_2 B'}{N_1} \right) h\nu,$$

$$E_\nu = N_2 A / N_1 \left(B - \frac{N_2}{N_1} B' \right).$$

It is to be noted that if we introduce the excitation temperature T_a by

$$\frac{N_2}{N_1} = \frac{g_2}{g_1} e^{-h\nu/k T_a}$$

E_ν is formally equivalent to the Planck function for T_a. Hence

$$E_\nu = \frac{2h\nu^3}{c^2} \Big/ \left(e^{h\nu/k\,T_a} - 1\right) \equiv P_\nu(T_a)$$

Therefore, in any non-equilibrium state, we may write

$$\cos\theta \frac{dI_\nu}{d\tau_\nu} = I_\nu - P_\nu(T_a). \tag{1}$$

The equation of transfer for the continuum can be written

$$\cos\theta \frac{dI_\nu}{d\tau} = I_\nu - P_\nu(T_c) \tag{2}$$

where

$$d\tau \cos\theta = -\kappa dx$$

and T_c represents the temperature distribution as derived from limb darkening.

We may superpose these two equations of transfer (1) and (2) by remembering that the total intensity I_ν suffers simultaneously two kinds of absorption κ and κ_ν. If we denote κ_ν/κ by η, the resulting equation of transfer can now be written as

$$\cos\theta \frac{dI_\nu}{d\tau} = (1+\eta)I_\nu - \eta P_\nu(T_a) - P_\nu(T_c). \tag{3}$$

This equation cannot be solved unless the distributions of T_a and T_c are given at all depths. As T_c is normally given by limb darkening, the remaining problem to be considered in the theory of line formation concerns T_a. The assumption

$$T_a = T_c \text{ everywhere}$$

has usually been called local thermodynamic equilibrium, while the alternative assumption

$$P_\nu(T_\nu) = I_\nu, \text{ averaged over all solid angles,}$$

has been called monochromatic radiative equilibrium.

These assumptions have so far been very useful in many problems, but if the problem involves both the uppermost layers, including the chromosphere and the deeper reversing layer, either assumption could be made satisfactorily only by considering a very complicated stratified atmosphere. In fact, the chromosphere may make an important contribution, even in the case of weak lines, the effect of which must be considered if we are interested in centre-limb variations. In the present state of our knowledge it seems that the best way would be to use an empirical distribution of T_a and to avoid reference to either assumption. Although to solve the equation in this way may not be tantamount to solving the problem of line formation, it will lead to a sufficient check on the model solar atmosphere we wish to use in evaluating the saturation effect.

In what follows I have used the Böhm–Vitense Model II (**10**), which as far as I can see represents the empirical distribution of T_a through the upper layers, with minimum deviations from the continuous limb-darkening. Since the excitation temperatures naturally vary from line to line, this procedure is justifiable only from a statistical point of view. In the uppermost layers, for which limb darkening measures give us no data, we can equate T_c to T_a without violating any observed limb darkening. In deeper layers, where we have no empirical determination of T_a, the discrepancy between T_a and T_c might in principle be considerable, depending on the degree of departure from thermodynamic equilibrium. But in this particular wavelength region the limb darkening coefficient happens to be about 1·5, and the difference between "absorption"

and "scattering" for weak lines is thus smaller than for other regions. Thus, irrespective of the mode of formation, we can safely put $T_a = T_e$ in deep layers. The equation of transfer (3) now becomes

$$\cos\theta \frac{dI_\nu}{d\tau} = (1+\eta)I_\nu - (1+\eta)P_\nu(T_a), \tag{4}$$

where T_a is the temperature distribution of Böhm–Vitense's Model II.

(4) is to be regarded as an empirical equation, rather than as referring to pure absorption, although formally there is no difference. P_ν will not be assumed to be linear in τ. In the next section exact solutions will be given for equation (4) for general $\eta(\tau)$ and $P_\nu(\tau)$.

7. *Centre-limb variation of equivalent width.*—From equation (4) the intensity I_ν is given by

$$I_\nu(0,\theta) = \int_0^\infty P_\nu \, e^{-(\tau+\tau_\nu)\sec\theta} \, d(\tau+\tau_\nu)\sec\theta,$$

where

$$\tau_\nu = \int_0^\tau \eta d\tau.$$

If we introduce an auxiliary function

$$\Phi^*(\tau,\theta) = \int_\tau^\infty P_\nu \, e^{-\tau\sec\theta} \, d\tau \sec\theta,$$

the intensity outside the line is $\Phi^*(0,\theta)$.

The line absorption $I_0 - I_\nu$ is now transformed as follows:

$$\begin{aligned} I_0(0,\theta) - I_\nu(0,\theta) &= \Phi^*(0,\theta) - \int_0^\infty P_\nu \, e^{-\tau\sec\theta} e^{-\tau_\nu\sec\theta} \, d\tau\sec\theta \\ &\qquad - \int_0^\infty P_\nu \, e^{-\tau\sec\theta} \, \eta \, e^{-\tau_\nu\sec\theta} d\tau\sec\theta \\ &= \Phi^*(0,\theta) + \Phi^*(\tau,\theta)\, e^{-\tau_\nu\sec\theta}\Big|_0^\infty - \int_0^\infty \Phi^*(\tau,\theta)(-\eta\sec\theta)\, e^{-\tau_\nu\sec\theta} d\tau \\ &\qquad - \int_0^\infty P_\nu \, e^{-\tau\sec\theta} \, \eta \, . \, e^{-\tau_\nu\sec\theta} d\tau\sec\theta \\ &= \int_0^\infty (\Phi^*(\tau,\theta) - P_\nu \, e^{-\tau\sec\theta}) \eta \, e^{-\tau_\nu\sec\theta} \, d\tau\sec\theta. \end{aligned}$$

Hence the line depth $r(\theta)$ can be written

$$r(\theta) = \frac{I_0(0,\theta) - I_\nu(0,\theta)}{I_0(0,\theta)} = \int_0^\infty g(\tau,\theta) \, . \, \eta \, . \, e^{-\tau_\nu\sec\theta} d\tau, \tag{5}$$

where

$$g(\tau,\theta) = \frac{1}{\Phi^*(0,\theta)} [\Phi^*(\tau,\theta) - P_\nu(\tau)\, e^{-\tau\sec\theta}] \sec\theta \tag{6}$$

It is to be noted that this expression for the weighting function is identical with that derived by Unsöld for general $P_\nu(\tau)$, but for $\eta \ll 1$, (9). It can easily be shown that the weight function (6) may also be written as

$$g(\tau,\theta) = \frac{1}{\Phi^*(0,\theta)} \int_\tau^\infty \frac{dP_\nu(\tau)}{d\tau} e^{-\tau\sec\theta} d\tau\sec\theta \tag{7}$$

This last expression gives higher accuracy in numerical computation. It also has a definite physical meaning, namely that the weight function at τ is proportional to the observable effective emissivity gradient below τ.

If $P_\nu(\tau)$ is represented by a linear function $1+\beta_0\tau$, (7) reduces to

$$g(\tau,\theta)=\frac{\beta_0}{1+\beta_0\cos\theta}\,e^{-\tau\sec\theta} \tag{8}$$

If, moreover, η is small compared with unity, the line depth becomes

$$r(\theta)=\int_0^\infty \frac{\beta_0}{1+\beta_0\cos\theta}\,e^{-\tau\sec\theta}\,\eta\,d\tau \tag{9}$$

This is the expression frequently used by Unsöld, which is valid only for very small line depths. It is the correction factor $e^{-\tau_\nu\sec\theta}$ in our formula (5) that measures the degree of saturation with which we are primarily concerned.

For very large η, the line depth in a "linear" atmosphere, corresponding to equations (5) and (8), tends to a finite value

$$r(\theta)\to\frac{\beta_0\cos\theta}{1+\beta_0\cos\theta}. \tag{10}$$

In a general temperature distribution it becomes

$$r(\theta)\to g(0,\theta)\cos\theta=\frac{1}{\Phi^*(0,\theta)}\int_0^\infty \frac{dP_\nu(\tau)}{d\tau}\,e^{-\tau\sec\theta}\,d\tau \tag{11}$$

from equations (5) and (7). It is of interest to compare these two series of limiting line depths. The comparison is made in Table IV.

TABLE IV

Comparison of limiting line depths

$\cos\theta$	1·0	0·8	0·6	0·4	0·3
Present work	0·88	0·85	0·82	0·81	0·76
Linear approximation	0·60	0·55	0·47	0·38	0·31

The Böhm–Vitense model gives decidedly greater limiting depths and a much less marked decrease in line depth from centre to the limb than does the linear approximation. These features would be inherent in every modern model of the solar atmosphere in which there is a very sharp decrease to a very low surface temperature near the upper boundary. This is apparent in our formula (11) according to which the limiting line depth is proportional to the observed effective emissivity gradient in the reversing layer. Modern models of this kind therefore give less saturation effects in the lines than an atmosphere based on the linear approximation.

The weight functions (7) were evaluated by numerical integration after converting the temperature distribution into the emissivity distribution $P_\nu(\tau)$ for λ6310; they are tabulated in Table V for $\cos\theta=1{\cdot}0$ and 0·3 for a number of optical depths, and are compared with the weight function (8) for the linear approximation with $\beta_0=1{\cdot}5$. The comparison shows that in the model we are using there is a greater contribution to the line depth from the upper layers than there is in the linear approximation, especially near the limb. This can also be understood from equation (7) as a consequence of the adopted sharp decrease in temperature towards the surface.

η was calculated for each line on the same model, using the Saha and Boltzmann formulae, partition functions being taken from Claas' tables (**11**). Continuous absorption coefficients were read from Vitense's diagrams (**12**). The resulting

TABLE V

Comparison of weight functions

	Present work		Linear approximation	
τ_{6310}	$\cos\theta = 1.0$	0.3	1.0	0.3
0.00	0.877	2.525	0.600	1.034
0.04	772	1.917	576	0.905
0.1	571	0.824	543	742
0.2	500	531	491	531
0.4	388	320	402	273
1.0	198	043	221	037
1.5	0.120	0.008	0.134	0.007

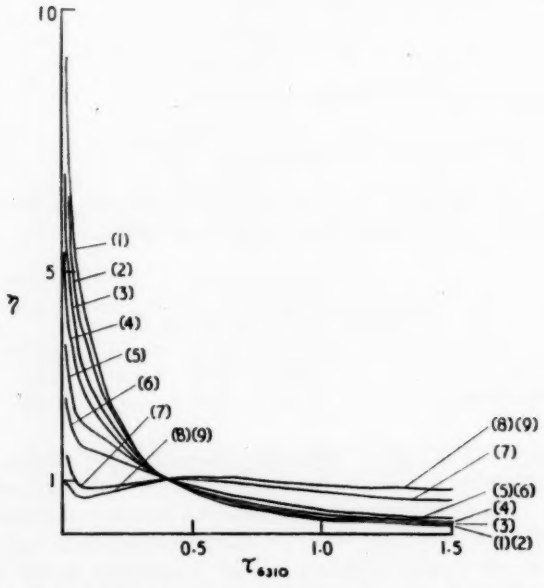

FIG. 2.—*Relative η's of nine lines. Numbers refer to the line number in Table I.*

η's for the nine lines studied are shown in Fig. 2. The numbers in the diagram refer to line numbers in Table I. The smaller the number the steeper the decrease of η with depth. For a number of lines with smaller numbers the η's increase very rapidly at very small optical depths not shown in the diagram.

The calculated centre-limb variations of central line depths from formula (5) are shown in Fig. 3 by broken lines and compared with observation (continuous lines). Numbers on each side of the diagram refer to line numbers in Table I. Those on the left refer to both observed and calculated curves, those on the right to observed curves only. On the whole the agreement with observation seems as good as one could hope. It is well established that lines of stronger limb strengthening are always associated with steeper η distributions. However, if there is an anisotropy or depth-variation of turbulence in the reversing layer, as will be discussed later in detail, this comparison can be only qualitative, since the limb profiles may be shallower on account of larger turbulent velocities in the

upper layers. Centre-limb variations for separate parts of the profile would then give no significant test of the adopted model. It is well known, however, that centre-limb variations of the equivalent widths are not affected by turbulence, provided this is of large scale. Though we do not necessarily postulate that the turbulence is of large scale, the comparison of centre-limb variations of equivalent widths would be more significant. This is especially true because even the strongest lines we measured are still on the linear part of the curve of growth.

The first step was to determine the wave-length distribution of the absorption coefficient for the centre of the disk, and with this then to calculate the expected profiles for other positions on the disk. Integration of the calculated profiles gave calculated equivalent widths, which were compared with observation. The

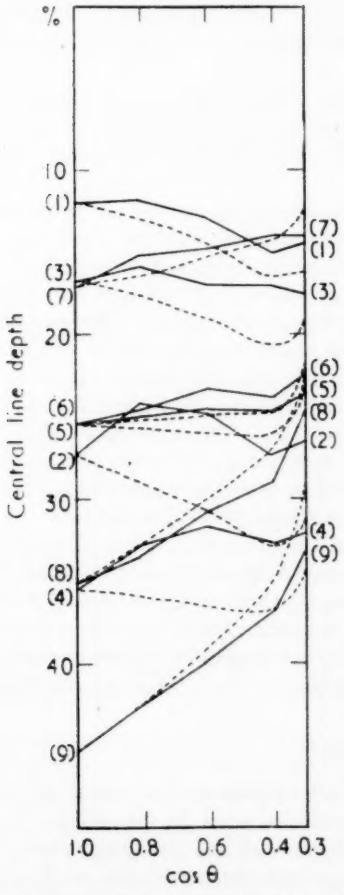

FIG. 3.—*Centre limb variations of line depths at the centre of lines. Continuous lines: observations. Broken lines: calculations. Numbers on both sides of the diagram refer to line numbers.*

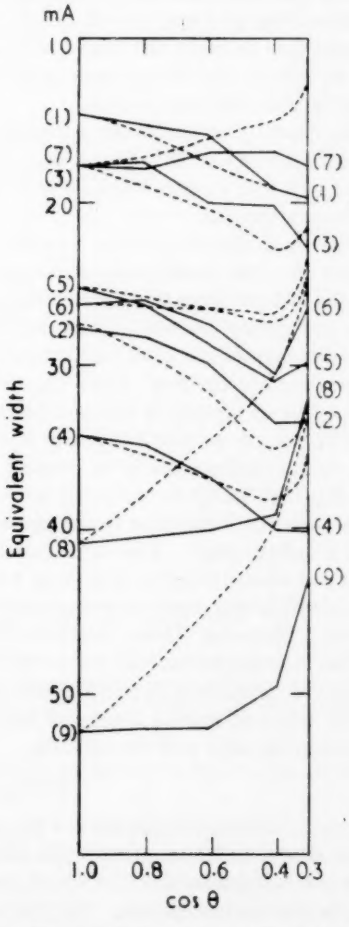

FIG. 4.—*Centre limb variations of equivalent widths. Continuous lines: observations. Broken lines: calculations. Numbers on both sides of the diagram refer to line numbers.*

results are in Fig. 4. Once more the numbers on the left refer to the observed and calculated values, whereas those on the right refer to observed values only. The agreement appears satisfactory except for lines of high excitation potential, especially those of ionized iron. For two or three of these lines the observed equivalent widths definitely exceed the calculated equivalent widths near the limb. This discrepancy may possibly be associated with an error in estimating the excitation from the ground state. The excitation was calculated by Boltzmann's formula, using the temperature, empirically determined, either from the limb darkening or from the central intensities in the visible region. For excitation from the ground state, however, the effective radiation comes from the far ultra-violet, of which we are quite ignorant. In this wave-length region there might be an excess of radiation such as was suggested by Böhm (**13**). But we shall not examine this problem in full detail here, for the discrepancy under discussion appears not to affect the final conclusion of this work appreciably. We would like to believe that the adopted model is good enough to evaluate the saturation effect in the observed profiles.

8. *Centre-limb variations of Doppler widths.*—We do not know exactly whether the turbulence we are going to deal with is predominantly of large scale or small scale. In this section we shall determine the true Doppler widths on both of these assumptions.

We shall first derive the Doppler widths assuming small scale turbulence. In this case the distribution of the absorption coefficient over the profile can be derived directly from the line depths using the known relation between $r(\theta)$ and η. The absorption coefficient distributions were calculated and half half-widths were determined for each line at various positions on the disk. The results are in the fourth column of Table II. The table shows that the widths of all lines except that of vanadium increase towards the limb, as was pointed out by Allen.

The vanadium line $\lambda 6251{\cdot}845$ is evidently broadened by hyperfine structure (**14**), and we cannot use it for discussing turbulence. The other lines, of Cr, Fe and Ni, may safely be assumed to be free of hyperfine structure effects, since these elements have even atomic numbers and their primary isotopes have even mass numbers (**15**). The vanadium line is excluded from what follows.

If one wishes to get average true widths for each $\cos\theta$ from Table II, one finds values which are more scattered about the mean values than are the observed widths. However, if true widths are plotted against the corresponding equivalent widths, there is a beautifully linear relation. Accordingly in Fig. 5 we employ the more exact procedure of plotting true widths (represented by the larger symbols) against effective optical depths of line formation. These effective depths are calculated by means of the relation

$$(\tau+\tau_{0\cdot5_\nu})\sec\theta=1$$

where $\tau_{0\cdot5_\nu}$ means τ_ν at the part of the profile where η has half its central value η_0. There seems to be no doubt that the true widths again lie on straight lines. Since the half half-width of thermal motion is about 23 mA, the rest of the width must be due to turbulence. We may conclude that the turbulence velocities in a given direction increase with optical depth, and that the velocity at $\tau\approx0{\cdot}4$ is greater in the horizontal direction than vertically.

At this point one might raise the objection that turbulent velocities apparently decreasing with height could have resulted from an overestimate on our part of

the saturation effects, as the stronger lines which need more correction for this effect proved to have narrower true widths. The answer is given by a comparison of $\lambda 6238$ with $\lambda 6248$, both lines belonging to the same multiplet. In spite of the fact that $\lambda 6238$ is the weaker of the two, it actually has a greater observed width. This would be quite incomprehensible from the point of view of saturation effect, unless the true width of $\lambda 6238$ is greater than that of $\lambda 6248$. Another example of this kind is given by comparing $\lambda 6369$ and $\lambda 6229$. Again the weaker $\lambda 6369$ has a greater observed width than the stronger $\lambda 6229$. The tendency for the line of sight components of turbulence velocities to decrease with height may thus be said to be clearly visible in the observed widths themselves. If we take the brightness difference of the ascending and descending granules into account,

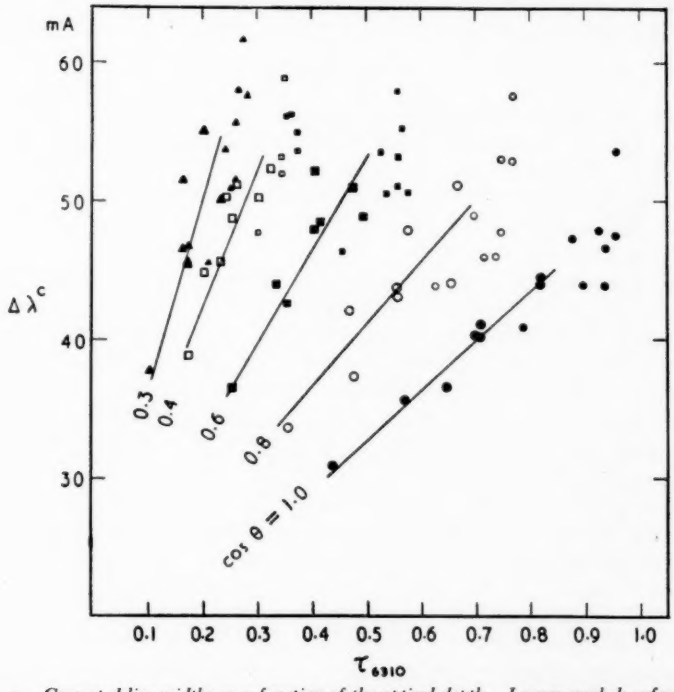

FIG. 5.—*Corrected line widths as a function of the optical depth. Larger symbols refer to half half-widths of the absorption coefficient, whereas smaller symbols refer to half half-widths derived from 1/10-widths.*

the variation of velocities with height would be intensified, as we would naturally expect greater contrast in deeper layers.

One might also suspect that the anisotropy found near $\tau = 0{\cdot}4$ is due to the brightness difference of the ascending and descending granules (**16**). In fact, if the descending granules had zero brightness, the vertical velocities would be measured at about half their real values, supposing no account to be taken of any velocity shift of the whole line. But it seems difficult to explain the strong anisotropy at $\tau \approx 0{\cdot}4$ on this basis, and there seems no doubt that at about this level the horizontal motions are predominant. It is quite possible, however, that there are ascending and descending granules of diameters about 100 km

with surface brightness ratio as high as 3 : 1, corresponding to a temperature difference of about 1000 deg., and if so the line widths are probably affected. The velocity field of turbulence derived in the next section is to be understood as provisional.

If the turbulence increases with depth the lines would be widened in the wings more than at the centre, since the wings are formed effectively at a greater depth. To check this the line widths were computed for a point where the absorption coefficient is 1/10th that at the line centre. The damping parameter a can be taken to be near zero for these faint lines and then the ratio of 1/10-width to half-width is 1·82. The 1/10-widths were therefore reduced by this factor to give fictitious half-widths corresponding to the derived 1/10-widths. The fictitious half half-widths were plotted in Fig. 5 (small symbols) against effective depths given by the relation

$$(\tau+\tau_{0\cdot1\nu})\sec\theta=1$$

where $\tau_{0\cdot1\nu}$ means τ_ν at the point of the profile where $\eta=0\cdot1\eta_0$. This diagram tends to confirm the distribution of velocities with depth suggested by the half half-widths. Were a taken to be about 0·1 instead of zero, the widths would be reduced by about 3 per cent and the fit in the diagram would not be appreciably altered. But in view of the low accuracy of the 1/10-widths this argument is not very significant.

On the assumption of large scale turbulence we again obtained about the same velocity distribution with depth as is shown in Fig. 5. The widths were calculated in the following way. For simplicity, lines at the centre of the solar disk were assumed to be broadened by small scale turbulence only. This assumption is plausible in view of the fact that the line widths there are consistent with the small scale turbulence velocities derived from the curve of growth by Wright (**17**), and ten Bruggencate and Houtgast (**18**). From these profiles at the disk centre, profiles at other positions on the disk were computed using the previous calculations of the centre-limb variation of the absorption at each point of the line profile. The calculated profile widths were compared with those observed and the amount of blurring necessary to bring them into agreement gives the velocities of the large scale turbulence. However the variation of velocity with depth which was suggested by the half half-widths is not apparent in the observed line profiles. Velocities derived from the 1/10-widths are about the same as the velocities from the half half-widths of the same lines, in spite of the difference of average depth of the layers in which they originate. If we take damping into consideration the situation becomes worse.

Although we do not attach great weight to the 1/10-widths, we are inclined to believe that the turbulence responsible for the line widths is predominantly of small scale. It does not necessarily follow, however, that the small scale turbulence suggested has to be much smaller in size than the scale height. The small scale turbulence we have in mind can be as big as the scale height and accordingly may have a free path comparable with this. This can be understood if one bears in mind that turbulence of this size also includes much smaller turbulence and that the greater part of the effects of "small scale" turbulence comes from the smaller turbulence elements (**19**).

Wright (**17**), found 1·0 km/sec for the velocity of the small scale turbulence from the curve of growth at the centre of the disk. The corresponding half

half-width after adding the thermal velocity is 28 mA at λ6300. This is to be interpreted as the velocity at the depth where lines lying on the Doppler part of the curve of growth are formed. These lines have equivalent width about 130 mA. Since the equivalent width of our strongest line is 52 mA, the effective depth of the Wright velocity should be much higher in the photosphere than $\tau = 0{\cdot}4$. It seems probable from Fig. 5 that our vertical velocity is very near the Wright value there and our assumption that the turbulence is of small scale thus does not contradict Wright's results. But it is evident that the larger value of small scale turbulence found by ten Bruggencate and Houtgast (**18**), viz. 1·7 km/sec, is inconsistent with our profiles, since the corresponding half half-width in Fig. 5 is this time 35 mA.

9. *Variation of turbulence with depth in the reversing layer.*—The velocity field of turbulence at various depths was derived from Fig. 5 after subtracting the thermal velocities for the corresponding temperatures, and this is shown in Fig. 6. In this diagram the most probable turbulence velocities ξ_t are drawn separately, according to whether they are ascending or descending, and the optical depths for λ 5010 are also shown. Strong asymmetry around $\tau \approx 0{\cdot}4$ is again evident here. In deeper layers, where at present we have no means of measuring horizontal velocities, we do not know whether, for example at $\tau \approx 1$, the turbulence is predominantly vertical or horizontal, or isotropic. At any rate it looks as though the upward motion at $\tau \approx 1$ of some of the granules escaping from the top of the convection layer into the radiative equilibrium zone are deflected into horizontal motions at $\tau \sim 0{\cdot}4$ and that these are finally converted into downward motion. As the speed of vertical motion at $\tau \approx 1$ is about the same as of horizontal motion at $\tau \approx 0{\cdot}4$, there should be no difficulty in satisfying continuity conditions.

Allen's anisotropy (**1**) of 1·74 km/sec and 2·79 km/sec for the vertical and horizontal motions respectively now have to be interpreted as the velocities at $\tau \approx 1$ and say $\tau \approx 0{\cdot}2$ respectively, now that we find evidence for a strong variation of turbulence with optical depth within the reversing layer. Our velocities, however, appear to be somewhat lower than the corresponding Allen values, a difference which may be associated with differences in the way of correcting for saturation effects.

Quite recently McMath *et al.* (**20**), have found increasing large scale turbulence towards the limb from the zigzag appearance of λ 4626, CrI, and λ 5853, BaII. They found that ξ_t increases from 0·6 km/sec at the centre of the disk to 0·8 km/sec at the limb. This points to a variation of velocity of the kind found by Allen and supported by the present work. We do not know, however, whether the McMath results, which undoubtedly refer to much higher layers than ours, are directly related to our velocity field.

The turbulence variation with optical depth proposed here is the opposite of that suggested by Su-Shu Huang (**21**), for F type stars and also the Sun. Su-Shu Huang found a strong increase of turbulence with height in F-type giants and a very weak increase in the Sun. But as far as the Sun is concerned his argument is not very convincing, since he based his conclusions on Allen's profile measures. We do not believe that the turbulence/height relation need necessarily be the same in F giants and G dwarfs. In the F-type stars the convection layer must be located much higher than on the Sun, and may include the whole reversing layer, whereas in the Sun there is a layer in radiative equilibrium

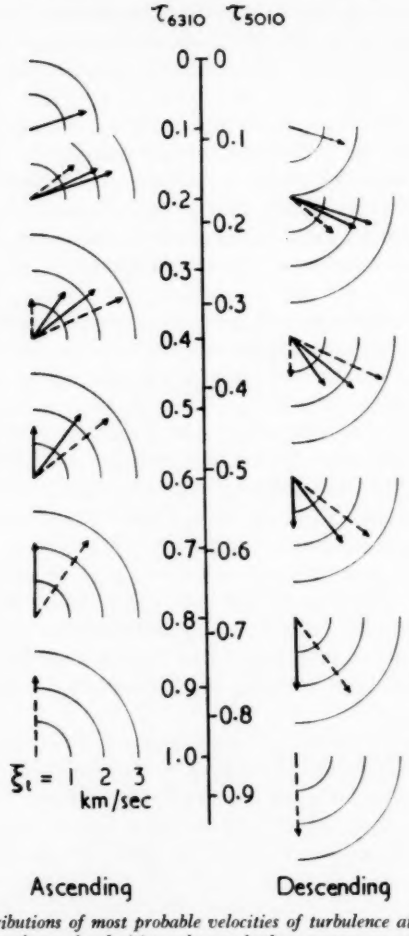

FIG. 6.—*Angular distributions of most probable velocities of turbulence at various depths. Continuous arrows are observed velocities, whereas broken arrows are extrapolated values.*

above the convection layer, acting as a barrier to the granules ascending from below. What we see in the F-type stars is the increasing turbulence with height which is associated with decreasing density. But what we see in the Sun is only the tail end of convection prevailing beneath $\tau \approx 1$. It is understandable that the granular elements surging into the reversing layer are decelerated or deflected, or diminish in number as they ascend, giving a decreasing turbulence with height.

Summing up, we may conclude that the vertical motions of the granule elements from the convection layer are gradually deflected and converted into horizontal motions as they penetrate the radiative equilibrium zone, and are finally converted into downward motions back to the convection layer, without much change in their original speed of about 2 km/sec. The size of the granules would be about the scale height, and the mean free path would be the path length of the circulation just described. No substantial part of the granulation energy

is transferred to the reversing layer. The turbulence observed in the highest part of the reversing layer and in the chromosphere is to be regarded only as a secondary disturbance arising from a small fraction of the granulation energy. This secondary turbulence will probably increase with height, due to the decreasing density.

The author has great pleasure in acknowledging with thanks his indebtedness to Professor F. J. M. Stratton, President of Commission 38, for a grant permitting him to stay at the Cambridge Observatories, and to Professor R. O. Redman, for encouragement and for the facilities put at the author's disposal, as well as for reading and revising the manuscript of this paper in detail. He is especially indebted to Dr H. von Klüber, without whose active guidance and valuable discussions this work could not have been done.

The Observatories,
Cambridge :
1957 *February* 1.

References

(1) C. W. Allen, *M.N.*, **109**, 343, 1949.
(2) C. D. Shane, *Lick Obs. Bull.*, No. 507, 1941.
(3) P. J. Treanor, *M.N.*, **109**, 389, 1949.
(4) S. Tolansky, *High Resolution Spectroscopy*, p. 145, London, 1947.
(5) Z. Suemoto, *Publ. Astr. Soc. Japan*, **2**, 137, 1951.
(6) C. Candler, *Modern Interferometers*, p. 303, Glasgow, 1951.
(7) R. R. McMath, *Ap. J.*, **123**, 1, 1956.
(8) C. W. Allen, *Mem. C.S.O., Canberra*, No. 5, 1934; *M.N.*, **96**, 508, 1936; *Ap. J.*, **85**, 165, 1937.
(9) A. Unsöld, *Physik der Sternatmosphären*, II Auf., Berlin, 1955.
(10) E. Böhm-Vitense, *Zs. f. Ap.*, **34**, 209, 1954.
(11) W. J. Claas, *Rech. Astr. d'Utrecht*, **12**, Part 1, 1951.
(12) E. Vitense, *Zs. f. Ap.*, **28**, 81, 1951.
(13) K. H. Böhm, *Zs. f. Ap.*, **35**, 179, 1954.
(14) A. Abt, *Ap. J.*, **115**, 199, 1951.
(15) A. C. Candler, *Atomic Spectra*, 2nd Vol., p. 208, Cambridge, 1937.
(16) R. S. Richardson and M. Schwarzschild, *Ap. J.*, **111**, 351, 1950.
(17) K. O. Wright, *Publ. Domin. Ap. Obs.*, **8**, 1, 1948.
(18) P. ten Bruggencate and J. Houtgast, *Zs. f. Ap.*, **20**, 149, 1941.
(19) M. H. Wrubel, *Ap. J.*, **112**, 424, 1950.
(20) R. R. McMath, O. C. Mohler, A. K. Pierce, L. Goldberg, *Ap. J.*, **124**, 1, 1956.
(21) Su-Shu Huang, *Ap. J.*, **114**, 287, 1951.

CHROMOSPHERIC INTERFEROMETRY

*P. J. Treanor, S.J.**

(Communicated by the Director of the University Observatory, Oxford)

(Received 1956 December 6)

Summary

The interference spectrum of the brighter lines in the chromosphere of the uneclipsed Sun has been photographed by means of the Oxford 35 m solar telescope, used in conjunction with a Fabry–Perot etalon of high reflectivity and large range, and a low dispersion spectrograph. The very narrow spectroscope slit was set tangentially to the 34 cm solar image. Under these conditions, the emission lines of hydrogen, helium and calcium appear as a system of interference fringes, with a resolving power of nearly 10^5.

A method is developed for the quantitative photometric analysis of the fringe system, from which it is possible to determine chromospheric line-profiles as a function of height, and the chromospheric intensity gradient.

This technique has been employed to determine the profile of the D_3 line of helium. It is found to be nearly independent of height over the range 1500–4250 km, and, after correction for the effect of fine structure and photometric broadening, corresponds closely to a Gaussian distribution of the form $I = I_0 \exp[-(\delta\lambda/0{\cdot}34)^2]$. These results are interpreted as implying that there is little self-absorption, and that the atoms which give rise to the line are subject to turbulent velocities of the order of 17 km/sec.

---

1. *Introduction.*—The application of interferometric techniques to solar studies, initiated by Fabry and Perot in 1902 (**6**), received an impetus some years ago, when it became possible to exploit the progress in the production of high quality silver and dielectric reflecting films and narrow band interference filters (**12**).

In the field of photospheric interferometry, the observational achievements of the past few years have been of considerable significance. Investigations of the mean solar magnetic field by Thiessen (**18**) and by von Klüber (**25**), the study of the Einstein shift by Adam (**1**), the fine structure analysis by Hindmarsh (**7**), and Kinman's search for solar deuterium (**9**) are examples from a varied field of interferometric solar researches, each of which has made a definite contribution to outstanding problems in solar physics.

Nevertheless, as the writer pointed out (**20**), the small range between successive orders makes the Fabry–Perot interferometer a somewhat difficult and limited instrument for use in the study of an absorption spectrum, and it is largely for this reason that it has been overtaken by the grating. In studying the emission spectra of the chromosphere, of solar prominences, and of the corona, these limitations are not encountered, and the great versatility of the etalon commends it in various ways. In it we have a compact spectroscope whose dispersion and resolving power can be chosen at will. With relatively high luminous efficiency, it combines the possibility of simultaneous study of line structures and

* Henry Skynner Research Fellow in Astronomy, Balliol College, Oxford.

displacements over extended areas (a fact made use of by Jarrett and von Klüber (**8**) in their coronal interferometry), or of recording on a single plate high resolution interference spectra of the whole of the photographically accessible spectrum. The potential value of such an instrument for the simultaneous study of chromospheric line structures, or for using to the best advantage the rare and brief moments of total eclipse, is sufficiently evident.

Attempts to realize this promise of interference spectroscopy in the study of solar emission spectra have in fact almost all been made under the difficult and chancy conditions of total eclipse. A number of early attempts from Sproul Observatory (**26**) to obtain coronal fringes failed, as the writer has pointed out (**21**), because of defective experimental design. The success of Jarrett and von Klüber's coronal interferometry (**8**) in the eclipse of 1952 was due entirely to the highly controlled conditions of their observations. On the other hand, Brück and Jackson in their attempt (**5**) to secure an interference spectrum of the chromospheric lines during the eclipse of 1952 February 25 did not succeed in photographing fringes, since the line width, to which from their observations they were able to assign a minimum value of $1{\cdot}2\,\mathrm{cm}^{-1}$ (0·24 A at 4471), exceeded the range of the etalon.

Now the stronger chromospheric lines, and the lines in solar prominences, can be observed outside of eclipse under favourable conditions by setting the slit of the spectrograph across or tangentially to the solar limb so that it intersects the chromosphere and the overlying prominences. The possibility of developing and testing an interferometric technique in the more tranquil atmosphere prevailing outside of eclipse is clearly worth exploring. This fact is emphasized by the success of Harrison's recently invented echelle grating in obtaining high order interference spectra of prominences outside of eclipse (**13**). The fact that the chromospheric emission is confined to a narrow layer of less than 10″ of arc immediately bordering on the solar limb naturally makes the problem of chromospheric interferometry observationally more difficult, since quite small excursions of the Sun's limb, due to scintillation or guiding errors, and light scattered atmospherically or instrumentally from the photosphere, frequently produce an intolerably heavy scatter spectrum.

In the summer of 1955, the new Oxford 35 m solar telescope (**16**) had been completed, but awaited the installation of its large spectrograph, the place of which was occupied by the Hilger medium glass prism spectrograph which had been used with this telescope to obtain material for Bishop's study of the latitude variation of D_3 (**2**). The dispersion of this instrument is about 40 A/mm at 5876 A. This arrangement provided the writer with an opportunity to attempt to develop a technique for photographing the interference spectrum of the chromosphere outside of eclipse and for analysing the fringe systems in order to obtain from them the line profiles as a function of height, and the chromospheric intensity gradient.

2. *Photography of the chromospheric interference spectrum*

2.1. *General arrangement.*—The writer has discussed elsewhere the factors determining the best arrangement of an etalon in conjunction with a spectrograph for solar studies (**20**). When absolute wave-lengths are not required, and when the image-forming properties of the spectroscope are limited only by slit width and plate grain, as in the Hilger instrument, the arrangement of the etalon, in a

collimated beam before the slit, and that in which it follows the formation of the spectrum, are equivalent. The choice of the former arrangement was necessitated by the strongly inclined focal plane of the Hilger Spectrograph.

The general arrangement of the system is shown in Fig. 1. The solar image, 32 cm in diameter, was formed on a screen A containing a rectangular slot, which was re-imaged on the slit of the spectrograph by means of the field lens, collimator and ring-lens system BCD. The slot was so related to a circle ruled on the screen, of the same diameter as the solar image, that when the solar image was guided on the circle the slit was tangential to the re-imaged solar limb, with the base of the slit at the point of contact. The slit was about 2 cm in height. Under these conditions, the full height of the slit corresponds to an elevation of 8″ above the solar limb. The guiding was controlled during exposures (of one to two minutes' duration) by varying the orientation of a plane parallel guiding plate F.

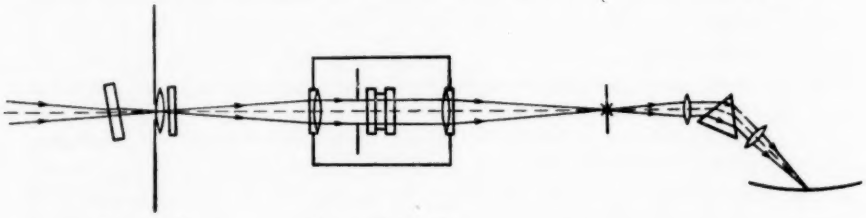

FIG. 1.—*Experimental arrangement for chromospheric interferometry.*

The etalon E was placed in the collimated beam. The Hilger plates, 2 cm in diameter, had a wedge angle of 15′, and were so oriented that the two principal first order ghosts produced images of the slot in the focal plane of the slit, to either side of the principal image, so that no scattered light from these ghosts could enter the system. The etalon was tilted a few degrees about a horizontal axis, so that the centre of the fringe system fell vertically below the slit. In this way, several chromospheric fringes could be formed along the length of the slit.

2.2. *Some considerations of experimental designs.*—The success of this kind of work depends greatly on the right choice of slit width, etalon spacer and reflectivity, and of the focal lengths of the field lens, collimator, and ring-lens system.

2.2.1. *Slit width.*—If there were no scattered light from the solar limb, it would be possible to use a wide slit, since the only effect of so doing, in the case of an isolated emission line, would be to admit a longer arc of each fringe, without altering its intensity. In fact, however, the emission fringes will be accompanied by a continuous photospheric scatter spectrum. It is obvious that the intensity of a continuous spectrum is directly proportional to slit width. On this general ground one would use as narrow a slit as possible, the useful limit being set at 0·03 mm by plate grain and light loss by slit diffraction. In fact, the scatter spectrum is not continuous, but takes the form of a channelled spectrum. However, for all but the very narrowest slit widths, the channels overlap and obey the same intensity law as a continuous spectrum, and even when they do not the use of a narrow slit will, as Shane has shown (**17**), reduce scatter from adjacent orders. We conclude, therefore, that a very narrow slit is essential.

2.2.2 *Etalon range.*—It is known that the strong chromospheric lines are greatly broadened. Hα extends over more than 2 A, D_3 over more than 1 A. The range of a Fabry–Perot etalon is given by

$$\mu = \lambda^2/2t \qquad (1)$$

where λ is the wave-length, t the spacer length. We can therefore only use spacers of less than 1 mm for Hα and less than about 2 mm for D_3. There is one significant qualification on this limit. If the slit width is sufficiently small for adjacent parabolic channels to be separated, it remains possible to resolve adjacent orders without overlap. An interesting example of this is illustrated in Plate 2(*c*) in which 3 orders of Hβ are clearly distinguished by their relation to the channel system, although they just exceed the etalon's range.

2.2.3. *Resolving power.*—The resolving power of an etalon of reflectivity r, in order n is given by

$$\lambda/\delta\lambda = [2{\cdot}98r^{1/2}/(1-r)]n. \qquad (2)$$

Having fixed t by considerations of range, we can increase the resolving power only by increasing r. However, since plate irregularities and defective parallelism may be expected to broaden the fringes to 1/30th of an order, the maximum resolution we can expect under working conditions with reflectivities exceeding 0·92 is about $30n$, where n is the order of interference, that is to say 100 000 at 6000 A for a 1 mm spacer, a value that will not be increased by increasing the reflectivity.

2.2.4. *Dispersion.*—In order that this resolving power of 10^5 may not be lost by plate granularity, the dispersion should be great enough for the resolving limit, 0·06 A at 6000 A, to exceed the dimensions of plate grain (say 0·03 mm), a condition that is well satisfied by a dispersion of 1 A/mm. Since the dispersion of the etalon is given by

$$D = f_d/\lambda a \text{ mm/A}, \qquad (3)$$

where f_d is the focal length of the ring lens and a the tilt of the etalon in radians, we can obtain the desired dispersion by various combinations of a and f_d.

In order to preserve the solar image size on the one hand, and on the other to preserve its intensity, the focal lengths of C and hence the field lens B, should be more or less equal to that of D. But the focal length of the field lens determines the size of the image of the solar telescope objective, which is formed on the etalon, and which must be kept sufficiently small to ensure that there is no loss of beams by multiple reflection. A 50 cm field lens already forms an image 0·7 cm in diameter on the etalon. Accepting this indirect upper limit to the focal length of D, we obtain the required dispersion for tilts not exceeding 5°. In this way the optical constants of the system are completely determined.

2.3. *Observations.*—To satisfy the preceding requirements, the spectrograph slit was reduced in width to 0·02 mm, which, however, on account of the tilt of the focal plane, corresponds to a slit image width of 0·04 mm. Etalon spacers of invar steel, 1 mm and 0·5 mm in length, were employed. Through the kindness of Dr Kuhn, silver coatings were deposited shortly before use, with mean measured reflectivities and tranmissions of 95·5 and 2·5 per cent respectively at 5500 A, giving a theoretical resolving power, for the 1 mm spacer, of 260 000. On each plate of the chromosphere, control fringes were photographed using the 6438 A line from a Cd discharge. The actual resolving power deduced from microphotometric measurements of the profiles of the Cd fringes, was 90 000, in good

agreement with the indications of the previous section. The lenses C and D were visual achromats of 45·7 cm focal length. The field lens B was a spectacle lens of 50 cm focal length. A stop, only slightly larger than the image of the objective, was placed immediately in front of the etalon, to eliminate scattered light and to ensure that the Cadmium lamp, when interposed in the space between B and C, illuminated the same area of the etalon as the Sun. The Cadmium lamp was also used to adjust the etalon for parallelism *in situ* and to orientate the etalon with respect to the slit.

A plate normally contained five exposures. Two of these were of the chromosphere. The third was an exposure made through a rhodium step wedge calibrated previously in the D region by Bray (**3**), using the solar centre as source. A fourth exposure was made without the wedge, as a test for uniformity of illumination along the slit, again using the solar centre. The interferometer was left in position for these exposures. All of these exposures were made with the narrow slit. The final exposure, superimposed on the fourth, and with a wide slit, was the Cd lamp exposure already referred to. In addition to serving as an adjustment check, it provided a system of sharp fringes from which the centre of the chromospheric fringe system could be determined. Plate 3(*a*) shows a greatly enlarged portion of this fringe system, superimposed on the interference spectrum of the solar centre. Exposure times were equalized by means of neutral filters at A.

During the summer of 1955 a successful series of interference photographs was taken with a separator of 1 mm (**23**). These showed fringe systems of Hα, Hβ, and of the H and K lines. The most perfect fringe system however was that shown by the D_3 line of neutral helium, as was to be expected in view of the ratio of the line width to the etalon range. Plate 2(*a*) and (*b*) show enlargements from this fringe system. It has, superimposed upon it, a strong photospheric interference spectrum of scattered light. On account of the great intrinsic width of the line, the fringes are extended in the direction of the etalon's dispersion, while being narrowly confined perpendicularly to this direction on account of the very narrow slit. Hence they present (in negative prints) the appearance of black stitches. Plate 2(*b*) shows a still greater enlargement, in which the channelled spectrum and the plate grain appear.

A careful inspection of the Hα fringes made it clear that one was observing slightly overlapping orders of a heavily self-reversed line. To confirm this deduction, a further series of plates was obtained in the spring of this year, using a separator of 0·5 mm and Kodak II N infra-red plates, in place of the Ilford R.40 plates used in the previous summer, since the sensitivity of the latter plate falls off rapidly at Hα. Plate 3(*b*) shows the self-reversed Hα line now completely free from overlapping of orders. The reduction in the scattered light is due largely to the realuminising of the telescope mirrors during the intervening winter. The sensitivity of the II N emulsion extends far into the infra-red, so that the spectrum of the solar centre shows the atmospheric A band near 7600 A. With the 0·5 mm spacer and the increased wave-length, the range of the etalon is 5·8 A, so that the channels are still well resolved and reveal the structure of the band in an unexpected way (Plate 3(*c*)).

3. *Photometric analysis of the interference fringe system.*—We shall now proceed to consider how to interpret quantitatively the chromospheric fringe systems just described. It is evident that the intensity distribution along any fringe in the direction of etalon dispersion is closely related to the profile of the line that

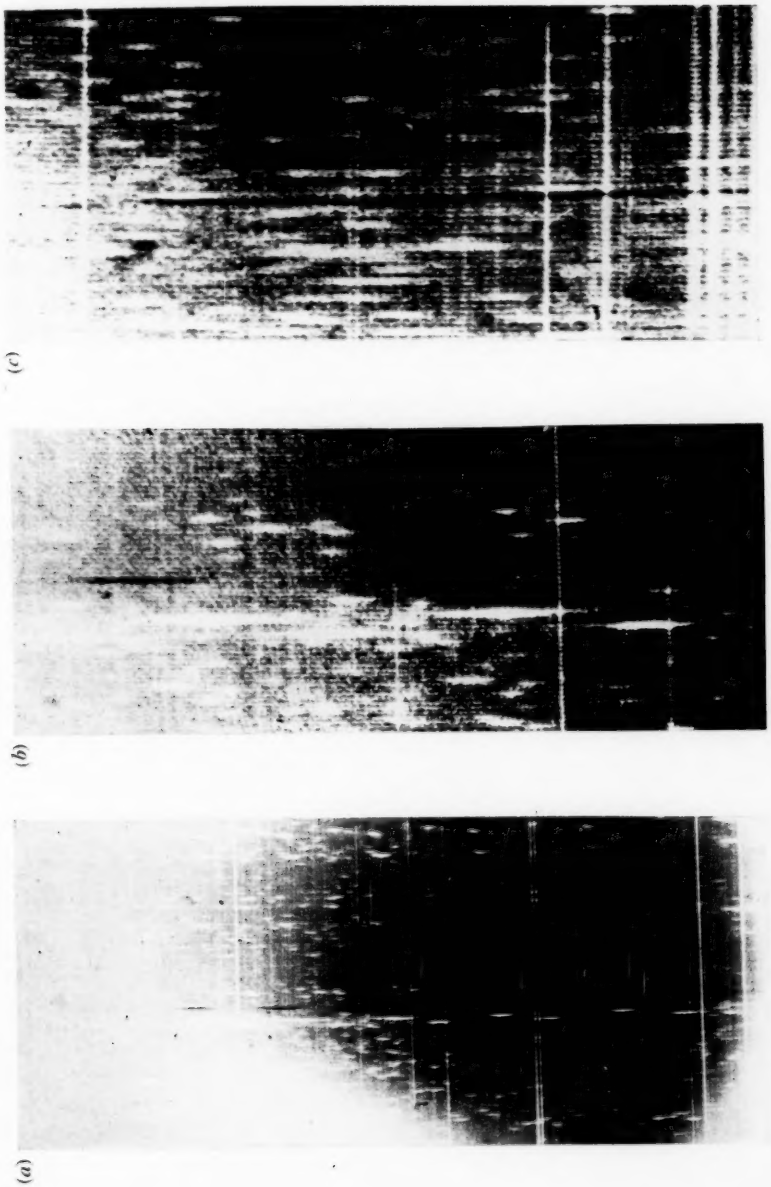

(c)

(b)

(a)

(a) *Chromospheric fringe system for the* D_3 *line.*
(b) *The same enlarged, showing the channelled spectrum.*
(c) *Nearly overlapping fringes of* Hβ.
(*Negative prints.*)

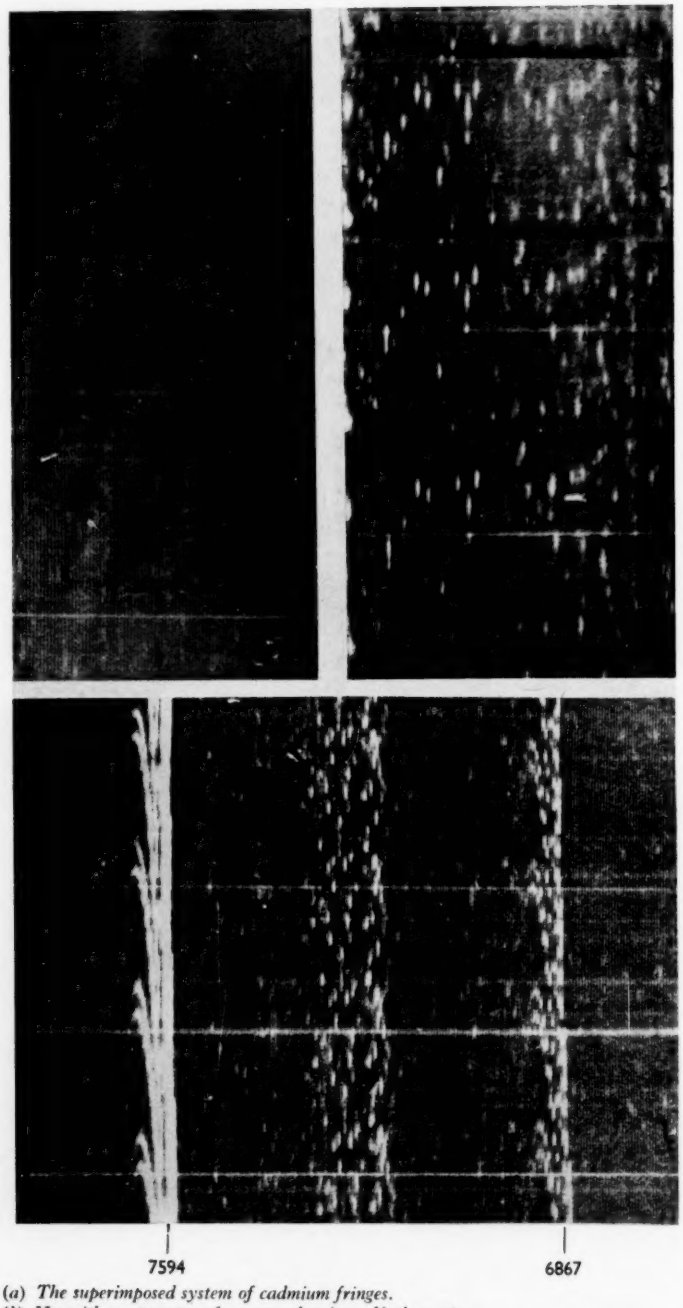

(*a*) *The superimposed system of cadmium fringes.*
(*b*) Hα *with a separator of* 0·5 *mm showing self-absorption.*
(*c*) *Bands of atmospheric oxygen* (6870 *and* 7600A) *in the interferometric photospheric spectrum.*
(*Negative prints.*)

P. J. Treanor, Chromospheric interferometry.

produces it, and that the falling off in overall intensity from fringe to fringe is closely related to the chromospheric intensity gradient. However, since the Sun and the fringe system are imaged in the same plane on the slit, different points on a single fringe correspond not merely to different wave-lengths within the line, but also to different heights in the chromosphere. What is strictly true however is that if we denote the position of any point in the fringe system by x, where x is measured from the edge of the spectrum which is coincident with the Sun's limb, then to each x will correspond an intensity I_x, of which the plate blackening is a measure, which refers to the intensity of the chromosphere at a definite height h_x and at a definite wave-length λ_x. The problem of interpreting the fringe system, therefore, reduces itself to two stages. First, we must determine I, h, and λ for a series of closely adjacent values of x covering the whole fringe system. This part of the problem alone involves the experimental technique. The second part of the interpretation is to use the purely solar data, I, h and λ, so obtained, to construct the true profile at any given height, and to measure the intensity gradients. We shall consider these stages in turn.

3.1. *Determination of height.*—Provided the origin of x measurement is truly the point of contact of the tangential slit with the limb of the Sun, a point at distance x along the slit corresponds to a height h above the limb, such that

$$x^2 = 2hR \tag{4}$$

where R is the radius of the solar image. h may therefore be determined at once. It must however be remembered that the height h is the height down to which the line of sight from the observer descends into the solar chromosphere, so that the light from x is produced by the integrated contributions of all heights above h.

3.2. *Determination of wave-length.*—The problem of determining wave-lengths from one side only of a Fabry–Perot ring system is treated in detail by Tolansky (**19**). The following simple treatment is quite adequate for the present case where only a wave-length scale is required.

The dispersion formula (3) may be written in the form

$$\frac{dr}{d\lambda} = f^2/\lambda r \tag{5}$$

where f is the focal length of the collimator and r the radius of the fringe.

Integrating (5) we obtain

$$\lambda = k_1 r^2 + k_2. \tag{6}$$

To determine the wave-length corresponding to a point x we must determine r for the point x, and evaluate k_1 and k_2. Since the centre is not on the plate, r cannot be measured directly. The position of the centre may however be determined approximately. If, choosing the nth fringe as origin, we measure the coordinates R_{n+1}, R_{n+2} of the fringes $n+1$, $n+2$, it may easily be shown from the geometry of the fringe system that the radius of the nth fringe is given by

$$r_n = \frac{2R_{n+1}^2 - R_{n+2}^2}{R_{n+2} - 2R_{n+1}}. \tag{7}$$

In this way the centre may be determined in relation to the origin of x (preferably by measurements on a sharp fringe system such as that provided by the Cd lines), and the values of r computed for each value of x. Now consider two wave-lengths λ_1 and $\lambda_1 + \mu$, where μ is the wave-length range of the etalon. Denoting

the radius of a fringe of the former wave-length by r_1, and the next fringe of the same wave-length by r_2, we have, by (6) and the definition of range,

$$\lambda_1 = k_1 r_1^2 + k_2$$

$$\lambda_1 + \mu = k_1 r_2^2 + k_2$$

whence

$$k_1 = \mu/(r_2^2 - r_1^2) = \mu/\overline{(r_{n+1}^2 - r_n^2)}. \tag{8}$$

Since the difference of square of successive radii is, for a given wave-length, a constant of the system, it is preferable to use a suitably determined mean value from several fringes to compute k_1. This is the mean value indicated in the denominator of the last term in equation (8). To determine k_2 we need only identify and determine the radius r_0 of a fringe of known wave-length λ_0 (e.g. the centre of the D_3 line), yielding

$$k_2 = \lambda_0 - k_1 r_0^2. \tag{9}$$

Hence, finally, in any fringe

$$(\lambda - \lambda_0) = \mu(r^2 - r_0^2)/\overline{(r_{n+1}^2 - r_n^2)}. \tag{10}$$

3.3. *Determination of the chromospheric intensity.*—Consider the microphotometer tracings obtained by running a very short and narrow microphotometer slit across the fringe system at each value of x for which we require a determination of I_x, the chromospheric intensity at x. The appearance of this tracing will resemble Fig. 2, which is reproduced from an actual record. The tracing shows the density variations in the channelled spectrum of the scattered light, together with sections of the absorption line profiles, as in Shane's method (**17**), of which this is in fact an application to an emission line. The section of the D_3 fringe traversed in each run appears as a peak superimposed on the scatter spectrum. When this density curve is converted to an intensity curve, by means of the wedge calibration, the area under the section of the D_3 fringe, discounting the scattered light contribution, is a measure of the chromospheric intensity. It would be very laborious to have to reduce each trace in this way. Bishop has shown (**2**) however, from high magnification tracings from direct spectra of the D_3 line taken with the same spectroscope and measured with the same slit as that here employed, that the area required and hence the intensity of the chromosphere, bears a linear relation to the intensity difference between the peak and the level of scattered light. This result is not surprising, since it reflects the fact that the Moll microphotometer with a narrow slit (**15**) does not appreciably distort the profile of the D_3 peak, the form of which is constant, since it is determined almost wholely by spectroscopic slit width and plate grain.

3.3.1. *Corrections.*—The simple method so described is sufficient when the scatter spectrum is free from absorption lines in the region of the chromospheric line profile. If these are present, the profile can be determined from regions of the scattered light spectrum where the fringe system of the chromospheric line is absent. After determining the wave-length of the chromospheric section traversed in any run, one would then know what percentage of the scattered light adjacent to the chromospheric fringe, and corresponding to the continuous background, should be subtracted from the peak intensity to give the chromospheric intensity.

If there is any variation in instrumental transmission intensity along the spectroscope slit, this must be determined, and an appropriate correction to the intensity determined for each value of x.

The intensity so determined is of course proportional to the flux received from the chromosphere over a short wave-length interval, determined here by the length of the microphotometer slit, and the interferometric dispersion. This latter quantity varies according to equation (5), and it would appear at first sight as though one should apply a correction for this, such as must be applied to allow for the variation of dispersion in the microphotometry of prismatic spectra.

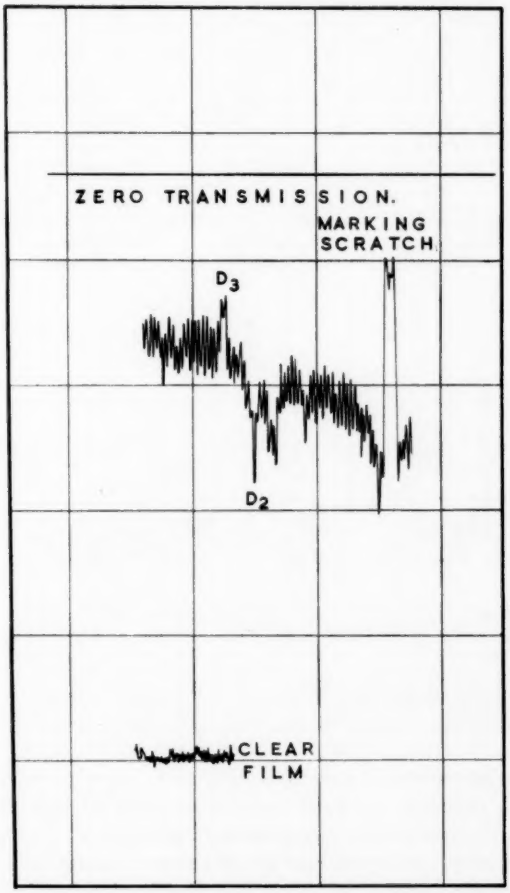

FIG. 2.—*Typical microphotometer trace across a chromospheric fringe.*

Further consideration of this analogy indicates that this is not the case. For it is a characteristic of the Fabry–Perot instrumental pattern, in contrast to the slit pattern of a spectroscope, that its width remains always a constant fraction of its range: consequently its half width in mm on the plate decreases with dispersion, from fringe to fringe, the monochromatic peak intensity remaining constant. The just analogy should therefore be a prism spectroscope whose slit width is made to vary directly with the dispersion. The writer has analysed this question quantitatively elsewhere (**22**).

the radius of a fringe of the former wave-length by r_1, and the next fringe of the same wave-length by r_2, we have, by (6) and the definition of range,

$$\lambda_1 = k_1 r_1^2 + k_2$$

$$\lambda_1 + \mu = k_1 r_2^2 + k_2$$

whence

$$k_1 = \mu/(r_2^2 - r_1^2) = \mu/\overline{(r_{n+1}^2 - r_n^2)}. \tag{8}$$

Since the difference of square of successive radii is, for a given wave-length, a constant of the system, it is preferable to use a suitably determined mean value from several fringes to compute k_1. This is the mean value indicated in the denominator of the last term in equation (8). To determine k_2 we need only identify and determine the radius r_0 of a fringe of known wave-length λ_0 (e.g. the centre of the D_3 line), yielding

$$k_2 = \lambda_0 - k_1 r_0^2. \tag{9}$$

Hence, finally, in any fringe

$$(\lambda - \lambda_0) = \mu(r^2 - r_0^2)/\overline{(r_{n+1}^2 - r_n^2)}. \tag{10}$$

3.3. *Determination of the chromospheric intensity.*—Consider the microphotometer tracings obtained by running a very short and narrow microphotometer slit across the fringe system at each value of x for which we require a determination of I_x, the chromospheric intensity at x. The appearance of this tracing will resemble Fig. 2, which is reproduced from an actual record. The tracing shows the density variations in the channelled spectrum of the scattered light, together with sections of the absorption line profiles, as in Shane's method (**17**), of which this is in fact an application to an emission line. The section of the D_3 fringe traversed in each run appears as a peak superimposed on the scatter spectrum. When this density curve is converted to an intensity curve, by means of the wedge calibration, the area under the section of the D_3 fringe, discounting the scattered light contribution, is a measure of the chromospheric intensity. It would be very laborious to have to reduce each trace in this way. Bishop has shown (**2**) however, from high magnification tracings from direct spectra of the D_3 line taken with the same spectroscope and measured with the same slit as that here employed, that the area required and hence the intensity of the chromosphere, bears a linear relation to the intensity difference between the peak and the level of scattered light. This result is not surprising, since it reflects the fact that the Moll microphotometer with a narrow slit (**15**) does not appreciably distort the profile of the D_3 peak, the form of which is constant, since it is determined almost wholely by spectroscopic slit width and plate grain.

3.3.1. *Corrections.*—The simple method so described is sufficient when the scatter spectrum is free from absorption lines in the region of the chromospheric line profile. If these are present, the profile can be determined from regions of the scattered light spectrum where the fringe system of the chromospheric line is absent. After determining the wave-length of the chromospheric section traversed in any run, one would then know what percentage of the scattered light adjacent to the chromospheric fringe, and corresponding to the continuous background, should be subtracted from the peak intensity to give the chromospheric intensity.

If there is any variation in instrumental transmission intensity along the spectroscope slit, this must be determined, and an appropriate correction to the intensity determined for each value of x.

The intensity so determined is of course proportional to the flux received from the chromosphere over a short wave-length interval, determined here by the length of the microphotometer slit, and the interferometric dispersion. This latter quantity varies according to equation (5), and it would appear at first sight as though one should apply a correction for this, such as must be applied to allow for the variation of dispersion in the microphotometry of prismatic spectra.

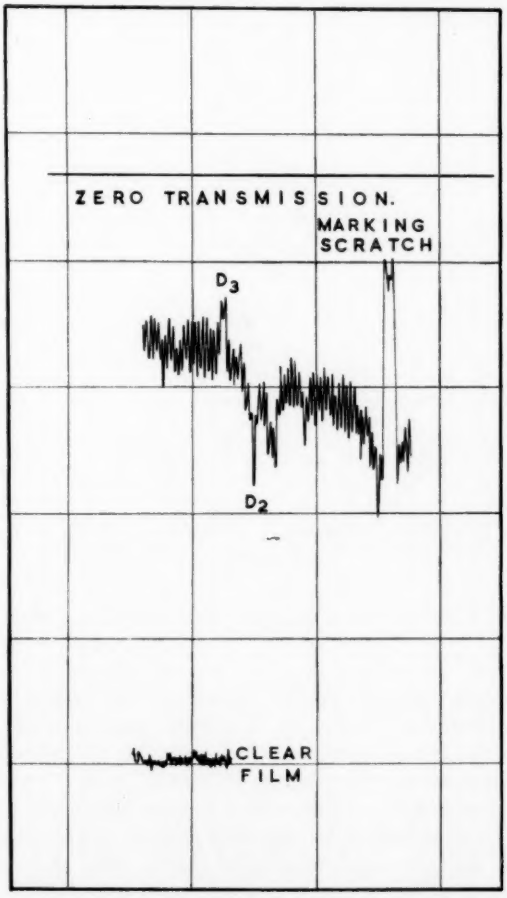

FIG. 2.—*Typical microphotometer trace across a chromospheric fringe.*

Further consideration of this analogy indicates that this is not the case. For it is a characteristic of the Fabry–Perot instrumental pattern, in contrast to the slit pattern of a spectroscope, that its width remains always a constant fraction of its range: consequently its half width in mm on the plate decreases with dispersion, from fringe to fringe, the monochromatic peak intensity remaining constant. The just analogy should therefore be a prism spectroscope whose slit width is made to vary directly with the dispersion. The writer has analysed this question quantitatively elsewhere (**22**).

3.4. *Line profiles.*—By the methods of Sections 3.1–3.3 we may extract all the solar information that the chromospheric fringe system will yield, in the form of tables of associated values of h, I and λ for successive values of x. From these values, we may obtain true line profiles at required heights, by a procedure suggested by Plaskett, which we shall call the method of monochromatic intensity gradients.

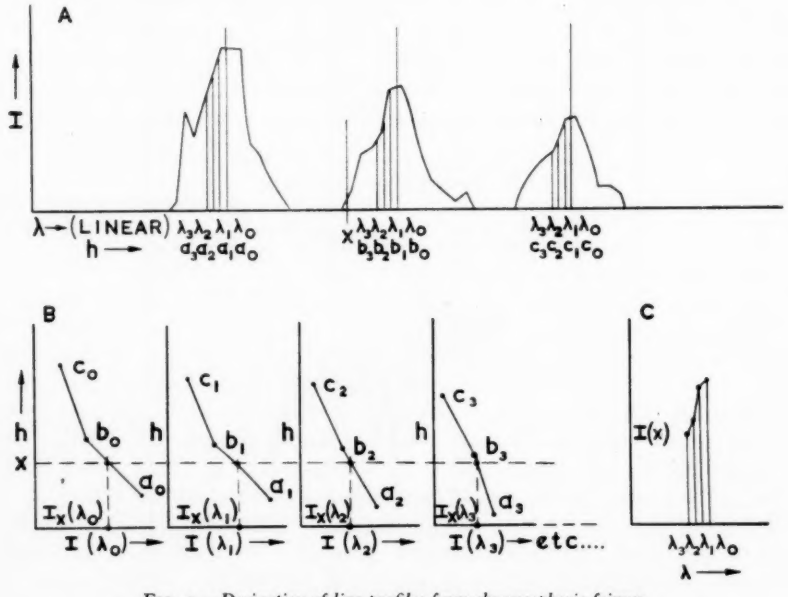

FIG. 3.—*Derivation of line profiles from chromospheric fringes.*
(A) *Fringe profiles*; (B) *Monochromatic intensity curves*; (C) *Resultant profile.*

To carry out this method, we first plot from our tabular values the *fringe* profiles, with ordinates I, abscissa λ. Fig. 3(A) presents such a plot obtained from one of our D_3 fringe systems. Now mark off from the line centre λ_0 a series of equidistant ordinates corresponding to λ_1, λ_2 etc. Next read from the fringe profiles the intensity I at λ_0 on each fringe available, and obtain the corresponding heights h_a, h_b, h_c etc. by interpolation from the table. For each λ in turn, we can now plot height as a function of intensity. This stage is shown schematically for 4 wave-lengths in Fig. 3(B), and these curves give essentially monochromatic intensity variation with height in the chromosphere. From this array of curves, we can now read off the monochromatic intensity at any desired height, for the series of wave-lengths λ_0, λ_1, λ_2 and in this way construct the profile at any height represented on all the graphs.

The profiles at different heights are therefore obtained independently from each plate. In combining them, profiles at some common height must be normalized, since the absolute intensity will vary from plate to plate owing to the varying conditions of exposure.

3.5. *Chromospheric intensity gradients.*—Having obtained the profiles at a series of heights from individual plates, it is clearly easy to determine the integrated

chromospheric gradient for the line as a whole by plotting the area of successive profiles from the same plate as a function of height. The mean gradient adopted must of course be the mean of the gradients so determined from individual plates.

TABLE I

Computed and observed profiles of D_3

λ	C_1	C_2	C_3	C	O	O–C	σ
5875·140	14·1	00·0	14·1	16·1	17·6	+1·5	±1·5
·190	20·9	00·1	21·0	23·2	26·8	+3·6	2·0
·240	29·5	00·1	29·6	31·8	36·5	+4·7	1·8
·290	40·0	00·2	40·2	42·0	42·4	+0·4	1·3
·340	51·9	00·4	52·3	53·6	53·5	−0·1	2·3
·390	64·4	00·7	65·1	65·3	65·0	−0·3	1·4
·440	76·6	01·1	77·7	76·9	75·1	−1·8	1·4
·490	87·3	01·8	89·1	87·1	84·5	−2·6	1·3
·540	95·2	02·6	97·8	94·5	92·2	−2·3	1·9
·590	99·7	03·7	103·4	98·3	97·8	−0·5	1·6
·640	99·7	05·0	104·7	100·0	100·0	0·0	0·3
·690	95·2	06·5	101·7	97·7	97·4	−0·3	2·3
·740	87·3	08·1	95·4	92·2	93·6	+1·4	2·7
·790	76·6	09·5	86·1	84·3	86·1	+1·8	1·4
·840	64·4	10·9	75·3	74·5	76·2	+1·7	1·6
·890	51·9	11·9	63·8	64·0	61·8	−2·2	2·2
·940	40·0	12·5	52·5	53·3	50·6	−2·7	2·2
·990	29·5	12·5	42·0	43·3	43·4	+0·1	2·5
5876·040	20·9	11·9	32·8	34·4	34·4	0·0	2·9
·090	14·1	10·9	25·0	26·5	26·2	−0·3	2·0
·140	09·1	09·5	18·6	20·3	20·2	−0·1	3·0

Successive columns denote: (1) λ, the wave-length; (2) C_1, the computed Doppler profile of the strong components; (3) C_2, the corresponding profile of the weak components; (4) $C_3 = C_1 + C_2$, the computed blend; (5) C, the computed blend, subjected to photometric distortion; (6) O, the observed blended profile; (7) O–C; and (8) the standard deviation σ of the observed values.

4. *The profiles of the D_3 line*

4.1. Seven notably successful plates showing the fringe system of the D_3 line due to neutral helium at 5875·6 A were selected for profile determination. Apart from its astrophysical interest, this line is particularly suitable as a test of the method, since it is not observed in absorption in the photosphere, which is disturbed only by water vapour lines in the wings (beyond the wave-length range measured) at 5876·162 and 5876·452 A, and, within the line, only by much weaker lines of water vapour the effect of which we may fairly safely neglect.

The reduction was carried out by the methods of Section 3, and requires only a little further comment. The choice of a tangential slit in making the exposures was taken only because a suitable device for accurate guiding, which would have permitted the use of a slit slightly inclined to the tangent position, and encroaching a little on the photosphere, was not available at the time. With the arrangement used, the limb does not appear on the plate, and we can do no more than to assume

that its mean position coincides with the base of the slit, which is what we endeavoured to achieve by guiding. Consequently, our individual absolute height determinations are more uncertain than they need have been, but the relative heights and the mean heights from several plates can hardly be seriously wrong.

The scheme for wave-length determination worked fairly well, except for the lowest of the heights measured, 1500 km, where an apparent line shift of 0·08 A appeared. It is believed that this effect is not real, but is due to the choice of the centre of the D_3 line to determine k_2. Krat (**11**) has found that below 1500 km the centre of the D_3 line is shifted by asymmetry towards the red. The use of fringes in this lower region as a standard, though not for profile measurement, accounts for our blue shift. Its effect on the profile determination is practically negligible.

The scattered light was rather high, mainly due to the poor condition of the final Coudé mirror. This factor increases the random error, as can be seen from the very ragged profiles of Fig. 3(A), and also limited the range of h over which the microphotometer (a Moll thermocouple instrument) could usefully record. For the same reason, it was necessary to use a slit height corresponding to a wave-length interval of 0·18 A. A correction for this smearing is therefore required in interpreting the profile, but owing to the much greater width of the helium line, the effect is not too serious. The tracings were made over two, three or four fringes, at intervals of 0·126 mm (1 division on the head of the plate-raising screw).

Profiles were determined for heights of 1500, 2250, 3000, 3750 and 4250 km above the solar limb, and are displayed in Fig. 4. Those for the extreme heights are means from only 2 plates; intermediate heights depend on 4 or 5 plates each. The peak intensities at the various heights have been brought into arbitrary agreement in the figure. Since the profiles show no systematic variation with height, they can be combined to derive a mean profile, corresponding to a mean height of about 3000 km. The mean points, together with their standard deviations, are shown in Fig. 5. In deriving this mean the extreme profiles have been given half weight.

4.2. *Interpretation of the profiles.*—The D_3 line of helium originates from the transition 2^3P–3^3D. The three components of the main triplet structure of the line have recently been completely resolved by Brochard, Chabbel, Chantral and Jacquinot (**4**) using a discharge cooled by liquid hydrogen. The measured intensities agree very well with the theoretical values. The two stronger components are separated by only 0·04 A, and these together with three much fainter components (the line is really sextuplet) may be lumped together, to form with the third line of the triplet what is equivalent to a doublet with components at 5875·61 and 5875·96 with intensity ratio 7·96 : 1. In our analysis we have used the now conventional value of 8 : 1.

The fact that the profile of D_3 does not vary with height in the chromosphere within the range of heights measured makes it likely that self-absorption in the line may be neglected. From this it follows that the intensity ratio of 8 : 1 may be assumed for the fine structure of the line under chromospheric conditions. It also follows that the broadening of the line is not a curve of growth effect, but represents faithfully the distribution of intensity with wave-length prevailing in the atomic population. The most obvious source of the broad distribution is a combination of thermal and turbulent velocities, and this explanation is rendered

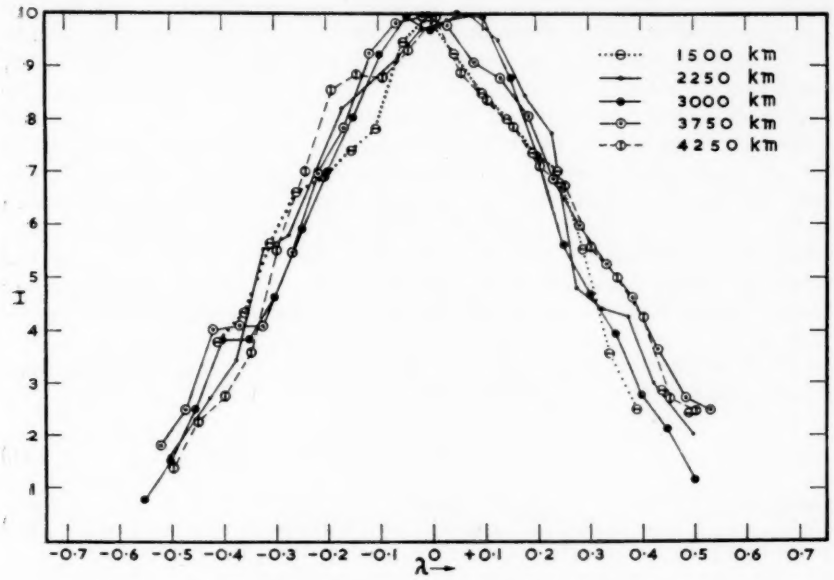

FIG. 4.—*Observed profiles of the* D_3 *line at various heights.*

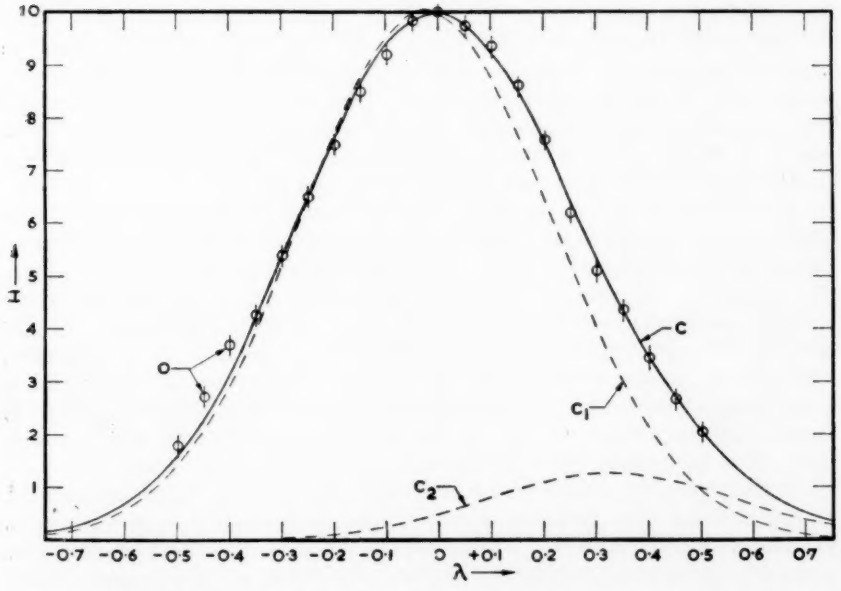

FIG. 5.—*Observed mean profile, compared with a computed Doppler profile. The symbols* C_1, C_2, C *and* O *have the meanings assigned to them in Table I.*

that its mean position coincides with the base of the slit, which is what we endeavoured to achieve by guiding. Consequently, our individual absolute height determinations are more uncertain than they need have been, but the relative heights and the mean heights from several plates can hardly be seriously wrong.

The scheme for wave-length determination worked fairly well, except for the lowest of the heights measured, 1500 km, where an apparent line shift of 0·08 A appeared. It is believed that this effect is not real, but is due to the choice of the centre of the D_3 line to determine k_2. Krat (**11**) has found that below 1500 km the centre of the D_3 line is shifted by asymmetry towards the red. The use of fringes in this lower region as a standard, though not for profile measurement, accounts for our blue shift. Its effect on the profile determination is practically negligible.

The scattered light was rather high, mainly due to the poor condition of the final Coudé mirror. This factor increases the random error, as can be seen from the very ragged profiles of Fig. 3(A), and also limited the range of h over which the microphotometer (a Moll thermocouple instrument) could usefully record. For the same reason, it was necessary to use a slit height corresponding to a wave-length interval of 0·18 A. A correction for this smearing is therefore required in interpreting the profile, but owing to the much greater width of the helium line, the effect is not too serious. The tracings were made over two, three or four fringes, at intervals of 0·126 mm (1 division on the head of the plate-raising screw).

Profiles were determined for heights of 1500, 2250, 3000, 3750 and 4250 km above the solar limb, and are displayed in Fig. 4. Those for the extreme heights are means from only 2 plates; intermediate heights depend on 4 or 5 plates each. The peak intensities at the various heights have been brought into arbitrary agreement in the figure. Since the profiles show no systematic variation with height, they can be combined to derive a mean profile, corresponding to a mean height of about 3000 km. The mean points, together with their standard deviations, are shown in Fig. 5. In deriving this mean the extreme profiles have been given half weight.

4.2. *Interpretation of the profiles.*—The D_3 line of helium originates from the transition 2^3P–3^3D. The three components of the main triplet structure of the line have recently been completely resolved by Brochard, Chabbel, Chantral and Jacquinot (**4**) using a discharge cooled by liquid hydrogen. The measured intensities agree very well with the theoretical values. The two stronger components are separated by only 0·04 A, and these together with three much fainter components (the line is really sextuplet) may be lumped together, to form with the third line of the triplet what is equivalent to a doublet with components at 5875·61 and 5875·96 with intensity ratio 7·96 : 1. In our analysis we have used the now conventional value of 8 : 1.

The fact that the profile of D_3 does not vary with height in the chromosphere within the range of heights measured makes it likely that self-absorption in the line may be neglected. From this it follows that the intensity ratio of 8 : 1 may be assumed for the fine structure of the line under chromospheric conditions. It also follows that the broadening of the line is not a curve of growth effect, but represents faithfully the distribution of intensity with wave-length prevailing in the atomic population. The most obvious source of the broad distribution is a combination of thermal and turbulent velocities, and this explanation is rendered

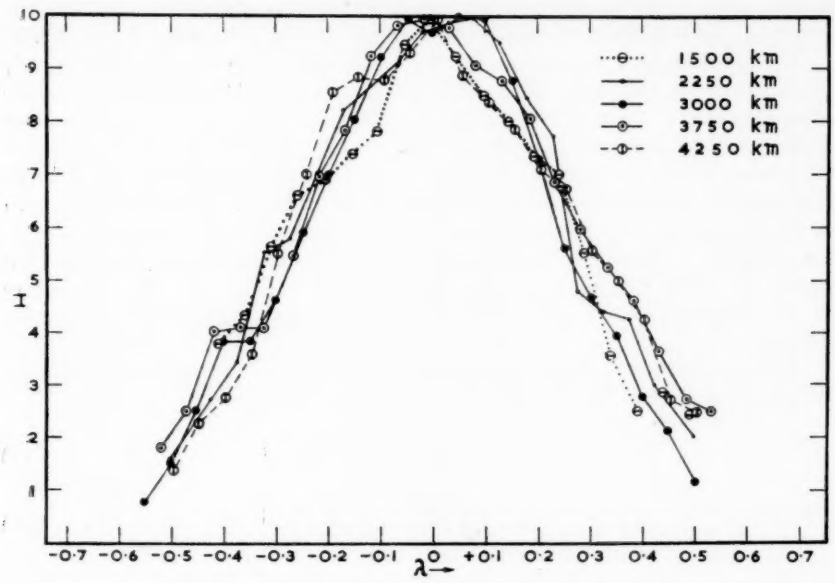

FIG. 4.—*Observed profiles of the* D_3 *line at various heights.*

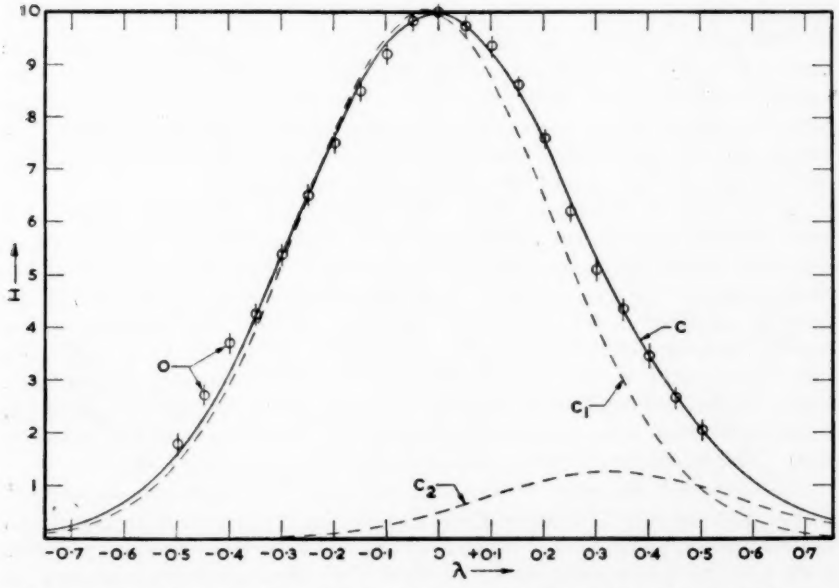

FIG. 5.—*Observed mean profile, compared with a computed Doppler profile. The symbols* C_1, C_2, C *and* O *have the meanings assigned to them in Table I.*

immediately plausible by the approximately Gaussian form of the determined profile, even before correction for microphotometric distortion and for fine structure, since neither of these effects will greatly alter the form of the profile.

Using these clues, we have sought for a Doppler profile of half-width slightly smaller than the half-width of the observed curve, which after smearing with the microphotometer slit pattern, and after the addition of a fine structure component of the same smeared form, and 1/8th of the intensity, distant 0·35 A, will reproduce the observed curve. For this purpose we have approximated the microphotometer pattern to a Gaussian form $I = I_0 \exp[-(\delta\lambda/0{\cdot}108)^2]$. The result is shown in Fig. 5, and Table I. A true profile of the form $I = I_0 \exp[-(\delta\lambda/0{\cdot}340)^2]$, after smearing and adding the fine structure component, reproduces the observed profile to within the limits of experimental error. Note that the asymmetry of the combined profile has moved the peak intensity towards the satellite by 0·025 A.

If the broadening of the line were entirely thermal, its profile for an assumed temperature of 4800 deg. would be given by

$$I = I_0 \exp[-(\delta\lambda/D\lambda)^2] \tag{11}$$

where

$$D\lambda = \frac{\lambda}{c}\sqrt{\frac{2RT}{\mu}} = 0{\cdot}0875 \text{ A}. \tag{12}$$

The distribution of turbulent velocities which in combination with this thermal distribution will reproduce the deduced profile is only slightly narrower than the profile itself, and corresponds to a turbulent velocity (at height $1/e$ in the distribution) of 16·7 km/sec.

The profile that we have determined ($D\lambda = 0{\cdot}34$) is slightly narrower than that of Peripelkin and Melnikov (**14**) who like us found Doppler profiles invariant with height but with $D\lambda = 0{\cdot}377$. This is the only result with which strict comparison may be made, since Unsöld's measures (**24**) yielding $D\lambda = 0{\cdot}316$ rested on rather slight and uncorrected observational material, and Krat's recent profiles (**10, 11**) ($D\lambda = 0{\cdot}26$), refer mainly to lower levels.

4.3. *A note on the D_3 gradient.*—The absence from the plate of the solar limb, besides creating some uncertainty in the determination of heights, left no means for determining the effect of seeing on the measured gradient of the chromosphere. In view of both these limitations, the determination of the intensity gradient was not pursued seriously. A pilot investigation of our profiles, however, yielded an intensity distribution of the form $I = I_0 \exp(-\beta h)$, with a mean value of $\beta = 0{\cdot}42 \times 10^{-8}\,\text{cm}^{-1} \pm 0{\cdot}06$. Using ordinary spectra taken a few months previously with the same telescope and spectrograph, Bishop (**2**) found an identical mean value for the D_3 gradient, before correction for scintillation. This correction, however, increased his value by 50 per cent.

In conclusion, the author wishes to acknowledge the help and encouragement he has received from Professor Plaskett, most particularly in connection with the deduction of the profiles. Thanks are also due to Dr Kuhn and his colleagues at the Clarendon laboratory for the excellent silver films and the measurement of their optical constants; to Dr Bray for the calibration data of the step wedge, and to Mr Bishop for providing me with much useful information from his own researches, partly unpublished, on the D_3 line. Finally the author acknowledges

his indebtedness to Balliol College for the Research Fellowship during the tenure of which this research has been carried out.

University Observatory,
Oxford:
1956 *November* 29.

References

(1) Adam, M. G., *M.N.*, **115**, 367, 1955; *Comm. Univ. Obs., Oxford*, No. 49.
(2) Bishop, R. O., *M.N.*, **116**, 593, 1956; *Comm. Univ. Obs., Oxford*, No. 60.
(3) Bray, R. J., *M.N.*, **114**, 540, 1954; *Comm. Univ. Obs., Oxford*, No. 45.
(4) Brochard, J., Chabbel, R., Chantrel, H. and Jacquinot, P., *Jn. Phys. et Rad.*, **13**, 433, 1952.
(5) Brück, H. A. and Jackson, D. A., *Proc. Roy. Soc.* A, **216**, 183, 1953.
(6) Fabry, C. and Perot, A., *Ap. J.*, **15**, 73 and 261, 1902.
(7) Hindmarsh, W. R., *M.N.*, **115**, 367, 1955; *Comm. Univ. Obs., Oxford*, No. 47.
(8) Jarrett, A. H. and von Klüber, H., *M.N.*, **115**, 343, 1955.
(9) Kinman, T. D., *M.N.*, **116**, 77, 1956; *Comm. Univ. Obs., Oxford*, No. 55.
(10) Krat, T. B., *Izv. Glav. Ast. Obs. Pulkova*, No. 152, XIX, 20, 1954.
(11) Krat, T. B., *Izv. Glav. Ast. Obs. Pulkova*, No. 153, XIX, 6, 1955.
(12) Kuhn, H., *Rep. Prog. in Phys.*, **14**, 80, 1951.
(13) McMath, R. R., *The Sun* (ed. Kuiper G. K.), p. 615, Chicago, 1953.
(14) Peripelkin, E. J. and Melkinov, O. A., *Obs. Bull. Pulkova*, No. 122, XIV, 5, 1935.
(15) Plaskett, H. H., *M.N.*, **95**, 60, 1934; *Comm. Univ. Obs., Oxford*, No. 4.
(16) Plaskett, H. H., *M.N.*, **115**, 543, 1955; *Comm. Univ. Obs., Oxford*, No. 52.
(17) Shane, C. D., *Lick. Obs. Bull.*, **16**, 76, 1932; **19**, 199, 1941.
(18) Thiessen, G., *Zs. f. Ap.*, **26**, 130, 1949.
(19) Tolansky, S., *High Resolution Spectroscopy*, p. 133, London, 1947.
(20) Treanor, P. J., *M.N.*, **109**, 37, 1949; *Comm. Univ. Obs., Oxford*, No. 28.
(21) Treanor, P. J., *Observatory*, **70**, 176, 1950.
22 Treanor, P. J., " Wavelength measurement and Intensity Determination by interferometric and other methods ", p. 68. Thesis, Oxford, 1950.
(23) Treanor, P. J., *Nature*, **176**, 1166, 1955.
(24) Unsöld, A., *Zs. f. Ap.*, **3**, 77, 1931.
(25) von Klüber, H., *M.N.*, **114**, 242, 1954.
(26) Wright, W. R. and Curtis, H. D., Sproul Obs. Bull. No. 11.

OSCILLATOR STRENGTHS FROM ARC SPECTRA OF DILUTED COPPER ALLOYS

C. W. Allen and A. S. Asaad

(Received 1956 December 11)

Summary

The method of determining absolute oscillator strengths from arc spectra of diluted copper alloys has been described. The scale has been averaged from various absolute measurements and calculations that are available. Absolute values are tabulated for certain lines in the spectra of Al, Si, Cr, Mn, Fe, Co, Ni, Cu, Ga, Ag, Sn, Pb, and Bi. A relation between oscillator strength and excitation potential has been found as in earlier work, but this is now shown to be due mainly to the weakness of those transitions for which the moving electron is equivalent in the lower level. Some empirical rules for estimating oscillator strengths in complex spectra are given.

---

1. *Introduction.*—Oscillator strengths are essential to the interpretation of astronomical spectrum line intensities. More values are required and those available are strongly in need of comparative check.

An independent measurement of the absolute oscillator strength (f-value) of a spectrum line involves the difficult technique of determining the number of atoms in the medium emitting or absorbing the spectrum. Relative measurements are much more straightforward. In the present work relative measurements only are made but these are standardized by any absolute measurements or calculations that are available. The method allows the comparison of one atom with another to give absolute f-values for a large number of atoms. The essential requirement for this purpose is a source of light containing several atoms in known abundance ratios. Relative measurements then lead to (*a*) absolute f-values of atoms for which no values were previously available, and (*b*) checks on absolute values previously observed or calculated for different atoms.

This procedure has been applied to the determination of absolute f-values of the neutral atoms Al, Si, Cr, Mn, Fe, Co, Ni, Cu, Ga, Ag, Sn, Pb and Bi. The source was a direct current arc between poles of copper alloys containing known and very small amounts ($<0{\cdot}05$ per cent) of the other elements. The poles were obtained from Johnson, Matthey and Co., London.

2. *Experimental procedure.*—The alloy arc spectra were obtained by means of a 10-foot Eagle-mounted concave grating spectrograph in the first order. The ruled grating area was $7{\cdot}5$ cm $\times$ $4{\cdot}0$ cm, the rulings 14438 lines to the inch, and the first order dispersion $5{\cdot}54$ A/mm. A rhodium on quartz step filter was placed at the sagittal focus a little way in front of the slit to provide photometric calibration. A lens close to the step filter focused the arc onto the grating and the arc length was such that the arc image came just within the grating ruled area. The slit width was $0{\cdot}06$ mm—about three times the theoretical resolving distance.

The data for the absorptions of the filter steps were provided by the makers (Hilger), and checked as a function of wave-length by means of a photo-cell. The absorption of the six steps was rather accurately neutral. Any differential absorption by the quartz plate was eliminated by passing both arc and colour correction spectra through it.

The spectrographic regions and the photographic emulsions employed were 3200–4600 A on Ilford Zenith plates and 3900–5400 A on Ilford Pan. H.P. 3 plates. D76 developer was used at 65 deg. F.

The arc was operated from a 240-volt d.c. generator, the arc current was 3 amps, the pole separation was 3 mm, the poles were always similar and the negative electrode on top. The copper alloy electrodes were $3\frac{1}{2}$ inches long (at start) and $\frac{1}{8}$ inch diameter. The alloy rods were available in two series, one labelled CA containing Sb, Bi, Cr, Ga, Pb, Ag, Sn, Al and the other labelled CB containing Co, Fe, Mn, Ni, Si. Each series was in nine concentration grades extending from grade 0 containing 0·05 per cent by weight of each alloy to grade 8 containing about 0·0001 per cent of each. The compositions were given by the makers (Johnson, Matthey and Co.). Grade 0 was determined by chemical analysis and the other grades calculated from the amount of dilution with pure copper.

Two colour standards were available. During the early part of the work use was made of a tungsten strip lamp operating at a brightness temperature that was measured by an optical pyrometer. This was satisfactory in the visible spectrum but for $\lambda < 3800$ A the faintness of the source and the absorption of the glass bulb produced errors. Later, when a heavy electric generator became available, use was made of the positive pole of a carbon arc. For this purpose German " Spektra-Kohlen " rods of $\frac{1}{4}$ inch diameter were inserted in an arc that held the positive rod horizontally and the negative at an angle of 120° to it. A high enough current (10 amps) was forced through the arc to bring the positive pole to the volatilization temperature of 3995 deg. K (**1**). The arc was focused onto a screen (at the spectrograph sagittal focus) which contained an aperture to select the positive pole.

3. *Measurement.*—Photometric measurements were made by means of a Hilger Recording Microphotometer. With very many narrow lines to be measured it was necessary to run the photometer rather faster than would allow full photometric resolution, but this did not affect the photometry since the same speed on similar lines was used in the various filter steps for obtaining the calibrations.

For each plate a calibration curve was prepared which enabled the microphotometer deflection for the centre of any line to be converted into intensity. The continuous background was also converted into intensity and subtracted. The curves for various plates were on arbitrary scales but one plate was taken as standard and the others converted to this standard by comparing the faint copper lines. Comparison showed that the standardized individual lines had a probable error of 15 per cent.

Alloy lines were all sharp enough for the observed width to be entirely instrumental and central intensities were used without correction. However the copper lines had a great variety of widths (because of autoionization) and for these the intensity was represented by the central intensity multiplied by the ratio of the observed to the instrumental width.

Curves giving a correction for sensitivity as a function of wave-length (colour correction) were prepared from the density measurements of the colour standard spectra. Independent calibration curves were prepared for this purpose using a continuous spectrum and step filter. The densities at various wave-lengths were converted into intensities by the calibration curve for the plate and then compared with the calculated intensity. For the calculation of carbon arc positive pole intensity the black-body formula was used with a colour temperature of 3950 deg. K (**1**). For tungsten strip lamp calculations the colour temperature was obtained from the optical pyrometer brightness temperature using the optical constants of tungsten (**2**). In the region 3900–5400 A the colour correction from the carbon arc and tungsten lamp agreed well and a mean was used. In the region 3200–4600 A there was disagreement for $\lambda < 3800$ A. However, throughout most of this region ($\lambda > 3400$ A) it has been possible to compare Fe line intensities in the arc with values expected from King's furnace absorption measurements (**3**). This comparison also leads to a colour correction which agrees well with the carbon arc but not with the tungsten lamp. The colour correction for the 3200–4600 A region has therefore been averaged from the carbon arc and from the Fe line intensities. Lines in the two regions are standardized to the same scale by means of the overlap 3900–4600 A.

4. *Conversion to ϖf-values.*—The measurements lead to a set of line intensities I on a uniform but arbitrary scale.

The emission intensity of a spectrum line from an upper level 2 to a lower level 1 is

$$I = \text{const. } N_2(-f_{21})/\lambda^3 = \text{const. } N_2(\varpi_1/\varpi_2)f_{12}/\lambda^3,$$

where N_2 is the number of atoms in the upper level, ϖ_2 and ϖ_1 are the upper and lower statistical weights, f_{21} and f_{12} the emission and absorption oscillator strengths, and λ the wave-length. We use ϖf ($= \varpi_1 f_{12} = -\varpi_2 f_{21}$) to describe our results since this is symmetric in the initial and final levels. Then

$$\varpi f = \text{const. } (\varpi_2/N_2)\lambda^3 I. \tag{1}$$

Boltzmann's equation relating N_2, the population of atoms in the 2 level, with N_0, the population in the ground term 0, may be written

$$(\varpi_2/N_2)/(\varpi_0/N_0) = \exp(E_2/kT) \tag{2}$$

in the usual notation. Hence

$$\varpi f = \text{const. } \lambda^3 I(\varpi_0/N_0)\exp(E_2/kT). \tag{3}$$

This equation converts the measurements I into values of ϖf on a scale that is common for all atoms concerned. For its application we need relative values of N_0 and also T.

The values of N_0 are in proportion to the concentration by mass of the element in the copper alloy divided by the atomic weight. If an appreciable fraction of the atoms is not in the ground term (at 4300 deg. K) we use the partition function in place of ϖ_0. The partition functions have been obtained from Claas' table (**4**) with a little extrapolation.

The excitation temperature T was obtained by a comparison of our $\lambda^3 I$ with the ϖf values published by King and others (**3, 5, 6, 7, 8, 9**). For a particular atom (3) becomes

$$\log(\lambda^3 I/\varpi f) = \text{const.} - E_2 \cdot 5040/T. \tag{4}$$

The slope of $\log(\lambda^3 I/\varpi f)$ against E_2 gave the values of T in Table I. The E_2 ranges for Mn and Ni were too small (<1 volt). There were good ranges for Fe (2 volts), Co (3 volts) and Cr (3 volts) all of which appeared to give a satisfactory solution. However T from Cr is found to be anomalous; a similar anomaly has been found by Meggers *et al.* (**10**), by Sandage and Hill (**11**), and by Bretz (**12**). Cr, Mn and Ni were therefore given low weight and the temperature adopted was 4300 deg. K. For comparison it may be noted that Meggers (**10**) found an excitation temperature of 4940 deg. K for a 10 amp copper arc.

TABLE I

Atom	Fe	Co	Cr	Mn	Ni
T in deg. K	4350	4250	3800	4500	4500
Reference	(3)	(8)	(5)	(9)	(6, 7)

In the present work it has not been possible to use the method of temperature measurement devised by Schuttevaer *et al.* (**13**) since the spectrum lines used in their calculations (5153 and 5700 A) were too strong and liable to self-reversal. Attempts were made to determine T by comparison of measured arc line intensities with values calculated by various means. However, this led to some surprising anomalies which have already been described (**14**) and which invalidate any determination of T by this method. Attempts were also made to relate the excitation correction to E_2 by means of a curve instead of a straight line, but there appeared to be no evidence of curvature and the linear solution at $T=4300$ deg. K was adopted throughout. If later work should show that the appropriate excitation temperature for our arc should be corrected to T_c the corresponding correction to our published values denoted $\log \varpi f_{AA}$ in Tables III and IV would be

$$\log \varpi f - \log \varpi f_{AA} = (5040/T_c - 1{\cdot}17)(E_2 - 3{\cdot}4). \qquad (5)$$

In this expression 3·4 is taken as the mean E_2 in volts for the lines that provided the absolute standard.

5. *Derivation of the absolute scale.*—In Table II we compare $\log \varpi f_a$, representing our measures of ϖf on an arbitrary scale, with values of $\log \varpi f$ from various absolute measurements and calculations. The references are given for the measurements, and for the calculations (BD) indicates the use of the Bates–Damgaard tables (**15**). Lines for which our ϖf_a values are not thought reliable (e.g. Al and Cu resonance lines) are omitted from the table although calculations and measures may be available. The differences $\log \varpi f - \log \varpi f_a$ represent the correction required to standardize our measurements. These differences have been weighted and averaged to give a mean correction ($-1{\cdot}11$ in the log) which is then applied to ϖf_a to give ϖf_{AA} representing our measurements on an absolute scale.

The final results of (**19**) were received from Dr King after the final correction had been decided, but they do not demand any significant change in our constant. King also advises that the absolute values of (**20**) are being increased as a result of new vapour pressure determinations.

6. *Observational errors and tests.*—The overall accuracy of the values ϖf_{AA} can best be judged by the agreement of the various atoms as demonstrated

in Fig. 4 in Section 8. From this diagram one would judge the probable error of $\log \varpi f_{AA}$ to be about $\pm 0{\cdot}2$. However, some of the scatter is certainly due to the implicit assumption of *LS*-coupling, and the measurement error may be a little less. Although this final accuracy would thus appear to be satisfactory it is necessary to justify the reliability of assumptions and data that have been used. These are considered below.

TABLE II

Atom	λ	$\log \varpi f_a$	$\log \varpi f_{AA}$	$\log \varpi f$			
				(BD)			
Si	3905	+0·24	−0·87	−0·80			
				(16)	(17)	(18)	(19)
Cr	4254	+0·57	−0·54	−0·22	−0·50	−2·17	−0·42
	4289	+0·32	−0·79	−0·48	−0·74	−2·41	−0·66
	3578	+0·82	−0·29		−0·16	−1·70	
	3593	+0·73	−0·38		−0·23	−1·80	
				(18)	(19)		
Mn	4030	+0·54	−0·57	−0·43	−0·44		
	4033	+0·36	−0·75	−0·55	−0·69		
	4034	+0·21	−0·90	−0·72	−0·72		
				(20)	(21)	(19)	
Fe	3719	+0·60	−0·51	−1·04	−0·41	−0·54	
	3737	+0·47	−0·64	−1·05	−0·54		
				(16)			
Ni	3461	+0·54	−0·57	−1·19			
	3524	+0·94	−0·17	−0·89			
	3414	+0·77	−0·34	−0·92			
				(BD)			
Ga	4172	+0·44	−0·67	−0·64			
	4032	+0·10	−1·01	−0·92			
				(BD)			
Ag	3382	+0·56	−0·55	−0·26			

(*a*) *Atomic composition of arc plasma.*—We have been obliged to assume that the atomic composition of the plasma is the same as that of the pole. Since the poles are systematically consumed the alloy atoms must be volatilized into the arc plasma at a rate proportional to the pole concentration. Furthermore, since the alloy atoms are in such small proportions one would expect their diffusion to be controlled mainly by the diffusion of the dominating copper atoms. If this were accurately true the composition of the plasma would be the same as the pole, and also the distribution of the alloy atoms throughout the arc would be the same as the copper atoms. One can make a rough check on this distribution by studying spectra in which the arc is focused onto the slit (or onto the sagittal focus). It has been found that the distribution of intensity throughout the arc is much the same for all lines concerned, although there is perhaps a slight

tendency for light atoms to be more concentrated near the negative pole than heavier atoms. In the circumstances the similarity of composition of pole and plasma seems to be a fair working assumption. We have yet to see whether the assumption can be justified for all atoms.

The probable errors of the pole compositions are not stated but a study of inconsistencies in the tabulated values suggests that they are about 15 per cent for the grades that were employed. When line intensities I were plotted logarithmically against concentration C in the pole the slope $d\log C/d\log I$ was found to be about 1·2 instead of the expected 1·0. No clear explanation of this effect was found but we are inclined to regard it as being due mainly to errors in the relative concentration from one grade to the next. Any such error will not affect our results provided the same grades have been used for all lines measured. For the faint lines that were measured in the more concentrated grades only, a correction for this effect was devised and applied.

(*b*) *Effective excitation temperature.*—The various parts of an electric arc are doubtless at rather different temperatures and not in thermal equilibrium. However if we consider N_0 and N_2 in (2) to represent atomic populations throughout the whole arc we can define T for a whole arc. T, thus defined, may vary with E_2 and give rise to a curved relation between $\log(\lambda^3 I/\varpi f)$ and E_2 instead of (4). Our reason for choosing a single value of T was because no curvature could be detected in the data—not because any constancy of T or thermal equilibrium for the arc was assumed. Our results are not likely to be seriously influenced by errors in T unless $E_2 > 5$ volts. For the Cu lines E_2 reaches as high as 9 volts and considerable errors associated with T are possible.

Our adopted T depends almost entirely on the temperature standard of King's furnace. As a check we have determined the excitation temperature of the Sun's reversing layer by comparing Fraunhofer line intensities with the ϖf_{AA} values. The solar temperature obtained is 4850 ± 75 deg. K. Solar excitation temperatures from other sources are summarized by Hunaerts (**22**) from whose tables we might take 4750 deg. K as a representative value for molecules and 4400 deg. K for atoms. Our value is a little higher but not at all improbable, being the temperature for an optical depth of 0·06 (**23**). The solar temperatures we obtained from individual elements were Cr 4754 deg., Mn 4996 deg., Fe 4917 deg. and Co 4869 deg. These are in good agreement and do not show much Cr anomaly.

(*c*) *Self-absorption.*—It is rather difficult to prove conclusively that there has been no self-absorption but if it has only been slight it would produce no great differential effect from one atom to another. The chief evidence against self-absorption is that multiplets follow the LS intensity rules when expected to do so, and that our $\lambda^3 I$ values are proportional to the absorption ϖf values measured by King and others (**3, 5, 6, 8, 9**). Fig. 1 shows values of our $\lambda^3 I$ plotted logarithmically against published values of ϖf for Cr, Fe, Co. The lines are in groups selected by E_2. It is seen at once that there is no tendency for the slope to change with E_2 nor for the slope to be less than 1·0 as would be the case if self-absorption were effective.

7. *Results.*—The absolute values of ϖf derived in this work for the neutral atoms Al, Si, Cr, Mn, Fe, Co, Ni, Ga, Ag, Sn, Pb and Bi are set out in Table III. The first column contains the atom, the multiplet number from the Revised Multiplet Table (**24**) and sometimes a letter A or B explained in Section 8. The

wave-lengths are also from the Multiplet Table. The final absolute ϖf-values are denoted ϖf_{AA} and expressed logarithmically. For use in our discussion we also quote an experimental value for σ^2 defined (**15**) by

$$\sigma_{exp}{}^2 = S/\mathscr{S}(\mathscr{L})\mathscr{S}(\mathscr{M}) = \varpi f_{AA}\lambda/304\mathscr{S}(\mathscr{L})\mathscr{S}(\mathscr{M}) \qquad (6)$$

where S is the line strength, $\mathscr{S}(\mathscr{L})$ is the line strength relative to the multiplet strength (**23, 25**), $\mathscr{S}(\mathscr{M})$ which might be called the relative multiplet strength is available from tabulations (**23, 26**), and λ is in A. The lower excitation potential E_1 is given in the last column.

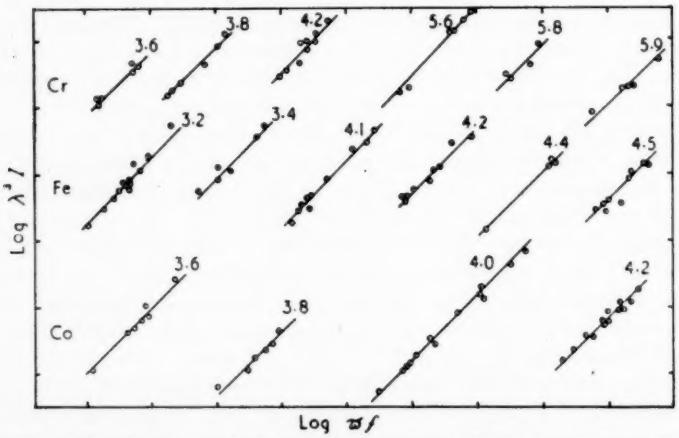

FIG. 1.—*Plots of log $\lambda^3 I$ against published log ϖf for groups of Cr, Fe and Co lines. The numbers represent E_2 for each group. The straight lines drawn in are at unit slope.*

There is some doubt about the Al resonance lines. Al was detected in the alloys as an unexpected impurity and a value for its abundance was given in the maker's report. However the low measured value of ϖf_{AA} suggests that the measured concentration is not accurate. Sb was contained in some of the alloys but no lines were seen.

The Cu results are quoted separately in Table IV. The details for Cu are somewhat reduced because both the accuracy and astrophysical interest may be less than for other elements. The three columns give (i) the lower term, (ii) the whole number part of the wave-length, and (iii) $\log \varpi f_{AA}$. The term data are from Shenstone (**27**). The lines are not separated into multiplets although they are in the order used for other elements in the Multiplet Table (**24**).

The copper resonance lines are far too strong for normal measurement but an attempt was made to correct for the severe self-reversal by evaluating the constants in a formula by Cowan and Dieke (**28**). The resulting measurement ϖf_{AA} is probably too small.

8. *Discussion of results.*—Our interests in the measurements are (i) to seek for useful regularities, and (ii) to investigate the excitation potential effect described earlier (**14**).

All the ϖf_{AA}-values are plotted against E_2 (upper EP) in Fig. 2. They show the tendency to increase with E_2 that had been noticed before (**14**), but now that some high potential copper lines have been added it would appear that the increase

TABLE III

Atom Mult.	λ	log wf_{AA}	log σ_{exp}^2	E_1	Atom Mult.	λ	log wf_{AA}	log σ_{exp}^2	E_1
Al(1)	3961·52	−1·3?	−0·8?	0·0	Cr(51)	3455·60	−0·07		2·5
	3944·01	−1·5?	−0·7?	0·0		3445·62	+0·53		2·5
					(52)	3436·19	+0·25		2·5
Si(3)	3905·53	−0·87	−0·06	1·9		3441·44	+0·51		2·5
						3447·43	+0·16		2·5
Cr(1)A	4254·35	−0·54	−0·34	0·0		3453·33	+0·22		2·5
	4289·72	−0·79	−0·33	0·0	(67)	3992·84	−0·09		2·7
(2)	3732·03	−2·44		0·0	(69)A	3841·28	+0·56	+0·71	2·7
	3730·81	−2·59		0·0		3850·04	+0·48	+0·92	2·7
(4)B	3578·69	−0·29	−1·16	0·0		3848·98	+0·17	+0·91	2·7
	3593·49	−0·38	−1·15	0·0		3854·22	+0·17	+0·80	2·7
(10)	4496·86	−1·12		0·9		3857·63	+0·13	+0·88	2·7
	4545·96	−1·37		0·9	(70)	3819·56	−0·22		2·7
	4580·06	−1·71		0·9	(71)	3815·43	+0·09		2·7
(21)B	4600·75	−1·21	−0·48	1·0	(139)	3804·80	+0·88		3·0
	4616·14	−1·15	−0·51	1·0		3797·72	+0·46		3·0
	4591·39	−1·77	−0·54	1·0		3793·29	−0·05		3·0
	4613·37	−1·64	−0·55	1·0		3793·88	+0·01		3·0
(22)B	4351·77	−0·66	−0·84	1·0		3792·14	+0·23		3·0
	4344·51	−0·64	−0·63	1·0		3791·38	+0·09		3·0
	4384·98	−1·40	−0·72	1·0					
	4371·28	−1·23	−0·69	1·0	Mn(2)B	4030·76	−0·57	−0·65	0·0
	4359·63	−1·22	−0·65	1·0		4033·07	−0·75	−0·71	0·0
	4351·05	−1·38	−0·67	1·0		4034·49	−0·90	−0·68	0·0
(23)B	3919·16	−0·89	−0·95	1·0	(5)A	4041·36	+0·68	+0·89	2·1
	3908·76	−1·07	−0·81	1·0		4055·54	+0·28	+0·85	2·1
	3941·49	−1·34	−0·71	1·0		4070·28	−0·59	+0·88	2·2
	3928·64	−1·25	−0·75	1·0		4018·10	+0·04	+0·89	2·1
	3921·02	−1·25	−0·69	1·0		4035·73	+0·28	+0·99	2·1
	3916·24	−1·72	−0·91	1·0		4048·76	+0·13	+0·87	2·2
	3886·79	−1·32	−0·69	1·0		4083·63	0·00	+0·72	2·2
	3885·22	−1·25	−0·69	1·0	(6)A	3806·72	+0·79	+0·80	2·1
	3894·04	−1·58	−0·77	1·0		3823·51	+0·66	+0·82	2·1
(24)	3849·53	−1·71		1·0		3843·98	−0·21	+0·79	2·2
	3852·22	−1·98		1·0		3809·59	−0·02	+0·65	2·1
(32)	4571·68	−0·54		2·5		3823·89	+0·01	+0·65	2·2
(33)A	4526·47	+0·17	+0·25	2·5		3833·86	+0·08	+0·82	2·2
	4535·72	−0·03	+0·24	2·5		3839·78	−0·07	+0·83	2·2
	4544·62	−0·25	+0·31	2·5	(8)A	3577·88	+0·61	+0·91	2·1
(38)A	3963·69	+0·97	+0·91	2·5		3607·54	+0·15	+0·99	2·1
	3969·75	+0·86	+0·90	2·5		3608·49	+0·42	+1·12	2·2
	3976·66	+0·79	+0·87	2·5	(16)A	4823·52	+0·15	+0·35	2·3
	3983·91	+0·69	+0·92	2·5		4783·42	+0·06	+0·36	2·3
	3991·12	+0·63	+0·95	2·5		4754·04	−0·04	+0·37	2·3
	3991·67	−0·30	+0·87	2·5	(18)A	3547·80	+0·81	+0·31	2·3
(40)A	3816·17	−0·13	+0·03	2·5	(21)A	4762·38	+0·54	+0·73	2·9
(43)B	3743·58	+0·75	+0·35	2·5		4766·43	+0·45	+0·81	2·9
	3749·00	+0·34	+0·05	2·5		4765·86	+0·24	+0·79	2·9
	3757·66	+0·21	+0·12	2·5		4727·48	−0·14	+0·89	2·9
(47)	3639·80	−0·41		2·5	(22)A	4451·59	+0·52	+0·84	2·9
	3636·59	+0·31		2·5		4464·68	+0·28	+0·89	2·9
	3649·00	−0·06		2·5		4470·14	−0·07	+0·88	2·9
						4472·79	−0·28	+0·87	2·9

TABLE III (*cont.*)

Atom Mult.	λ	log wf_{AA}	log σ_{exp}^2	E_1	Atom Mult.	λ	log wf_{AA}	log σ_{exp}^2	E_1
Mn(22)A	4436·35	−0·08	+0·93	2·9	Fe(23)A	3581·20	+0·38	+0·34	0·9
	4453·00	−0·20	+0·96	2·9		3647·84	−0·06	+0·02	0·9
	4502·22	−0·13	+0·97	2·9		3585·71	−0·87	0·00	0·9
	4498·90	−0·05	+0·97	2·9		3586·98	−0·7?	+0·57	1·0
	4490·08	−0·27	+0·89	2·9	(24)	3570·10	+0·21		0·9
						3565·38	0·00		1·0
Fe(4)B	3859·91	−0·63	−0·70	0·0		3558·52	−0·51		1·0
	3886·28	−1·05	−0·78	0·1	(41)	4383·55	+0·44		1·5
	3899·71	−1·42	−0·71	0·1		4404·75	+0·16		1·6
	3824·44	−1·15	−0·52	0·0	(42)A	4271·76	+0·11	+0·22	1·5
	3856·37	−1·28	−0·77	0·1		4307·91	+0·22	+0·46	1·6
	3878·58	−1·36	−0·79	0·1		4325·76	+0·27	+0·61	1·6
	3895·66	−1·62	−0·81	0·1		4202·03	−0·33	+1·07	1·5
	3922·91	−1·60	−0·95	0·1		4250·79	−0·45	+0·94	1·6
	3930·30	−1·46	−0·95	0·1	(43)A	4045·82	+0·54	+0·74	1·5
	3927·92	−1·49	−0·92	0·1		4071·74	+0·28	+0·76	1·6
	3920·26	−1·66	−0·85	0·1		3969·26	−0·11	+1·24	1·5
(5)B	3719·94	−0·51	−0·76	0·0		4005·25	−0·21	+1·18	1·6
	3737·13	−0·64	−0·72	0·1		4143·87	−0·23	+1·15	1·6
	3748·26	−1·04	−0·70	0·1		4132·06	−0·35	+1·06	1·6
	3679·92	−1·45	−0·84	0·0	(45)A	3815·84	+0·54	+0·83	1·5
	3705·57	−1·29	−0·82	0·1		3827·82	+0·40	+0·85	1·6
	3722·56	−1·22	−0·73	0·1		3841·05	+0·45	+1·07	1·6
	3733·32	−1·48	−0·84	0·1		3902·95	−0·01	+1·35	1·6
(6)B	3440·99	−1·07	−0·75	0·1	(152)A	4260·48	+0·68	+0·88	2·4
	3490·58	−1·24	−0·63	0·1		4235·94	+0·21	+0·79	2·4
	3476·70	−1·58	−0·60	0·1		4187·80	−0·19	+0·46	2·4
(15)B	5269·54	−1·40		0·9		4187·04	−0·09	+0·57	2·4
	5328·04	−1·44		0·9		4299·24	+0·11	+0·91	2·4
	5371·49	−1·53		1·0		4271·16	+0·21	+0·86	2·4
	5397·13	−1·89		0·9		4250·12	+0·31	+0·97	2·5
	5429·70	−1·74		1·0					
(20)A	3820·43	+0·33	+0·55	0·9	Co(3)	3909·93	−2·45		0·0
	3825·88	+0·09	+0·47	0·9		3979·52	−2·60		0·1
	3834·22	+0·12	+0·69	1·0		4027·03	−2·53		0·2
	3840·44	−0·29	+0·53	1·0	(4)B	3575·36	−0·99	−1·00	0·1
	3878·02	−0·62	+0·31	1·0		3594·87	−1·12	−0·96	0·2
	3872·50	−0·58	+0·37	1·0	(5)B	3513·48	−0·89	−1·10	0·1
	3865·53	−0·68	+0·43	1·0		3529·03	−1·02	−1·09	0·2
(21)A	3734·87	+0·38	+0·48	0·9		3533·36	−0·85	−0·80	0·2
	3749·49	+0·29	+0·58	0·9	(6)B	3431·58	−1·04	−0·98	0·1
	3758·24	+0·31	+0·76	1·0		3442·92	−1·19	−0·94	0·2
	3763·79	−0·02	+0·60	1·0		3455·24	−1·21	−0·77	0·2
	3767·19	−0·22	+0·57	1·0	(17)	3941·73	−1·81		0·4
	3709·25	−0·39	+0·70	0·9	(18)	3873·12	−0·64		0·4
	3727·62	−0·37	+0·54	1·0		3873·95	−0·77		0·5
	3743·36	−0·51	+0·58	1·0		3957·93	−1·85		0·6
	3798·51	−0·78	+0·28	0·9	(19)	3627·81	−1·11		0·5
	3799·55	−0·50	+0·40	1·0		3564·95	−1·00		0·6
	3795·00	−0·48	+0·44	1·0	(20)	3521·56	−0·87		0·4
	3787·88	−0·72	+0·38	1·0		3605·37	−1·17		0·5
(22)	3812·96	−0·68		1·0					
	3790·10	−1·12		1·0					

TABLE III (*cont.*)

Atom Mult.	λ	log wf_{AA}	log σ_{exp}^2	E_1	Atom Mult.	λ	log wf_{AA}	log σ_{exp}^2	E_1
Co(21)A	3502·28	−0·02	+0·19	0·4	Ni(7)B	3371·99	−1·41	−1·59	0·2
	3506·31	−0·16	+0·21	0·5	(8)	3366·17	−1·45		0·2
	3523·42	−0·39	+0·37	0·6	(9)	3320·26	−1·30		0·2
	3574·97	−0·70	+0·35	0·6	(17)	3461·65	−0·57		0·0
	3560·89	−0·72	+0·44	0·6		3452·89	−0·98		0·1
(22)A	3453·51	+0·50	+0·48	0·4	(18)A	3524·54	−0·17	+0·27	0·0
	3529·82	−0·04	+0·06	0·5		3492·96	−0·53	+0·18	0·1
	3509·84	−0·23	0·00	0·6		3510·34	−0·73	+0·33	0·2
	3495·68	−0·40	−0·05	0·6		3610·46	−1·10	+0·10	0·1
	3367·11	−1·13	+0·01	0·4		3597·70	−1·10	+0·10	0·2
	3385·22	−0·95	+0·27	0·5	(19)A	3414·76	−0·34	−0·24	0·0
(23)A	3405·12	+0·31	+0·40	0·4		3515·05	−0·43	−0·16	0·1
	3417·15	−0·57	−0·14	0·6		3458·47	−0·36	+0·08	0·2
	3433·04	−0·28	+0·25	0·6		3433·56	−0·78	+0·38	0·0
	3388·16	−0·88	+0·25	0·6		3361·56	−1·43	−0·27	0·1
	3474·02	+0·05	+1·07	0·6	(20)A	3392·99	−0·70	−0·44	0·0
	3462·80	−0·15	+0·98	0·6		3446·26	−0·58	−0·07	0·1
(25)	3412·34	−0·14		0·5		3423·71	−0·81	−0·10	0·2
(28)	4121·32	−0·26		0·9		3472·54	−0·92	+0·23	0·1
	4118·77	−0·38		1·0		3548·18	−1·35	−0·16	0·2
	3952·92	−1·17		0·9	(22)	3315·66	−1·24		0·1
(29)	4092·39	−0·95		0·9	(30)	3783·53	−1·29		0·4
	4110·53	−1·10		1·0	(31)	3973·56	−2·05		0·4
(31)	3995·31	−0·13		0·9		3831·69	−1·95		0·4
	4045·39	−1·11		1·0	(32)	3858·30	−0·95		0·4
(32)	3935·96	−0·83		0·9		3674·15	−1·8?		0·4
	3997·90	−0·73		1·0	(33)	3807·14	−1·19		0·4
(33)	3842·05	−0·62		0·9		3775·57	−1·25		0·4
(34)A	3845·47	+0·07	+0·17	0·9	(35)A	3619·39	−0·12	+0·12	0·4
	3894·07	+0·17	+0·38	1·0	(36)A	3566·37	−0·35	+0·02	0·4
(35)A	3569·37	+0·45	+0·64	0·9	(37)A	3380·57	−0·13	+0·43	0·4
	3587·19	+0·27	+0·58	1·0					
	3704·06	−0·79	+0·83	1·0	Ga(1)	4172·05	−0·67	−0·14	0·1
(36)A	3489·40	+0·33	+0·63	0·9		4032·98	−1·01	−0·18	0·0
	3518·34	−0·05	+0·41	1·0					
(58)	4086·30	−0·46		1·9	Ag(1)	3382·89	−0·55	+0·08	0·0
(62)	3732·39	−0·34		1·9					
	3730·48	−0·51		1·9	Sn(2)	3330·62	−0·04		1·1
(64)	3543·26	−0·47		1·9		3801·02	+0·15		1·1
(95)	3735·93	−0·62		2·1	(3)	3262·34	+0·99	+1·01	1·1
(98)	3708·82	−0·50		2·0	(5)	4524·74	+0·19	+1·06	2·1
(115)	3662·16	−0·05		2·3					
(145)	3702·24	+0·4?		2·9	Pb(1)	3639·57	+0·23	+1·13	1·0
						4057·81	+0·31	+1·03	1·3
Ni(3)	3437·28	−1·33		0·0		3683·47	+0·47	+1·26	1·0
	3548·18	−1·35		0·3	(2)	3739·94	+0·97		2·7
(4)	3670·43	−2·17		0·2	(3)	3572·73	+1·00	+1·07	2·7
	3664·10	−1·78		0·3					
(5)	3391·05	−1·12		0·0	Bi	3397·21	−0·56		1·9
	3571·87	−1·22		0·2					
(6)	3369·57	−0·77		0·0					
	3500·85	−1·46		0·2					
	3612·74	−1·40		0·3					

TABLE III (*cont.*)

Atom Mult.	λ	log wf_{AA}	log σ_{exp}^2	E_1	Atom Mult.	λ	log wf_{AA}	log σ_{exp}^2	E_1
Mn(22)A	4436·35	−0·08	+0·93	2·9	Fe(23)A	3581·20	+0·38	+0·34	0·9
	4453·00	−0·20	+0·96	2·9		3647·84	−0·06	+0·02	0·9
	4502·22	−0·13	+0·97	2·9		3585·71	−0·87	0·00	0·9
	4498·90	−0·05	+0·97	2·9		3586·98	−0·7?	+0·57	1·0
	4490·08	−0·27	+0·89	2·9	(24)	3570·10	+0·21		0·9
						3565·38	0·00		1·0
Fe(4)B	3859·91	−0·63	−0·70	0·0		3558·52	−0·51		1·0
	3886·28	−1·05	−0·78	0·1	(41)	4383·55	+0·44		1·5
	3899·71	−1·42	−0·71	0·1		4404·75	+0·16		1·6
	3824·44	−1·15	−0·52	0·0	(42)A	4271·76	+0·11	+0·22	1·5
	3856·37	−1·28	−0·77	0·1		4307·91	+0·22	+0·46	1·6
	3878·58	−1·36	−0·79	0·1		4325·76	+0·27	+0·61	1·6
	3895·66	−1·62	−0·81	0·1		4202·03	−0·33	+1·07	1·5
	3922·91	−1·60	−0·95	0·1		4250·79	−0·45	+0·94	1·6
	3930·30	−1·46	−0·95	0·1	(43)A	4045·82	+0·54	+0·74	1·5
	3927·92	−1·49	−0·92	0·1		4071·74	+0·28	+0·76	1·6
	3920·26	−1·66	−0·85	0·1		3969·26	−0·11	+1·24	1·5
(5)B	3719·94	−0·51	−0·76	0·0		4005·25	−0·21	+1·18	1·6
	3737·13	−0·64	−0·72	0·1		4143·87	−0·23	+1·15	1·6
	3748·26	−1·04	−0·70	0·1		4132·06	−0·35	+1·06	1·6
	3679·92	−1·45	−0·84	0·0	(45)A	3815·84	+0·54	+0·83	1·5
	3705·57	−1·29	−0·82	0·1		3827·82	+0·40	+0·85	1·6
	3722·56	−1·22	−0·73	0·1		3841·05	+0·45	+1·07	1·6
	3733·32	−1·48	−0·84	0·1		3902·95	−0·01	+1·35	1·6
(6)B	3440·99	−1·07	−0·75	0·1	(152)A	4260·48	+0·68	+0·88	2·4
	3490·58	−1·24	−0·63	0·1		4235·94	+0·21	+0·79	2·4
	3476·70	−1·58	−0·60	0·1		4187·80	−0·19	+0·46	2·4
(15)B	5269·54	−1·40		0·9		4187·04	−0·09	+0·57	2·4
	5328·04	−1·44		0·9		4299·24	+0·11	+0·91	2·4
	5371·49	−1·53		1·0		4271·16	+0·21	+0·86	2·4
	5397·13	−1·89		0·9		4250·12	+0·31	+0·97	2·5
	5429·70	−1·74		1·0					
(20)A	3820·43	+0·33	+0·55	0·9	Co(3)	3909·93	−2·45		0·0
	3825·88	+0·09	+0·47	0·9		3979·52	−2·60		0·1
	3834·22	+0·12	+0·69	1·0		4027·03	−2·53		0·2
	3840·44	−0·29	+0·53	1·0	(4)B	3575·36	−0·99	−1·00	0·1
	3878·02	−0·62	+0·31	1·0		3594·87	−1·12	−0·96	0·2
	3872·50	−0·58	+0·37	1·0	(5)B	3513·48	−0·89	−1·10	0·1
	3865·53	−0·68	+0·43	1·0		3529·03	−1·02	−1·09	0·2
(21)A	3734·87	+0·38	+0·48	0·9		3533·36	−0·85	−0·80	0·2
	3749·49	+0·29	+0·58	0·9	(6)B	3431·58	−1·04	−0·98	0·1
	3758·24	+0·31	+0·76	1·0		3442·92	−1·19	−0·94	0·2
	3763·79	−0·02	+0·60	1·0		3455·24	−1·21	−0·77	0·2
	3767·19	−0·22	+0·57	1·0	(17)	3941·73	−1·81		0·4
	3709·25	−0·39	+0·70	0·9	(18)	3873·12	−0·64		0·4
	3727·62	−0·37	+0·54	1·0		3873·95	−0·77		0·5
	3743·36	−0·51	+0·58	1·0		3957·93	−1·85		0·6
	3798·51	−0·78	+0·28	0·9	(19)	3627·81	−1·11		0·5
	3799·55	−0·50	+0·40	1·0		3564·95	−1·00		0·6
	3795·00	−0·48	+0·44	1·0	(20)	3521·56	−0·87		0·4
	3787·88	−0·72	+0·38	1·0		3605·37	−1·17		0·5
(22)	3812·96	−0·68		1·0					
	3790·10	−1·12		1·0					

TABLE III (*cont.*)

Atom Mult.	λ	log wf_{AA}	log σ_{exp}^2	E_1	Atom Mult.	λ	log wf_{AA}	log σ_{exp}^2	E_1
Co(21)A	3502·28	−0·02	+0·19	0·4	Ni(7)B	3371·99	−1·41	−1·59	0·2
	3506·31	−0·16	+0·21	0·5	(8)	3366·17	−1·45		0·2
	3523·42	−0·39	+0·37	0·6	(9)	3320·26	−1·30		0·2
	3574·97	−0·70	+0·35	0·6	(17)	3461·65	−0·57		0·0
	3560·89	−0·72	+0·44	0·6		3452·89	−0·98		0·1
(22)A	3453·51	+0·50	+0·48	0·4	(18)A	3524·54	−0·17	+0·27	0·0
	3529·82	−0·04	+0·06	0·5		3492·96	−0·53	+0·18	0·1
	3509·84	−0·23	0·00	0·6		3510·34	−0·73	+0·33	0·2
	3495·68	−0·40	−0·05	0·6		3610·46	−1·10	+0·10	0·1
	3367·11	−1·13	+0·01	0·4		3597·70	−1·10	+0·10	0·2
	3385·22	−0·95	+0·27	0·5	(19)A	3414·76	−0·34	−0·24	0·0
(23)A	3405·12	+0·31	+0·40	0·4		3515·05	−0·43	−0·16	0·1
	3417·15	−0·57	−0·14	0·6		3458·47	−0·36	+0·08	0·2
	3433·04	−0·28	+0·25	0·6		3433·56	−0·78	+0·38	0·0
	3388·16	−0·88	+0·25	0·6		3361·56	−1·43	−0·27	0·1
	3474·02	+0·05	+1·07	0·6	(20)A	3392·99	−0·70	−0·44	0·0
	3462·80	−0·15	+0·98	0·6		3446·26	−0·58	−0·07	0·1
(25)	3412·34	−0·14		0·5		3423·71	−0·81	−0·10	0·2
(28)	4121·32	−0·26		0·9		3472·54	−0·92	+0·23	0·1
	4118·77	−0·38		1·0		3548·18	−1·35	−0·16	0·2
	3952·92	−1·17		0·9	(22)	3315·66	−1·24		0·1
(29)	4092·39	−0·95		0·9	(30)	3783·53	−1·29		0·4
	4110·53	−1·10		1·0	(31)	3973·56	−2·05		0·4
(31)	3995·31	−0·13		0·9		3831·69	−1·95		0·4
	4045·39	−1·11		1·0	(32)	3858·30	−0·95		0·4
(32)	3935·96	−0·83		0·9		3674·15	−1·8?		0·4
	3997·90	−0·73		1·0	(33)	3807·14	−1·19		0·4
(33)	3842·05	−0·62		0·9		3775·57	−1·25		0·4
(34)A	3845·47	+0·07	+0·17	0·9	(35)A	3619·39	−0·12	+0·12	0·4
	3894·07	+0·17	+0·38	1·0	(36)A	3566·37	−0·35	+0·02	0·4
(35)A	3569·37	+0·45	+0·64	0·9	(37)A	3380·57	−0·13	+0·43	0·4
	3587·19	+0·27	+0·58	1·0					
	3704·06	−0·79	+0·83	1·0	Ga(1)	4172·05	−0·67	−0·14	0·1
(36)A	3489·40	+0·33	+0·63	0·9		4032·98	−1·01	−0·18	0·0
	3518·34	−0·05	+0·41	1·0					
(58)	4086·30	−0·46		1·9	Ag(1)	3382·89	−0·55	+0·08	0·0
(62)	3732·39	−0·34		1·9					
	3730·48	−0·51		1·9	Sn(2)	3330·62	−0·04		1·1
(64)	3543·26	−0·47		1·9		3801·02	+0·15		1·1
(95)	3735·93	−0·62		2·1	(3)	3262·34	+0·99	+1·01	1·1
(98)	3708·82	−0·50		2·0	(5)	4524·74	+0·19	+1·06	2·1
(115)	3662·16	−0·05		2·3					
(145)	3702·24	+0·4?		2·9	Pb(1)	3639·57	+0·23	+1·13	1·0
						4057·81	+0·31	+1·03	1·3
Ni(3)	3437·28	−1·33		0·0		3683·47	+0·47	+1·26	1·0
	3548·18	−1·35		0·3	(2)	3739·94	+0·97		2·7
(4)	3670·43	−2·17		0·2	(3)	3572·73	+1·00	+1·07	2·7
	3664·10	−1·78		0·3					
(5)	3391·05	−1·12		0·0	Bi	3397·21	−0·56		1·9
	3571·87	−1·22		0·2					
(6)	3369·57	−0·77		0·0					
	3500·85	−1·46		0·2					
	3612·74	−1·40		0·3					

TABLE IV

Copper lines

Low term	λ	log ϖf_{AA}	Low term	λ	log ϖf_{AA}	Low term	λ	log ϖf_{AA}	Low term	λ	log ϖf_{AA}
4^2S	3247	−1·2?	z^4F^0	4354	−0·33	z^4D^0	3488	+0·39	z^2F^0	3800	+0·17
	3273	−1·5?		3365	+0·95		3472	+0·61		3527	+0·86
m^2D	5105	−3·5?		3396	−0·46		3613	+0·91		3797	−0·28
	3594	−4·42		3384	+0·05		3632	+0·33	z^2P^0	4525	+0·11
	3727	−4·09		3354	+0·61		3656	+0·32		4003	+0·06
	3457	−3·56		3335	+0·50		3734	+0·42		3979	−0·67
	3337	−2·68		3381	+0·90		3650	−0·1?		3964	−0·18
	3530	−2·65		3349	+1·06		3602	+1·15		3811	+0·18
$4p^2P^0$	4480	−0·94		3329	+0·49		3614	+0·53		3659	+0·52
	4015	−1·77		3375	+0·11		3721	−0·16		3837	−0·42
	3825	−1·05		3319	+0·89		3632	+0·33		3817	−0·36
	3687	+0·03	z^4D^0	5292	+0·92		3546	+0·08		3671	+0·48
	3566	−1·43		5391	+0·42		3610	+0·53		3645	+0·63
	3481	−0·75		5250	+0·40		3498	+0·35		3635	+0·86
	3463	−1·71		5111	+0·24		3459	+0·15		3420	+0·25
	3433	−2·36		5144	+0·47		3474	−0·31	z^2D^0	4866	+0·83
z^4P^0	4275	+0·71		5016	+0·37	z^2F^0	5200	+0·34		4767	+0·51
	4378	+0·67		5432	+0·18		5034	+0·28		4050	−0·08
	4415	+0·36		5354	+0·05		5076	+0·64		4121	−0·03
	4104	−0·44		4230	−0·25		4642	+0·41		4080	+0·40
	4177	+0·06		4242	−0·09		4776	−0·40		4010	−0·41
	4248	+0·26		4336	−0·41		4123	+0·04		4075	+0·52
	4073	−0·40		3799	+0·02		4507	+0·98		3771	+0·63
	4111	−0·49		3780	−0·39		3860	+0·91		3699	−0·09
	3975	−0·51		3507	+0·63		3533	+1·00		3946	−0·25
z^4F^0	4651	+1·12		3655	+0·59		3695	−0·46		3888	−0·31
	4586	+0·92		3759	+0·06		3665	+0·09		4052	−0·25
	4539	+0·64		3624	+0·40		3652	+0·94		3860	+0·91
	4509	+0·50		3745	+0·41		3820	−0·32		3925	+0·28
	4704	+0·48		3627	+0·89		3648	+0·12		3712	+0·40
	4674	+0·55		3764	−0·24		3517	+0·16		3921	+0·17
	4697	+0·28		3741	+0·62		3813	−0·10		3487	+0·52
	4842	−0·57		3621	+0·96		3544	+0·44		3436	+0·32
	4328	−0·60		3620	+0·37		3641	+0·23			

in $\log \varpi f$ is not linear (as our previous analysis seemed to imply) but is bounded by a curve with a limiting $\log \varpi f$ of about 1·0. This is in better agreement with f-sum rule expectations.

In our previous work it was seen that the scatter could be reduced by comparing observed ϖf with the values calculated on the basis of the Bates–Damgaard tables (15). The corresponding relation using the ϖf_{AA}-values is shown in Fig. 3. We find the slope, the absolute values, and the interagreement of different atoms much the same as before. However the high level copper lines do not fit onto the linear curve.

A more useful relation is revealed if we convert ϖf_{AA} by means of (6) into σ_{exp}^2. This can only be done for certain multiplets permitted in LS-coupling. We plot the resulting values against *lower* excitation potential E_1 in Fig. 4. It is now found that the values segregate naturally into two groups A and B. A study of the spectroscopic transitions shows that A-lines are for transitions in which

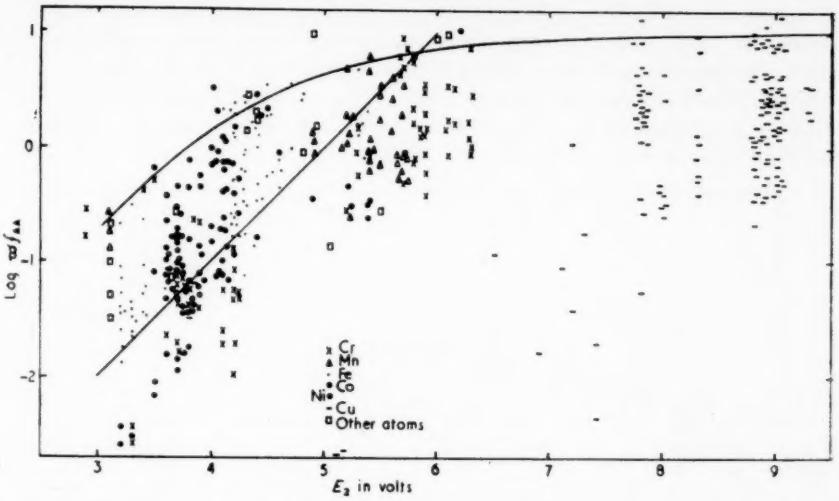

FIG. 2.—*Comparison of ϖf_{AA} with upper excitation potential. Each point represents a line. The curve represents the suggested maximum ϖf, and the straight line is the relation given earlier* (14).

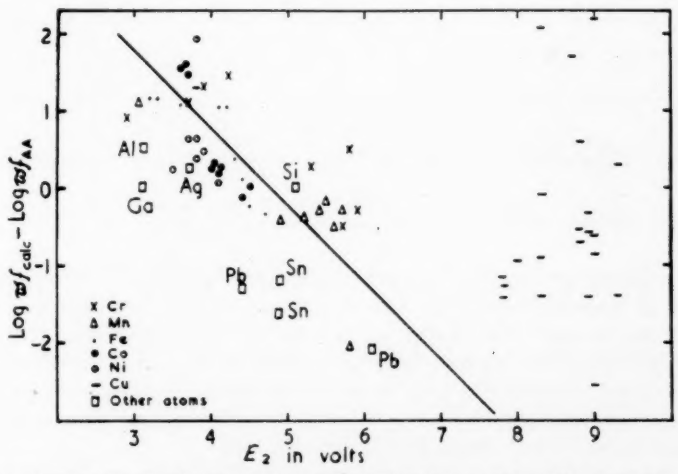

FIG. 3.—*Comparison of calculated and experimental values of ϖf. Each point represents a multiplet. The straight line shows the relation found previously* (14).

the moving electron is not equivalent in either the upper or the lower level, while for the B-lines the moving electron is equivalent in the lower level.

From Fig. 4 we might derive the following approximate empirical rules. For the A-lines σ^2 increases with E_1 in agreement with $\sigma_A{}^2 \simeq 1{\cdot}0 + 2{\cdot}5E_1$. For the B-lines there is not much evidence of the change of σ^2 with E_1 but we might write provisionally, $\log \sigma_B{}^2 \simeq -0{\cdot}95 + 0{\cdot}33E_1$. For complex atoms these relations could be used as a general method of predicting oscillator strengths although

it is not at present known how widely the rules are applicable. The relations could not have been expected from any studies of the *f*-sum rule nor the Bates–Damgaard procedure. It might be noted that σ_A^2 is in the range 1 to 20 whereas values of 1 to 5 are usually found when the Bates–Damgaard method is applied to strong lines. There is therefore order-of-magnitude agreement between A-group observations and calculations.

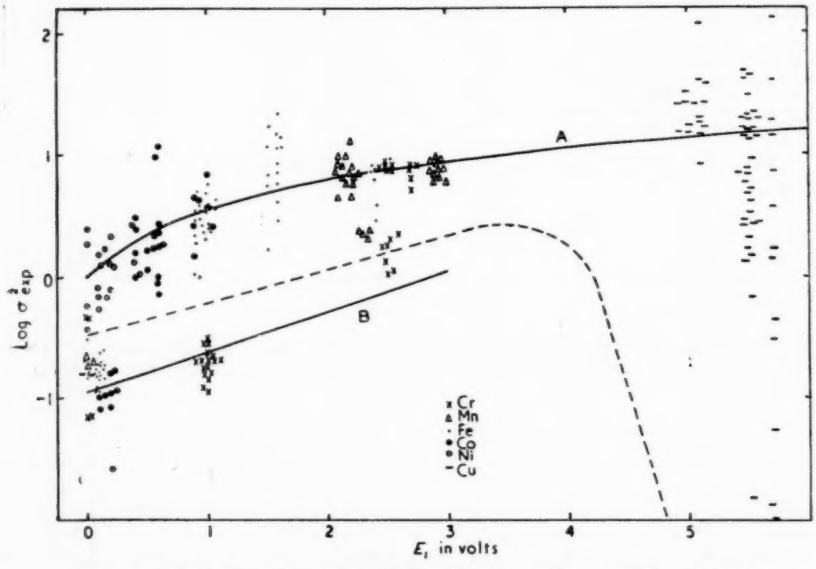

FIG. 4.—*Relation between experimental* σ^2 *and lower excitation potential. Each point represents a line.*
A *and* B *empirical curves for* A *and* B *line groups.*
– – – – *division between* A *and* B *line groups.*

The A-group are mostly $d^n s - d^n p$ transitions allowed in *LS*-coupling. In one case of inter-parentage, Cr(69), σ^2 is found to be normal instead of very weak. There are some cases of $d^n sp - d^n ss$ and $d^n sp - d^n sd$ transitions; Mn(16)(18) and Fe(152) tend to be weaker than the A-group normal, and the Cu multiplets exhibit a variety of intensities (due in part to the failure of *LS*-coupling). There are some other multiplets that are weaker than expected, Cr(33)(40), but much of this can be ascribed to departure from *LS*-coupling.

The B-group are mostly $d^n s^2 - d^n sp$ transitions but there are also some cases of $d^n s - d^{n-1} sp$, Cr(4)(43) and Fe(15).

The discussion of Fig. 4 shows clearly that the excitation potential effect of (14) is due mainly to the existence of low $d^n s^2$ configurations throughout the iron group of atoms.

The results for the non-iron atoms do not appear to be very regular. ϖf_{AA} values are compared with Bates–Damgaard calculations in Fig. 3. Si and Ga agree. For Al ϖf_{AA} is low, but this is thought to be due to error in the composition. The Ag value of ϖf_{AA} is also a little low. For Sn and Pb the ϖf_{AA} values are much higher than expected. Fig. 3 suggests that this could possibly be another manifestation of the excitation potential effect. On the other hand the

applicability of the method to the measurement of non-iron atoms cannot be regarded as established.

The authors wish to acknowledge that the idea of measuring absolute oscillator strengths by this method arose through a conversation with Dr W. F. Meggers in Rome, 1952. One of us (A. S. A.) has been in receipt of a research grant from the Egyptian Government.

University of London Observatory,
Mill Hill Park,
London, N.W.7:
1956 *December* 11.

References

(1) J. Euler, *Ann. d. Phys.*, **11**, 203, 1953.
(2) W. E. Forsythe and A. G. Worthing, *Ap. J.*, **61**, 146, 1925.
(3) R. B. King and A. S. King, *Ap. J.*, **87**, 24, 1938.
(4) W. J. Claas, *Proc. K. Ned. Ak. Wet.*, **52**, 518, 1949.
(5) A. J. Hill and R. B. King, *J.O.S.A.*, **41**, 315, 1951.
(6) R. B. King, *Ap. J.*, **108**, 87, 1948.
(7) H. van Driel, Thesis, Utrecht, 1935.
(8) R. B. King *et al.*, *J.O.S.A.*, **45**, 350, 1955.
(9) R. S. Seward, *Phys. Rev.*, **37**, 344, 1931.
(10) W. F. Meggers, C. B. Corliss and B. F. Scribner, *Science*, **121**, 624, 1955 and private communication.
(11) A. R. Sandage and A. J. Hill, *Ap. J.*, **113**, 525, 1951.
(12) M. Bretz, *Z. f. Ap.*, **38**, 259, 1956.
(13) J. W. Schuttevaer, M. J. de Bont and Th. H. van den Brock, *Physica*, **10**, 544, 1943.
(14) C. W. Allen and A. S. Asaad, *M.N.*, **115**, 571, 1955.
(15) D. R. Bates and A. Damgaard, *Phil. Trans.* A, **242**, 101, 1949.
(16) F. B. Estabrook, *Ap. J.*, **113**, 684, 1951; **115**, 571, 1952.
(17) M. H. Davis, P. M. Routly and R. B. King, *Proc. Conf. Stellar Atm.*, p. 47, Indiana. 1954.
(18) L. Huldt and A. Lagerqvist, *J.O.S.A.*, **42**, 142, 1952.
(19) R. B. King, Private communication containing new results by G. D. Bell, M. H. Davis. P. M. Routly and R. B. King.
(20) R. B. King, *Ap. J.*, **95**, 78, 1942.
(21) H. Kopfermann and G. Wessel, *Z. f. Phys.*, **130**, 100, 1951.
(22) J. Hunaerts, *Ann. d'Ap.*, **10**, 237, 1947.
(23) C. W. Allen, *Astrophysical Quantities*, London, 1955.
(24) Charlotte E. Moore, *A Multiplet Table of Astrophysical Interest, Contr. Princeton Univ. Ob.*, No. 20, 1945.
(25) H. N. Russell, *Ap. J.*, **83**, 129, 1936.
(26) L. Goldberg, *Ap. J.*, **82**, 1, 1935; **84**, 11, 1936.
(27) A. G. Shenstone, *Phil. Trans.*, **241** A, **297**, 1948.
(28) R. D. Cowan and G. H. Dieke, *Rev. Mod. Phys.*, **20**, 418, 1948.

STATISTICAL DYNAMICS AND ACCRETION

J. M. A. Danby and G. L. Camm

(Received 1956 October 8)

Summary

In Part I we discuss the velocity distribution of a cloud of non-interacting particles in the gravitational field of a point mass. It is assumed that at great distances the velocity-distribution is Maxwellian, and that the cloud and the point mass are in uniform relative motion. Values are obtained for the density, for the mean velocity, and for the components of velocity-dispersion at points on the axis of symmetry near the centre of attraction.

These results are applied in Part II to the problem of accretion by stars of interstellar matter. It is found that, in the physical conditions usually assumed for interstellar matter, collisions between particles are relatively unimportant, and the rate of accretion is so extremely slow as to be negligible.

PART I.—THE MOTION OF A CLOUD OF PARTICLES IN A GRAVITATIONAL FIELD

1. *Introduction.*—The problem of the motion of a cloud of particles in the gravitational field of a star arises in connection with the theory of stellar accretion. It was considered many years ago by Eddington (**8**); later it was treated very differently by Hoyle and Lyttleton (**9, 10**), and their theory of accretion has been followed up more recently by Bondi (**2, 3**), Dodd (**5, 6**) and McCrea (**12**). As first presented, both theories of accretion were purely dynamical in form, but the assumptions underlying the mechanism which leads to accretion were so different that the conclusions reached were diametrically opposed.

Both theories were concerned with the behaviour of a cloud of particles in the gravitational field of a single star. Both suppose that the small particles in interstellar space whose behaviour they consider all have the same vector velocity at great distances from the star. This is clearly an over-simplification, and the main purpose of this paper is to examine the two theories when we assume that the particles have a Maxwellian distribution of velocities at great distances. Eddington assumed that the particles were effectively non-interacting, and he calculated the number of particles, per unit of time, which, moving in the gravitational field of the star, are deflected so as to strike its surface. For densities sufficiently low it is reasonable to ignore collisions, and Eddington's result is readily generalized (in Section 8) to cover the case in which the particles have a velocity distribution at great distances.

In the Hoyle–Lyttleton theory, it is supposed that particles will collide with each other on the leeward side of the accretion axis—the line through the centre of attraction parallel to the initial velocity vector of the particles. The effect of these collisions, which are inelastic, is to annihilate the velocity components perpendicular to the axis, and the consequent loss of kinetic energy will prevent many of the particles from escaping from the star's gravitational field. It is clear that if initially there is no dispersion of velocities then all particles will intersect the accretion axis and the density on the axis will be infinite. However, if there is a velocity dispersion, then the particles will not in general intersect the accretion axis, so that the density near the axis will be greatly reduced, and the likelihood of collisions is correspondingly lowered.

For densities sufficiently high it is certain that collisions are the controlling mechanism; in that case the problem of accretion is one of gas dynamics, and the methods of Bondi and Dodd are applicable. But the circumstances which lead to so high a density have still to be established, and this is our immediate aim. We first determine the velocity distribution and density of the interstellar particles near the centre of attraction in terms of the velocity distribution and density at great distances, on the assumption that the effects of collisions between particles may be ignored. A special case of this problem, when the cloud has no mean motion relative to the attracting mass, has already been solved by Eakin and McCrea (7).

2. *The dynamics of a system of particles in the presence of a point source of attraction.*—We first examine the behaviour of a system of particles under the attraction of a point mass. It is supposed that the particles do not affect each other, either by collision or by gravitational forces. This is clearly an over-simplification, but it is equivalent to assuming that the mean free path between such encounters or collisions is comparable with the radius of the sphere within which the attraction of the point mass seriously affects the behaviour of the particles. What this radius will be is not known, of course, until the problem is solved. It is also assumed that the motion of the point mass continues to be uniform, so that we are ignoring the gravitational attraction of the particles on the point mass, and also the transfer of momentum which would arise if particles were to strike the attracting mass. In these circumstances we can suppose that the centre of attraction is at rest, and at great distances the particles have a Maxwellian distribution of velocities, with the same mean vector velocity at each point. The system is also assumed to be steady, as if a cloud of infinite extent were streaming past the point mass.

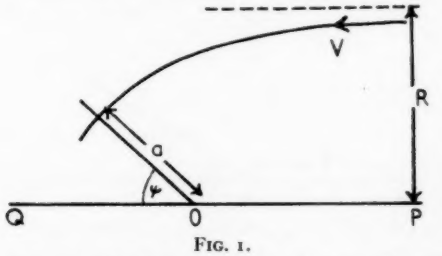

FIG. 1.

The density of the particles at any point can be calculated in two distinct ways. In the more direct method we consider first a stream of particles, all with the same vector velocity at infinity, and moving under the attraction of the point mass. At infinity all particles have velocity V in the direction parallel to OQ, where O is the centre of attraction. If ν is the number of particles per unit volume at infinity, then νV will cross unit area of the plane at infinity in unit time. All particles cross the cone of vertex O, axis OQ and semi-angle ψ at some point. We first examine those which enter this cone at a distance between a and $a+\delta a$ from the vertex. They all come from the cylindrical shell of radius R and thickness δR at infinity. If the gravitational force is μ/r^2 per unit mass, then the equation of a typical orbit in polar coordinates is

$$\frac{1}{r} = \frac{\mu}{R^2V^2}(1-\cos\theta) + \frac{1}{R}\sin\theta.$$

Consequently the relation between a and R is

$$\frac{1}{a} = \frac{\mu}{R^2V^2}(1+\cos\psi) + \frac{1}{R}\sin\psi. \tag{1}$$

Further,

$$\frac{\delta a}{a^2} = \frac{2\mu\delta R}{R^2V^2}(1+\cos\psi) + \frac{\delta R}{R^2}\sin\psi. \tag{2}$$

Now the total number of particles entering the element of the surface of the cone in unit time is $2\pi R\delta R\nu V$, and their normal velocity on crossing is RV/a. Thus the density at this part of the cone due to particles entering is

$$2\pi R\delta R\nu V/\{(RV/a)(2\pi a\sin\psi\,\delta a)\},$$

or

$$\frac{\nu\delta R}{\delta a}\operatorname{cosec}\psi.$$

Using equations (1), (2) we obtain for the density of entering particles the expression,

$$\tfrac{1}{2}\nu\left(\frac{2\mu}{aV^2}+\sin^2\frac{\psi}{2}\right)^{-1/2}\operatorname{cosec}\frac{\psi}{2}\left\{\frac{\mu}{aV^2}+\sin^2\frac{\psi}{2}+\sin\frac{\psi}{2}\left(\frac{2\mu}{aV^2}+\sin^2\frac{\psi}{2}\right)^{1/2}\right\}.$$

There are also particles which leave the cone through the element of surface $2\pi a\sin\psi\,\delta a$. By the same method we find that the number of particles per unit volume which are leaving the cone through the selected element is

$$\tfrac{1}{2}\nu\left(\frac{2\mu}{aV^2}+\sin^2\frac{\psi}{2}\right)^{-1/2}\operatorname{cosec}\frac{\psi}{2}\left\{\frac{\mu}{aV^2}+\sin^2\frac{\psi}{2}-\sin\frac{\psi}{2}\left(\frac{2\mu}{aV^2}+\sin^2\frac{\psi}{2}\right)^{1/2}\right\}.$$

Thus we obtain the particle density at (a,ψ) as

$$\nu\left(\frac{2\mu}{aV^2}+\sin^2\frac{\psi}{2}\right)^{-1/2}\operatorname{cosec}\frac{\psi}{2}\left(\frac{\mu}{aV^2}+\sin^2\frac{\psi}{2}\right). \tag{3}$$

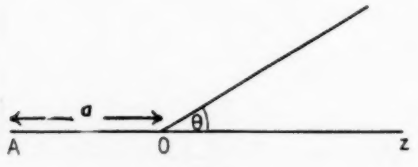

FIG. 2.

This result, which refers to a stream of particles all with the same vector velocity at infinity, can be extended to cover a much more general case. Let us suppose that the stream of particles which moves in the gravitational field of the point mass has a Maxwellian distribution of velocities with the same mean vector velocity at infinity. This system clearly will have axial symmetry about the line through the centre of attraction parallel to the mean motion. We take cartesian coordinates, x, y, z, with the origin, O, at the centre of attraction, and with the axis Oz directed towards the oncoming stream. The corresponding components of velocity are X, Y, Z: the velocity distribution function at infinity is

$$(2\pi)^{-3/2}\rho_0h^3\exp\{-\tfrac{1}{2}h^2[X^2+Y^2+(Z+c)^2]\}.$$

In this, ρ_0 is the density at infinity, $(-c)$ is the mean velocity, directed down the z-axis, and h^{-2} is the velocity-dispersion.

We shall confine our attention to the determination of the density of particles on the axis of symmetry. This is partly because we are reduced to the evaluation of a multiple integral, and on the axis of symmetry the evaluation is much simplified. It is also because on the axis the density will presumably take its maximum values.

We shall therefore evaluate the density at the point A, distant a from the centre of force, on the axis of symmetry, and on the leeward side. If in the velocity distribution function we put $X=-V\sin\theta\cos\phi$, $Y=-V\sin\theta\sin\phi$, $Z=-V\cos\theta$, we obtain the density at infinity of a stream of particles all moving with speed V along paths inclined at an angle θ to OA. In fact the number of particles per unit volume at infinity with speeds between V and $V+dV$, and moving in the solid angle $\sin\theta\,d\theta\,d\phi$ is

$$(2\pi)^{-3/2}\rho_0 h^3\exp\{-\tfrac{1}{2}h^2(V^2+c^2-2Vc\cos\theta)\}V^2\sin\theta\,d\theta\,d\phi\,dV.$$

Thus from (3) we see that the contribution which these particles make to the density at A is

$$(2\pi)^{-3/2}\rho_0 h^3\exp\{-\tfrac{1}{2}h^2(V^2+c^2-2Vc\cos\theta)\}\times\left(\frac{2\mu}{aV^2}+\sin^2\frac{\theta}{2}\right)^{-1/2}\operatorname{cosec}\frac{\theta}{2}\left(\frac{\mu}{aV^2}+\sin^2\frac{\theta}{2}\right)V^2\sin\theta\,d\theta\,d\phi\,dV.$$

The density at A is therefore the integral of this expression, and as the integration over ϕ is trivial, we have

$$\frac{\rho(a)}{\rho_0}=(2\pi)^{-1/2}h^3\int_{V=0}^{\infty}\int_{\theta=0}^{\pi}\left(\frac{\mu}{aV^2}+\sin^2\frac{\theta}{2}\right)\left(\frac{2\mu}{aV^2}+\sin^2\frac{\theta}{2}\right)^{-1/2}\times\exp\{-\tfrac{1}{2}h^2(V^2+c^2-2Vc\cos\theta)\}\sin\theta\operatorname{cosec}\frac{\theta}{2}V^2\,d\theta\,dV.$$

It is convenient to put $hV=u$, and to use two dimensionless parameters, defined by $p=hc$, $q^2=2\mu h^2/a$. In terms of these it is found that

$$\frac{\rho(a)}{\rho_0}=(2\pi)^{-1/2}\int_{u=0}^{\infty}\int_{\theta=0}^{\pi}\left(\frac{q^2}{u^2}+2\sin^2\frac{\theta}{2}\right)\left(\frac{q^2}{u^2}+\sin^2\frac{\theta}{2}\right)^{-1/2}\times\exp\{-\tfrac{1}{2}(u^2+p^2-2up\cos\theta)\}\cos\frac{\theta}{2}\,d\theta\,u^2\,du.$$

Finally, if we put $x=\sin\tfrac{1}{2}\theta$, we obtain

$$\frac{\rho(a)}{\rho_0}=\left(\frac{2}{\pi}\right)^{1/2}\int_{u=0}^{\infty}\int_{x=0}^{1}\exp\{-\tfrac{1}{2}(u-p)^2\}\exp\{-2upx^2\}\frac{q^2+2u^2x^2}{(q^2+u^2x^2)^{1/2}}\,dx\,du\,du. \quad (4)$$

It is evident that we can obtain an expression for the density at distance a on the "windward" side by similar methods—or we can simply reverse the direction of the mean motion. It is sufficient to change the sign of c, that is of p. On the windward side the density is given by

$$\frac{\rho(a)}{\rho_0}=\left(\frac{2}{\pi}\right)^{1/2}\int_{u=0}^{\infty}\int_{x=0}^{1}\exp\{-\tfrac{1}{2}(u+p)^2\}\exp\{2upx^2\}\frac{q^2+2u^2x^2}{(q^2+u^2x^2)^{1/2}}\,dx\,du\,du. \quad (5)$$

The behaviour of these two integrals is examined in some detail in Section 4.

3. *An alternative treatment.*—If we wish to find other properties of the stream of particles it is convenient to determine the velocity-distribution function at all points. Let us take cylindrical polar coordinates, ϖ, ϕ, z, with the origin at the centre of attraction, and the z-axis directed towards the streaming cloud of particles. The corresponding velocity components are Π, Φ, Z. From the rotational symmetry of the problem, the velocity-distribution will be independent of the angle ϕ. The velocity-distribution function $f(\varpi, z, \Pi, \Phi, Z)$, must satisfy

the generalized Boltzmann equation of continuity, which in these coordinates takes the form,

$$\Pi \frac{\partial f}{\partial \varpi} + Z \frac{\partial f}{\partial z} + \left(\frac{\Phi^2}{\varpi} - \frac{\mu \varpi}{r^3} \right) \frac{\partial f}{\partial \Pi} - \frac{\Pi \Phi}{\varpi} \frac{\partial f}{\partial \Phi} - \frac{\mu z}{r^3} \frac{\partial f}{\partial Z} = 0.$$

In this $r^2 = \varpi^2 + z^2$, and μ/r^2 is the force of attraction per unit mass.

It was pointed out by Jeans that f is simply a function of the first integrals of the set of equations,

$$\frac{d\varpi}{\Pi} = \frac{dz}{Z} = \frac{d\Pi}{\Phi^2/\varpi - \mu\varpi/r^3} = -\frac{d\Phi}{\Pi\Phi/\varpi} = -\frac{dZ}{\mu z/r^3}.$$

The appeal to Jeans' theorem has not been very productive in stellar dynamics, because it is rarely possible to find more than two of the integrals of the auxiliary equations. In the present case there are four integrals, all of which can be written down. They are:

$$\left.\begin{aligned} I_1 &= \Pi^2 + \Phi^2 + Z^2 - 2\mu/r, \\ I_2 &= \varpi\Phi, \\ I_3 &= (\Pi z - Z\varpi)^2 + r^2\Phi^2, \\ I_4 &= \Pi Z\varpi - z(\Pi^2 + \Phi^2) + \mu z/r. \end{aligned}\right\} \tag{6}$$

The first is related to the energy, the second to the angular momentum about the axis of symmetry, and the third to the modulus of the angular momentum vector.

The next problem is to find the function $f(I_1, I_2, I_3, I_4)$ which reduces at great distances to

$$(2\pi)^{-3/2}\rho_0 h^3 \exp\{-\tfrac{1}{2}h^2[\Pi^2 + \Phi^2 + (Z+c)^2]\}.$$

This can be done by using equations (6) to express Π, Φ and Z in terms of I_1, I_2, I_3, I_4, and r. The reduction is tedious, though quite straightforward. It introduces the angle θ, where $r\cos\theta = z$, $r\sin\theta = \varpi$, and we solve a quadratic equation for $\cos\theta$. This introduces a square root, the sign of which is ambiguous, and we therefore give this root a coefficient β, which will be either $+1$ or -1. Apart from this ambiguity, we can express

$$\Pi^2 + \Phi^2 + (Z+c)^2 = c^2 + 2cF(I_1, I_2, I_3, I_4, r) + I_1 + 2\mu/r.$$

Finally, if $F(I_1, I_2, I_3, I_4, r)$ tends to $G(I_1, I_2, I_3, I_4)$ as r tends to infinity, we have that $(c^2 + 2cG + I_1)$ is the combination of the four integrals which tends to $[\Pi^2 + \Phi^2 + (Z+c)^2]$ at great distances. We now replace the symbols I in this expression by their equivalent combination of space- and velocity-components. In this way, after much reduction, we determine the velocity-distribution function at any point to be

$$(2\pi)^{-3/2}\rho_0 h^3 \exp\left[-\tfrac{1}{2}h^2 \left\{ c^2 + I_1 + 2c\frac{I_1 Z - \beta I_1^{1/2}\mu r^{-1}\cos\theta + \beta I_1^{1/2} Z^2 \cos\theta + \beta I_1^{1/2} Z\Pi \sin\theta}{I_1 + \mu r^{-1} + \beta I_1^{1/2} Z\cos\theta + \beta I_1^{1/2}\Pi\sin\theta} \right\} \right], \tag{7}$$

where I_1 has been written for $(\Pi^2 + \Phi^2 + Z^2 - 2\mu/r)$, and $\beta^2 = 1$. With $c = 0$, this gives the expression obtained by Eakin and McCrea (7). It is obvious on inspection that this function gives the correct distribution of velocities at great distances. From the way it has been obtained, it must satisfy the equation of continuity—and by direct substitution it will be found to do so.

Clearly we can obtain the density at any point, or the mean velocity, or the dispersions in velocities, by making use of this velocity-distribution function,

but it is also plain that integrals involving the expression (7) are unlikely to be very tractable. We therefore confine attention to the axis of symmetry, on which $\sin\theta = 0$, and $\cos\theta$ is $+1$ on the windward side and -1 on the leeward. It should be noticed that, with $\sin\theta$ zero, the coefficient β is always multiplied by $\cos\theta$, so that if we change the sign of β we are changing from one side of the axis of symmetry to the other. Unfortunately it is not clear which side of the axis corresponds to $\beta = +1$. For the present, therefore, we shall put $\cos\theta = 1$, and retain β; so we have that on the axis of symmetry the velocity-distribution function is

$$f = (2\pi)^{-3/2}\rho_0 h^3 \exp\left[-\tfrac{1}{2}h^2\left\{c^2 + I_1 + 2c\frac{I_1 Z - \beta I_1^{1/2}(\mu r^{-1} - Z^2)}{I_1 + \mu r^{-1} + \beta I_1^{1/2} Z}\right\}\right].$$

The density is given by

$$\rho = \iiint f\, d\Pi\, d\Phi\, dZ.$$

To perform the integrations it is convenient to put

$$\Pi = V\sin\lambda\sin\nu, \qquad \Phi = V\sin\lambda\cos\nu, \qquad Z = V\cos\lambda.$$

The integration over ν is then trivial and we obtain the equation

$$\frac{\rho}{\rho_0} = (2\pi)^{-1/2}h^3 \iint \exp\left[-\tfrac{1}{2}h^2\left\{c^2 + V^2 - \frac{2\mu}{r} + 2c\frac{I_1 V\cos\lambda - \beta I_1^{1/2}(\mu r^{-1} - V^2\cos^2\lambda)}{I_1 + \mu r^{-1} + \beta I_1^{1/2} V\cos\lambda}\right\}\right] V^2\, dV\sin\lambda\, d\lambda.$$

The angle λ takes all values from 0 to π, and the speed V is positive and takes all values greater than $(2\mu/r)^{1/2}$. After some changes of the variables, and the introduction of the dimensionless parameters p and q used in the previous section, we obtain the expression for the density

$$\frac{\rho}{\rho_0} = \left(\frac{2}{\pi}\right)^{1/2}\int_{u=0}^{\infty}\exp\{-\tfrac{1}{2}(u-\beta p)^2\}\int_{x=0}^{1}\exp(-2\beta p u x^2)\,\frac{q^2 + 2u^2x^2}{(q^2 + u^2x^2)^{1/2}}\,dx\,u\,du. \qquad (8)$$

On comparison with the formulae (4) and (5), it is seen that the sign $\beta = 1$ corresponds to the leeward side, $\beta = -1$ to the windward side. This determines the sign of β in the formula (7), the expression for the velocity distribution.

4. *The determination of the density.*—The integral for the density can be handled simply in the case when $p = 0$, so that there is no mean motion. This is the case treated by Eakin and McCrea (7). We have

$$\begin{aligned}\frac{\rho}{\rho_0} &= \left(\frac{2}{\pi}\right)^{1/2}\int_{u=0}^{\infty}\exp(-\tfrac{1}{2}u^2)\int_{x=0}^{1}\frac{q^2 + 2u^2x^2}{(q^2 + u^2x^2)^{1/2}}\,dx\,u\,du,\\ &= \left(\frac{2}{\pi}\right)^{1/2}\int_{u=0}^{\infty}\exp(-\tfrac{1}{2}u^2)\,[x(q^2 + u^2x^2)^{1/2}]_0^1\,u\,du,\\ &= \left(\frac{2}{\pi}\right)^{1/2}\int_{0}^{\infty}\exp(-\tfrac{1}{2}u^2)\,(q^2 + u^2)^{1/2}\,u\,du,\\ &= \left(\frac{2}{\pi}\right)^{1/2}\int_{s=q}^{\infty}\exp[-\tfrac{1}{2}(s^2 - q^2)]\,s^2\,ds.\end{aligned}$$

For large values of q, the integral is expanded in asymptotic series, and we obtain the formula,

$$\frac{\rho}{\rho_0} = \left(\frac{2}{\pi}\right)^{1/2}[q + q^{-1} - q^{-3} + 3q^{-5} - 3\cdot 5q^{-7} + \ldots].$$

For small values of q, the integral can be expressed in ascending powers of q, in the form

$$\frac{\rho}{\rho_0} = \left(\frac{2}{\pi}\right)^{1/2}\left[\left(\frac{\pi}{2}\right)^{1/2}\exp(\tfrac{1}{2}q^2) - q^3/3 - q^5/3\cdot 5 - \dots\right].$$

When p is not zero, so that there is a streaming motion past the centre of attraction, we are primarily interested in the behaviour of ρ for large values of q, and small values of p. (It will be remembered that q^2 is inversely proportional to the distance from the centre of force.) Now the exponential terms in (8) are negligibly small except near $u=p$, $x=0$, in the case $\beta=+1$, or near $u=0$, $x=2^{-1/2}$ in the case $\beta=-1$. Thus, in the ranges of u and x where the integrand is not negligible, u^2x^2 is small compared with q^2. We shall therefore expand the integrand in descending powers of q, obtaining

$$\frac{\rho}{\rho_0} = \left(\frac{2}{\pi}\right)^{1/2} q\int_{u=0}^{\infty}\exp[-\tfrac{1}{2}(u-\beta p)^2]\int_{x=0}^{1}\exp(-2\beta pux^2) \times\left\{1+\sum_{n=1}^{\infty}(-1)^{n+1}\frac{(2n-2)!\,(2n+1)}{2^{2n-1}n!\,(n-1)!}\frac{u^{2n}x^{2n}}{q^{2n}}\right\}dx\,udu.$$

We write

$$\frac{\rho}{\rho_0} = \left(\frac{2}{\pi}\right)^{1/2} q\left[A_0+\sum_{n=1}^{\infty}(-1)^{n+1}\frac{(2n-2)!}{2^{2n-1}n!\,(n-1)!}A_n q^{-2n}\right], \tag{9}$$

where

$$A_n(p) = (2n+1)\int_{u=0}^{\infty}\exp[-\tfrac{1}{2}(u-\beta p)^2]\int_{x=0}^{1}\exp(-2\beta pux^2)\,x^{2n}\,dx\,u^{2n+1}\,du.$$

Of the several ways in which the functions $A_n(p)$ can be found, the simplest seems to be to make use of the differential equation satisfied by $A_n(p)$, namely,

$$4p^2\frac{d^2A_n}{dp^2}+4p(2n+1+p^2)\frac{dA_n}{dp}+(4n^2-1)A_n = (4n^2-1)\int_{u=0}^{\infty}\exp[-\tfrac{1}{2}(u+\beta p)^2]\,u^{2n+1}\,du. \tag{10}$$

The initial conditions are

$$A_n = 2^n n!, \quad \frac{dA_n}{dp} = -\beta\sqrt{\frac{\pi}{2}}\frac{(2n+1)!}{2^n n!}\left(\frac{2n-1}{2n+3}\right),$$

when $p=0$. This equation has been solved numerically for the special case $n=0$. For such other values of n as may seem necessary, say $n=1$, 2, 3, 4 and 5, it is best to make use of the three relations,

$$\left.\begin{aligned}
\frac{A_{n+1}}{2n+3} &= \frac{1}{4p}\frac{dA_n}{dp}+\left\{\frac{1}{4}+\frac{2n+1}{8p^2}\right\}A_n-\frac{2n+1}{8p^2}B_{2n+1}-\frac{\beta}{4p}B_{2n+2},\\
\frac{1}{(2n+3)^2}\frac{dA_{n+1}}{dp} &= -\frac{1}{8p^2}\frac{dA_n}{dp}-\frac{2n+1}{16p^3}A_n+\frac{2n+1}{8p^2}\beta B_{2n}\\
&\quad+\frac{2n+1}{4p}\left\{\frac{1}{4p^2}+\frac{1}{2n+3}\right\}B_{2n+1},\\
\frac{1}{(2n+3)^2}\frac{d^2A_{n+1}}{dp^2} &= \left\{\frac{2n+5}{8p^3}+\frac{1}{8p}\right\}\frac{dA_n}{dp}+\frac{(2n+1)(2n+5)}{32p^4}A_n\\
&\quad-\frac{\beta}{2n+3}\left\{\frac{(6n+5)(2n+1)}{8p}+\frac{(2n+1)(2n+3)(2n+5)}{16p^3}\right\}B_{2n}\\
&\quad-\frac{(2n+1)(2n+5)}{2n+3}\left\{\frac{2n+3}{32p^4}+\frac{1}{8p^2}\right\}B_{2n+1}
\end{aligned}\right\} \tag{11}$$

In these equations the quantities B_m which occur are functions of p, defined by the integral

$$B_m(p) = \int_0^\infty \exp[-\tfrac{1}{2}(u+\beta p)^2]\, u^m\, du.$$

It will be seen that

$$B_0(p) = \sqrt{\frac{\pi}{2}} - \beta \int_0^p \exp(-\tfrac{1}{2}x^2)\, dx,$$

$$B_1(p) = p \int_0^p \exp(-\tfrac{1}{2}x^2)\, dx + \exp(-\tfrac{1}{2}p^2) - \beta p \sqrt{\frac{\pi}{2}},$$

so that the values of these functions for different values of p can be readily obtained from tables of the error function. For the subsequent functions we make use of the recurrence relations

$$B_m = (m-1)B_{m-2} - \beta p B_{m-1}, \qquad m > 1.$$

Thus the procedure is to find values of the first few B's for different values of p. From these, and from the values of $A_0(p)$ and dA_0/dp obtained by numerical integration, we can use relations (11) to get values of A_1 and its first two derivatives. For each value of p these results can be checked from equation (10), the right-hand side of which is $(4n^2-1)B_{2n+1}$. These values of A_1 and dA_1/dp are now used to find A_2 and its first two derivatives. The procedure can be extended without difficulty, and it has been carried out as far as A_5.

It will be realized that the process has in effect to be carried out separately for the two values of β. The pairs of functions $A_n(\beta=+1)$ and $A_n(\beta=-1)$ behave quite differently. For $\beta=+1$, that is, on the leeward side, the functions B_n tend to zero rapidly as p increases. Indeed for large p,

$$B_m \sim m!\, p^{-m-1} \exp(-\tfrac{1}{2}p^2).$$

It is also found that as p increases, A_0 tends to a constant (which we shall show subsequently is $\pi/2$) and so we have from (11) that $A_{n+1}/A_n \to (2n+3)/4$ as p increases. Indeed it is found that, whereas $A_n(0) = 2^n n!$, the limit of A_n as p tends to infinity is $(2n+1)!\,\pi/n!\,2^{3n+1}$, which is smaller for $n>1$. Hence the series (9), which converges asymptotically quite rapidly for $q>3$, and p zero, will converge even more rapidly for $q>3$, and p large. We therefore obtain the functions $A_n(p)$ for large p by solving (10) in descending powers of p.

For $\beta=-1$, the problem cannot be tackled in this way. The integrals B_n increase rapidly with p, and we can show that

$$\underset{p\to\infty}{Lt}\ \{B_n/p^n\} = (2\pi)^{1/2}.$$

The function $A_0(p)$ decreases as p increases—in fact for large p,

$$A_0 \sim \tfrac{1}{2}\sqrt{\frac{\pi}{2}}\, p^{-1},$$

but the other A_n increase with p. It is found in fact that

$$\underset{p\to\infty}{Lt}\ \{A_n/p^{2n-1}\} = \tfrac{1}{2}\sqrt{\frac{\pi}{2}}(2n+1).$$

On comparing this result with equation (9), we may surmise that for large values of p and q, and for $\beta=-1$, the approximate value of ρ/ρ_0 is $\frac{1}{2}(q^2+2p^2)p^{-1}(q^2+p^2)^{-1/2}$. This will be confirmed by other methods.

5. *The determination of the density when the velocity of streaming is high.*—The method described for determining the density for small values of p would be difficult to justify if the value of p were large. An alternative method has been found, but it appears necessary to treat the windward and leeward sides of the axis separately. On the leeward side we have

$$\frac{\rho}{\rho_0} = \left(\frac{2}{\pi}\right)^{1/2} \int_0^\infty \exp\left[-\tfrac{1}{2}(u-p)^2\right] u\,du \int_0^1 \exp\left(-2pux^2\right) \frac{q^2+2u^2x^2}{(q^2+u^2x^2)^{1/2}}\,dx,$$

$$= \left(\frac{2}{\pi}\right)^{1/2} \int_0^\infty \exp\left[-\tfrac{1}{2}(u-p)^2\right] \int_0^u \exp\left(-2py^2/u\right) \frac{q^2+2y^2}{(q^2+y^2)^{1/2}}\,dy\,du.$$

In the inner integral we can replace the upper limit by infinity* thus adding to the right-hand side a quantity not exceeding $(2\pi)^{-1/2}qp^{-2}\exp\left(-\tfrac{1}{2}p^2\right)$. This is clearly negligible for q small and p large, and even for q and p large, but of the same order. The inner integral now becomes

$$\int_{y=0}^\infty \exp\left(-2py^2u^{-1}\right) \frac{q^2+2y^2}{(q^2+y^2)^{1/2}}\,dy,$$

$$= \tfrac{1}{2}q^2 \int_{t=0}^\infty \exp\left(-2pq^2u^{-1}\sinh^2\tfrac{1}{2}t\right)\cosh t\,dt,$$

$$= \tfrac{1}{2}q^2 \exp\left(pq^2u^{-1}\right) \int_0^\infty \exp\left(-pq^2u^{-1}\cosh t\right)\cosh t\,dt,$$

$$= \tfrac{1}{2}q^2 \exp\left(pq^2u^{-1}\right) K_1\left(pq^2u^{-1}\right).$$

Thus, for large values of p, the density is given by

$$\frac{\rho}{\rho_0} = \left(\frac{2}{\pi}\right)^{1/2} \int_0^\infty \exp\left[-\tfrac{1}{2}(u-p)^2\right] \tfrac{1}{2}q^2 \exp\left(pq^2u^{-1}\right) K_1\left(pq^2u^{-1}\right) du.$$

If we now put $u=p(1+z)$, the expression can be written as

$$\frac{\rho}{\rho_0} = (2\pi)^{-1/2} pq^2 \int_{-1}^\infty \exp\left(-p^2z^2\right) \exp\left[q^2/(1+z)\right] K_1\left\{q^2/(1+z)\right\} dz.$$

This integral can be expanded in inverse powers of p, using Watson's Lemma. The leading term is independent of p, so that for large values of p,

$$\frac{\rho}{\rho_0} \sim q^2 \exp\left(q^2\right) K_1\left(q^2\right),$$

and if q is also large, we obtain

$$\frac{\rho}{\rho_0} \sim \left(\frac{\pi}{2}\right)^{1/2} \left[q + \frac{3}{8}q^{-1} - \frac{15}{128}q^{-3} + \ldots\right].$$

This result confirms that the method described in the previous section can be applied to find the density on the leeward side even when p is large. We can therefore find (and use) the asymptotic form of $A_n(p)$ for large p, determined by equation (10).

With $\beta=-1$, the value corresponding to the windward axis, the integral must be treated rather differently. We write $q=s\cos\alpha$, $p=s\sin\alpha$, and for $0<\alpha<\pi/2$, and for large values of s, we examine the integral

$$\frac{\rho}{\rho_0} = \left(\frac{2}{\pi}\right)^{1/2} \int_{u=0}^\infty \exp\left[-\tfrac{1}{2}(u+s\sin\alpha)^2\right] \int_{x=0}^1 \exp\left(2sux^2\sin\alpha\right)$$

$$\times \frac{s^2\cos^2\alpha+2u^2x^2}{(s^2\cos^2\alpha+u^2x^2)^{1/2}}\,dx\,u\,du.$$

* The authors are indebted to Professor M. J. Lighthill, F.R.S., for suggesting the method which follows.

After some changes of variable, this can be written in the form

$$\frac{\rho}{\rho_0} = \left(\frac{2}{\pi}\right)^{1/2} s^3 \sin^2\alpha \int_{-1}^{\infty} \exp\left(-\tfrac{1}{2}s^2 z^2 \sin^2\alpha\right)(1+z) \int_0^{\pi/2} \exp\left[-2s^2 \sin^2\alpha(1+z)\sin^2\theta\right] \times \frac{\cos^2\alpha + 2\sin^2\alpha(1+z)^2\cos^2\theta}{\{\cos^2\alpha + \sin^2\alpha(1+z)^2\cos^2\theta\}^{1/2}} \sin\theta\, d\theta\, dz.$$

This also can be evaluated for large values of s, again using Watson's Lemma, and, after considerable algebra, we obtain the result

$$\frac{\rho}{\rho_0} = \frac{1+\sin^2\alpha}{2\sin\alpha} + \frac{\cos^4\alpha(1+6\sin^2\alpha)}{8s^2\sin^3\alpha} + \frac{\cos^4\alpha(7+9\sin^2\alpha+210\sin^6\alpha)}{32s^4\sin^5\alpha} + \ldots .$$

It is now convenient to tabulate ρ/ρ_0 as a function of p and q. It should be remembered that $p = hc$ and is thus the ratio of the mean speed to the root-mean-square speed of the particles at a great distance. The quantity q is $\sqrt{(2\mu h^2/r)}$, where μ/r^2 is the attraction per unit mass at a distance r. The first column of the table gives values of r in astronomical units. They have been calculated for the case in which the gravitational field is assumed to be the same as that of the Sun, and the root-mean-square velocity at infinity (h^{-1}) is assumed to be 1 km/sec. (This corresponds to a temperature of about 120 deg.) With these values of h and μ the value of q which corresponds to $r = 1$ astronomical unit is

TABLE I

The variation of density (ρ/ρ_0) as a function of distance from the centre of attraction and of the mean speed at infinity

	r (astr. units)	q \ p	0·0	0·5	1·0	2·0	3·0	4·0	7·0	10·0	∞
Windward axis	100	4·21	3·54	2·87	2·26	1·47	—	—	—	—	1·00
	50	5·96	4·88	3·91	3·02	1·87	—	—	—	—	1·00
	25	8·43	6·82	5·42	4·14	2·46	1·72	1·40	1·11	1·04	1·00
	10	13·3	10·7	8·46	6·42	3·70	2·48	1·92	1·31	1·14	1·00
	5	18·8	15·1	11·9	9·02	5·14	3·38	2·56	1·62	1·30	1·00
	2	29·8	23·8	18·8	14·2	8·04	5·32	3·90	2·31	1·73	1·00
	1	42·1	33·6	26·5	20·1	11·3	7·34	5·44	3·15	2·26	1·00
	0·5	59·6	47·5	37·5	28·3	16·0	10·3	7·64	4·37	3·11	1·00
	0·2	94·2	75·2	59·3	44·8	25·3	16·3	12·0	6·82	4·80	1·00
	0·1	133·2	106·3	83·9	63·3	35·7	23·0	17·0	9·61	6·73	1·00
	0·05	188·4	150·3	118·6	89·6	50·5	32·6	24·0	13·6	9·48	1·00
	0·01	421·3	336·2	265·2	200·3	112·9	72·8	53·7	30·3	21·1	1·00
Leeward axis	0·01	421·3	336·2	401·7	452·5	504·7	519·3	523·5	526·7	527·4	528·0
	0·05	188·4	150·3	179·6	202·4	225·7	232·2	234·1	235·5	235·8	236·1
	0·1	133·2	106·3	127·0	143·1	159·6	164·2	165·5	166·5	166·7	166·9
	0·2	94·2	75·2	89·8	101·2	112·8	116·1	117·0	117·7	117·9	118·1
	0·5	59·6	47·5	56·8	64·0	71·4	73·4	74·0	74·5	74·6	74·7
	1	42·1	33·6	40·2	45·3	50·5	51·9	52·4	52·7	52·7	52·8
	2	29·8	23·8	28·4	32·0	35·7	36·7	37·0	37·3	37·3	37·3
	5	18·8	15·1	18·0	20·3	22·6	23·2	23·4	23·6	23·6	23·6
	10	13·3	10·7	12·7	14·3	16·0	16·5	16·5	16·7	16·7	16·7
	25	8·43	6·82	8·11	9·12	10·2	10·4	10·5	10·6	10·6	10·6
	50	5·96	4·88	5·79	6·50	7·22	7·43	7·48	7·53	7·54	7·54
	100	4·21	3·54	4·17	4·66	5·17	5·31	5·35	5·38	5·38	5·39

42·1. In the third and subsequent columns are given the values of ρ/ρ_0 at different points on the axis for various values of p. The upper half of the table corresponds to the windward side of the axis, and the lower half to that part which lies beyond the centre of attraction.

There are several features of this table which call for comment. It is seen that on the windward side the density increases extremely slowly as we approach the centre of attraction unless the mean speed of the stream is very small. On the leeward side the increase of density is fairly rapid and becomes rather more rapid as the speed increases. However the density distribution is altered very little for values of p greater than 2. For a given q, ρ/ρ_0 decreases monotonically as p changes from $-\infty$ to $+\infty$.

It is not clear from the table whether the condensation which is particularly noticeable on the leeward side extends far beyond the range of distances included. The methods used do not lend themselves to the determination of density for small values of q except in the three cases of $p=0$, and $p\to\infty$ on either axis. Some results in these cases are given below. It will be seen from this table that the density at distances beyond 1000 astronomical units is very little in excess of the density at infinity.

TABLE II

The variation of density at large distances

r (astr. units)	500	1000	2000
q	1·884	1·332	0·942
$p=+\infty$ (windward axis)	1·00	1·00	1·00
$p=0$	1·86	1·41	1·29
$p=+\infty$ (leeward axis)	2·59	1·98	1·58

The assumptions which underlie these calculations may be repeated. It is assumed that a uniform stream of particles has taken up a steady state, solely under the attraction of a point mass which is at rest. In these hypothetical conditions we ignore for the moment such things as radiation pressure and the possible effects of collisions. The distances along the axis to which the tables refer are determined by the values of q, and also by the values assumed for the mass of the attracting particle and the velocity dispersion of the stream at infinity. A change in either of these quantities would lead to a different relation between r and q. It is for this reason that it was thought necessary to determine the density for a very large range of values of q.

6. *The velocity dispersion.*—Since we shall need to consider the possibility of close encounters between particles, it is necessary to get a measure of the velocity dispersion, and how it increases near the centre of force. Again we confine attention to the axis of the system, in order to be able to evaluate the integrals without too much difficulty. To obtain $\rho\overline{Z}$, $\rho\overline{\Pi^2}$ or $\rho\overline{Z^2}$, we multiply the velocity-distribution function (7) by Z, Π^2 or Z^2, and integrate over all values of the velocity components. The integrals are evaluated by the methods used in Section 4 to determine the density. Attention is confined to small values of the parameter p, and large values of q, that is, to the case when the mean motion is relatively small, and to the region near the centre of force.

TABLE III

The variation of the mean speed $(h\overline{Z})$ along the axis as a function of distance from the centre of attraction and of the mean speed at infinity

r (astr. units)	q \ p	2	1	0
100	4·21	−2·980	−1·268	0
10	13·3	−3·167	−1·296	0
1	42·1	−3·221	−1·302	0
1	42·1	−1·930	−0·974	0
10	13·3	−1·930	−0·974	0
100	4·21	−1·935	−0·977	0

Some values of the mean velocity and of the velocity dispersions parallel to the axis (σ_Z) and perpendicular to it (σ_π) are given in Tables III and IV. The qualitative behaviour of these quantities could have been predicted. On the windward axis there is a streaming motion towards the centre of attraction; the mean velocity is greater than at infinity. On the leeward side the streaming is perpendicular to the axis, and the mean velocity is reduced. The tables also suggest that for values of r exceeding, say, 200 astronomical units, the velocity distribution will be effectively Maxwellian.

TABLE IV

The variation of the velocity dispersions at points on the axis

r (astr. units)	$p=2$		$p=1$		$p=0$
	$h\sigma_\pi$	$h\sigma_Z$	$h\sigma_\pi$	$h\sigma_Z$	$h\sigma_\pi=h\sigma_Z$
100	1·62	3·23	2·11	3·17	2·57
10	4·13	11·77	6·11	10·18	7·74
1	12·73	38·02	19·17	34·27	24·34
1	28·81	10·82	27·38	16·68	24·34
10	9·15	3·55	8·69	5·35	7·74
100	3·00	1·46	2·86	1·91	2·57

PART II.—THE ACCRETION OF INTERSTELLAR MATTER

7. *The application to particles in interstellar space near an attracting star.*—We now apply the results of the preceding sections to different types of particle present in interstellar space. Of the two main points to consider, the first is whether the assumption required in the earlier sections—of non-interaction between particles—can be justified. If it can, we are able to estimate the density and velocity dispersion near the star. The remaining question to discuss is whether conditions near the star lead to so high a collision rate that accretion is necessarily a phenomenon in gas dynamics. In fact, it appears that, in the physical conditions normally assumed for interstellar matter, our hypothesis that the particles do

not interact has provided us with a very good approximation for the density distribution of matter in which collisions occur. Further, even in the region near the star where the approximation is not so convincing, it seems unlikely that collisions are so frequent as to necessitate the use of gas dynamics.

Data about the interstellar particles have been conveniently summarized by Spitzer (**13**). We shall need to distinguish between the H I regions, in which the hydrogen atoms are almost all non-ionized, and the H II regions, where they are ionized. We shall suppose, at any rate in the first instance, that the attracting star has the same mass as the Sun. In the H I regions the density of hydrogen atoms is estimated at 10 per cm^3; this corresponds to a mean free path of 20 ast. units. The temperature, originally given by Spitzer as 50 deg. K, is now considered to be about 125 deg. K (**15**). We assume a value of 120 deg. K, which gives the value of h^{-1} as 1 km/sec. With a gravitational field due to one solar mass, and with this temperature, the parameter q of the previous sections is related to the distance from the attracting star as in the first two columns of Table I. From the earlier calculations we conclude that at distances exceeding 200 ast. units the velocity-distribution of the hydrogen atoms is effectively Maxwellian. Although individual atoms will be involved in collisions, these will serve to maintain the Maxwellian distribution which is predicted by the present treatment, in which collisions have been ignored. Within 200 ast. units, the theoretical distribution departs further from the Maxwellian form, whereas in practice collisions become rather more frequent, for the mean free path within 200 ast. units is rather less than 10 ast. units. This implies that the method we have used is not strictly applicable at this short range. This can be verified much more directly. If we assume that the mean motion is zero at infinity, we can calculate (see the Appendix) the average number of collisions per unit volume per unit time, assuming that the velocity distribution is given by (7), with the constant c put equal to zero. We can also find the average number of collisions per unit volume per unit time in which one of the two particles loses sufficient energy to be temporarily "captured", i.e. so that its speed W becomes less than $(2\mu/r)^{1/2}$. It is only within about 200 ast. units that a large proportion of collisions lead to captures and therefore set up a velocity distribution seriously different from (7). The proportion of collisions which lead to captures is independent of the density, but the average number of collisions per unit volume per unit time is proportional to the square of the density. Consequently the expression (7) is reasonably accurate for $r>200$ ast. units even at much higher densities than we have considered. On the other hand for lower densities the number of collisions per unit volume per unit time falls off rapidly, so that although a high proportion of collisions will lead to temporary captures, the actual velocity distribution will not be affected seriously even at distances less than 200 ast. units.

Although the method we have used is not strictly applicable for un-ionized hydrogen atoms within 200 ast. units of the attracting star, we can make some useful deductions about the hydrogen atoms within this distance. In the first place it is clear that collisions are almost perfectly elastic. This contradicts the Hoyle–Lyttleton theory, in which collisions on the accretion axis are supposed to cause an actual loss of kinetic energy. In fact, if the collisions were completely inelastic, then the kinetic energy destroyed in this way—and presumably reappearing as radiation—would be sufficient to ensure that four cubic parsecs of un-ionized interstellar hydrogen would radiate more energy per second than

does the Sun. This seems to be far in excess of the energy output in the 21 cm band, or of any other interstellar radiation.

It is also apparent that although within 200 ast. units most collisions lead to captures these will usually be of a temporary nature. Many of the atoms which are so captured have kinetic energy little below that required to escape (see Appendix). They are likely to be involved in further collisions, most likely with atoms of much higher energy, and may well therefore recover much of the energy they originally lost. There is the further point that the average number of collisions experienced by any one particle is relatively small. If we confine our attention to the case of zero mean motion we can make a rough estimate in the following way. The mean free path is inversely proportional to the density which, at small distances from the centre of attraction, varies as $r^{-1/2}$. Thus $\lambda(r)$, the mean free path at a distance r, is $\lambda(a)(r/a)^{1/2}$. Let us consider the average

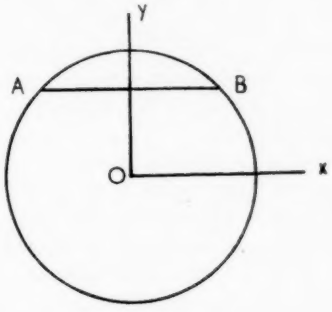

FIG. 3.

number of mean free paths per chord of a sphere of radius a. The number of mean free paths along the chord AB is given by

$$2\int_{x=0}^{(a^2-y^2)^{1/2}} \frac{dx}{\lambda(r)}, \qquad = \frac{2a^{1/2}}{\lambda(a)}\int_{x=0}^{(a^2-y^2)^{1/2}} r^{-1/2}\,dx.$$

The average number of free paths along any chord is then found to be

$$\frac{2a^{1/2}}{\lambda(a)}\int_{y=0}^{a}\frac{2y}{a^2}\left\{\int_{x=0}^{(a^2-y^2)^{1/2}} r^{-1/2}\,dx\right\}dy, \qquad = \frac{8}{5}\frac{a}{\lambda(a)}.$$

Hence the average number of mean free paths per chord of a sphere of radius 200 ast. units is about 30. This overlooks the fact that the actual orbits of particles between collisions are curved towards the centre of attraction, and that the direction of motion of a particle is changed at each collision. Of course, if the stream of particles has a mean motion, then this figure would be considerably reduced. The frequency of collisions depends on the velocity dispersion, but not on the mean motion. If the latter is large, the average distance travelled between two collisions would be very much larger than in the case of zero mean motion. For these higher speeds it would be better to estimate the number of collisions by dividing the average time taken to cross the region of relatively high density by the average time between two collisions. This gives a much smaller figure for the average number of collisions in a sphere of radius 200 ast. units.

The grains of interstellar dust in the H I regions present no serious difficulty. Were gravitation the only force acting on them, they would certainly need to be

taken into consideration, not only on their own account, but more particularly because of the possible effects of collisions between hydrogen atoms and dust particles. However, it is clear that the force of radiation from the star on these grains will in general greatly exceed the gravitational attraction, except in regions where the density of grains is so high that a certain amount of screening occurs.

So far, we have only considered un-ionized hydrogen atoms and dust grains. However it has been shown by Strömgren (**14**) that the brighter stars at least are surrounded by a large sphere in which all the hydrogen is ionized. For O and B type stars the radius of this sphere is of the order of parsecs, rather than ast. units. It now seems clear that for stars with an ionized envelope exceeding about 200 ast. units in radius, the effect of collisions in the un-ionized material outside can be neglected. Near the boundary of the ionized sphere there will be interaction between the neutral hydrogen from outside and the protons and radiation inside. The neutral hydrogen cannot penetrate far before it is ionized; the protons cannot escape far before recombination occurs. The boundary between the outer H I and inner H II regions is quite sharp. The dust grains do not come into consideration here, for in a region where the radiation is sufficiently energetic to ionize all the hydrogen, the radiation pressure will certainly repel the dust particles.

Within the H II region the density is about 1 proton per cm^3. As a result of the strong radiation the temperature is of the order of 10^4 deg. K, so that the root-mean-square velocity is about 9 km/sec. Unless the H II region is very small indeed, the ionization of incoming atoms will re-establish a Maxwellian velocity-distribution. Outside the region there is a mean streaming motion of the interstellar matter; this may persist to some extent inside, but it is likely to be checked by radiation pressure, and it seems more probable that the mean velocity within the sphere will be reduced. The sphere itself may be somewhat deformed by the external streaming. Even if streaming persists within the H II region, the parameter p, by which it is measured, will be small, for $p = hc$, and even if c, the mean velocity, is comparable with its value in the H I regions, the constant h is only one-ninth of its value outside. This reduction in the value of h enables us to deduce the velocity distribution in the H II regions at any rate approximately. Whereas in an H I region the parameter q takes the value 1·88 at 500 ast. units, in an H II region the value at this distance is only 0·21. If therefore the H II region has a radius of 500 ast. units—and this is a very modest figure—the Maxwellian distribution which is set up there differs insignificantly from our theoretical distribution, (7), which is only truly Maxwellian at infinity. We can therefore deduce that the more serious departures from the Maxwellian distribution which occur at $q = 3$ correspond to a distance of 2·5 ast. units—which is less than the radius of many O and B type stars.

In the H II regions, actual collisions between protons are extremely rare, but there will be close encounters between them, in which the electrostatic repulsions will produce deflections. The mean free path for the protons can be calculated by the method Chandrasekhar (**4**) has used in finding the mean free path for star systems, in which a star is deflected by the gravitational attraction of a near neighbour. The method leads to a formula for λ, the mean free path, namely

$$\lambda = K\overline{v^2}^2 m^2/\rho e^4 \log\{4mD\overline{v^2}/\pi e^2\},$$

where e and m are the charge and mass of the proton, $\overline{v^2}$ is the mean square

velocity, ρ is the number of protons per cm^3, D is the mean distance between protons, and K is constant. In the outer part of the H II regions, the value of λ is about 0·5 ast. units. However, it should be noted that, whereas for uncharged particles the mean free path between collisions varies inversely as the density, and is independent of the speed, for protons the mean free path between encounters varies inversely as the density, and more or less directly as the fourth power of the root-mean-square velocity. In these circumstances, the mean free path actually increases as the protons approach the star. At 2·5 ast. units ($q=3$), the mean free path has already risen to 2·5 ast. units. For smaller values of r, we have that $\rho \propto r^{-1/2}$, and $\overline{v^2} \propto r^{-1}$. If we use these approximations to find the average number of mean free paths per chord of a sphere of radius 2·5 ast. units, the value comes out to be 0·9. At $r=1$ ast. unit, the average number of mean free paths per chord is 0·12, so that only one proton in eight which enter this sphere will experience an encounter before leaving. It therefore seems to be established that encounters in the H II regions will not be frequent, and a theory which ignores encounters completely will not be seriously in error.

The calculations of this section have been based on the assumption that the attracting star has the same mass as the Sun. Now the parameter q is proportional to $(m/r)^{1/2}$, so that doubling the mass of the attracting star will produce the same density and velocity-distribution at twice the distance. For the bright stars which are surrounded by H II regions, an increase in mass would lead to an increase in the mean free path at a given distance. We may therefore conclude that collisions scarcely affect the motion at all in the H II regions, whatever the mass.

For those stars whose radiation is insufficient to ionize the hydrogen round them, collisions may be more effective for the more massive stars. As we have seen, for hydrogen atoms, the average number of mean free paths per chord of a sphere of radius 200 ast. units round a star with the Sun's mass is about 30, and the number varies as the square root of the mass. This, however, rather underestimates the effect of increasing mass, for the radius of the sphere in which a collision is likely to lead to a temporary capture also varies as the square root of the attracting mass. Thus the average number of mean free paths per chord of the sphere within which collisions are likely to lead to temporary captures varies directly as the mass of the attracting star.

It therefore seems possible that some hydrogen atoms will lose sufficient energy by collision to be captured by the gravitational field of the star, and that the rate of capture will be proportional to the mass of the star. The method we have used in this investigation does not reveal the rate of this accretion, but there are two reasons for supposing that it will be small. In the first place, since the kinetic energy is only exchanged at a collision, the average kinetic energy in any region will certainly exceed the energy of escape. Thus in the region within 200 ast. units, where, as we have seen, there will be some atoms which have been temporarily captured, further collisions between these and the fast-moving atoms will often raise the kinetic energy of the captured atoms above the escape level again. It is extremely important to distinguish between capture and accretion. A particle only undergoes accretion when it strikes the attracting star. Its kinetic energy may or may not exceed the escape energy. A particle is captured when, as a result of collisions, its kinetic energy falls below the escape energy. It is not automatically doomed to fall into the star, but at

least until involved in another collision it cannot escape to great distances. Since the paths of captured particles are entirely within regions of rather higher density, the frequency of subsequent collisions will be higher, but such collisions may raise the kinetic energy again. It is, of course, true that loss of energy is likely to make a particle pass closer to a star, where it is more likely to collide with other low-energy particles. And each such inward move increases the probability that a further collision will set the particle off on an orbit which meets the star. (In this connection it seems reasonable that the rate of accretion should be a function of the star's radius, and should increase with radius.) If we knew more precisely how the velocity-distribution is modified by collisions, we could estimate the rate at which atoms become more or less permanently captured. Presumably very near the star the atoms approach a Maxwellian velocity-distribution, provided the original density at infinity is sufficiently large, but the region which seems to be vital to the problem is the one in which collisions affect the velocity-distribution, but are not sufficiently frequent to produce a Maxwellian distribution.

The second feature which we have left aside, but which may well prevent any rapid accretion is the existence of the dust grains. These, we have explained, will actually be repelled by radiation pressure. They will scarcely be affected by collisions with the hydrogen atoms which have a much smaller mass, but the atoms may well be affected by such collisions. The grains in fact serve to check the inflow of hydrogen, and in clouds where the density of dust grains is high, the grains may prevent most of the hydrogen from approaching the star. Circumstances which favour this situation are either weak radiation or large mass, so that a barrier of dust grains forms relatively close to the star.

We can therefore conclude that in H II regions generally, and in the H I regions surrounding stars of relatively small mass, collisions do not appreciably affect the motion of the interstellar particles. In the H I regions round massive stars, collisions are likely to affect the motion, but they will not necessarily lead to a large scale accretion of hydrogen by the star.

8. *The modification of Eddington's treatment to allow for a velocity-distribution in the cloud.*—Since we have shown that collisions will not in general seriously affect the motion of particles in an interstellar cloud, we can calculate the rate of accretion by generalizing Eddington's result, so as to allow for a Maxwellian distribution of velocities at infinity. (The rate of accretion for non-interacting particles has in fact already been given by Eakin and McCrea (**7**), but the method which follows is more direct.) Let $N(V, \theta, \phi)$ be the number of particles per unit volume in the cloud approaching the star from infinity with velocity V in the direction (θ, ϕ). The rate of accretion for these particles is, by Eddington's formula,

$$\pi r_0^2[V + 2\mu/r_0 V]N(V, \theta, \phi),$$

where r_0 is the radius of the star, and μ/r^2 is the gravitational intensity which it produces. If we assume a velocity distribution at infinity of the form

$$(2\pi)^{-3/2}\rho_0 h^3 \exp[-\tfrac{1}{2}h^2(V^2 + c^2 - 2Vc\cos\theta)],$$

where c is the mean velocity of the star in the cloud, then

$$N(V, \theta, \phi) = (2\pi)^{-3/2}\rho_0 h^3 \exp[-\tfrac{1}{2}h^2(V^2 + c^2 - 2Vc\cos\theta)]V^2 \sin\theta,$$

and the total rate of accretion is

$$\pi r_0^2(2\pi)^{-3/2}\rho_0 h^3 \int_{V=0}^{\infty}\int_{\theta=0}^{\pi}\int_{\phi=0}^{2\pi}(V+2\mu/r_0V) \times \exp[-\tfrac{1}{2}h^2(V^2+c^2-2Vc\cos\theta)]V^2\sin\theta\,dV\,d\theta\,d\phi,$$

$$= \left(\frac{\pi}{2}\right)^{1/2} r_0^2\rho_0 h^3 \int_0^{\infty}\int_0^{\pi}(V^2+2\mu/r_0)\exp[-\tfrac{1}{2}h^2(V^2+c^2-2Vc\cos\theta)]V\sin\theta\,dV\,d\theta.$$

Now

$$\exp[-\tfrac{1}{2}h^2(V^2+c^2-2Vc\cos\theta)] = \exp[-\tfrac{1}{2}h^2(V^2+c^2)]\sum_{n=0}^{\infty}\frac{(h^2Vc\cos\theta)^n}{n!},$$

so the integral becomes

$$\left(\frac{\pi}{2}\right)^{1/2} r_0^2\rho_0 h^3\exp(-\tfrac{1}{2}h^2c^2) \times \sum_{n=0}^{\infty}\frac{h^{2n}c^n}{n!}\int_0^{\infty}\int_0^{\pi}\exp(-\tfrac{1}{2}h^2V^2)(V^{n+3}+2\mu V^{n+1}/r_0)\cos^n\theta\sin\theta\,dV\,d\theta.$$

This may be integrated term by term, and reduces to

$$(2\pi)^{1/2}r_0^2\rho_0\exp(-\tfrac{1}{2}h^2c^2\sum_{n=0}^{\infty}\left[\frac{2}{h}\frac{(n+1)(ch)^{2n}}{1\cdot3\cdot5\ldots(2n-1)(2n+1)} + \frac{2\mu h}{r_0}\frac{(ch)^{2n}}{1\cdot3\cdot5\ldots(2n-1)(2n+1)}\right].$$

As before, we put $p=hc$, and $q_0^2=2\mu h^2/r_0$, and then the rate of accretion becomes

$$(2\pi)^{1/2}r_0^2\rho_0 h^{-1}[2f_1(p)+q_0^2f_2(p)].$$

For small values of p, f_1 and f_2 may be expressed as

$$f_1(p)=\frac{1}{2}\left\{\exp(-\tfrac{1}{2}p^2)+(p+p^{-1})\int_0^p\exp(-\tfrac{1}{2}y^2)\,dy\right\} = -\sum_0^{\infty}\frac{(-1)^np^{2n}}{2^nn!(4n^2-1)},$$

$$f_2(p)=\frac{1}{p}\int_0^p\exp(-\tfrac{1}{2}y^2)\,dy=\sum_0^{\infty}\frac{(-1)^np^{2n}}{2^nn!(2n+1)};$$

if p is large, then we have

$$f_1(p)=(\tfrac{1}{8}\pi)^{1/2}\left(p+\frac{1}{p}\right)-\frac{1}{p^2}\exp(-\tfrac{1}{2}p^2)+\ldots,$$

$$f_2(p)=(\tfrac{1}{2}\pi)^{1/2}\frac{1}{p}-\frac{1}{p^2}\exp(-\tfrac{1}{2}p^2)+\ldots.$$

For normal values of M, r_0 and h, $q_0^2\gg1$ (see Table I), so the rate of accretion may be taken as

$$(2\pi)^{1/2}r_0^2\rho_0h^{-1}q_0^2f_2(p),$$

or

$$(8\pi)^{1/2}MGr_0\rho_0hf_2(p).$$

Graphs of $h.f_2(p)$ are given for various values of h and c in Fig. 4, and it will be seen that the introduction of the velocity distribution to Eddington's model (which is equivalent to $h^{-1}=0$) reduces the rate of accretion, and that this rate is a maximum for $p=0$, or $c=0$, when it is given by $(8\pi)^{1/2}MGr_0\rho_0h$. This is the rate of increase of the mass of the star due to accretion, so we may take

$$M\Big/\frac{dM}{dt}=(8\pi)^{-1/2}(Gr_0h\rho_0)^{-1}.$$

Values of this function for standard spectral types are given in Table V. The quantities r_0 for the different spectral types are those provided by Allen (1).

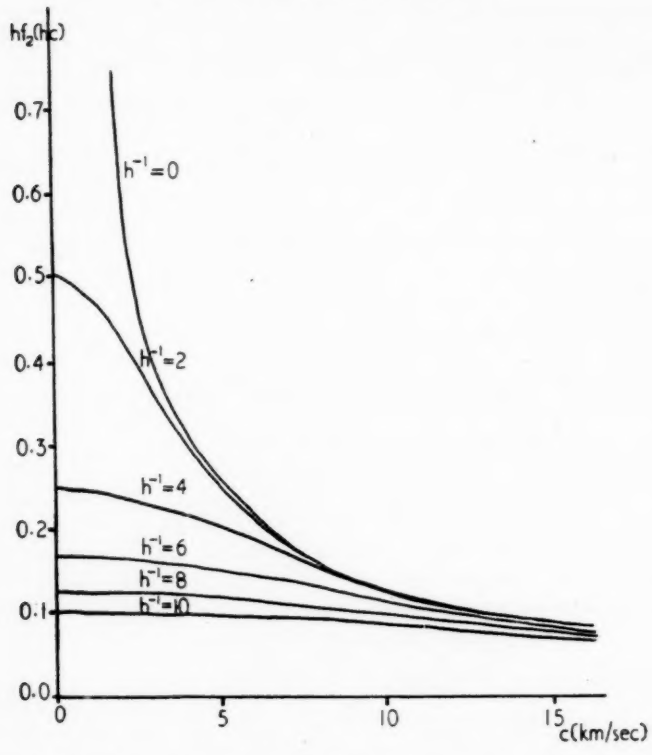

FIG. 4.—*The rate of accretion, measured by the function* $hf_2(hc)$, *as a function of the mean speed,* c, *for different values of the velocity-dispersion* h^{-1}.

TABLE V

Inverse rates of accretion for different spectral types. The quantity tabulated is $M\Big/\frac{dM}{dt}$, *in years, and the separate columns refer to supergiants, giants and dwarfs*

Sp	*S*—*g*	*g*	*d*	
O5	...	$6{\cdot}7\times10^{16}$		Stars in H II regions
B0	$6{\cdot}7\times10^{16}$	$1{\cdot}5\times10^{17}$		
B5	$4{\cdot}2\times10^{16}$	$3{\cdot}5\times10^{17}$		
A0	$3{\cdot}4\times10^{16}$	$6{\cdot}0\times10^{17}$		
A5	$2{\cdot}7\times10^{16}$	$7{\cdot}7\times10^{17}$		
F0	$2{\cdot}1\times10^{16}$	$9{\cdot}1\times10^{17}$		
F0	$1{\cdot}3\times10^{14}$	$5{\cdot}5\times10^{15}$		Stars in H I regions
F5	$1{\cdot}0\times10^{14}$	$6{\cdot}7\times10^{15}$		
G0	$8{\cdot}2\times10^{13}$	$8{\cdot}0\times10^{14}$	$8{\cdot}0\times10^{15}$	
G5	$6{\cdot}5\times10^{13}$	$5{\cdot}5\times10^{14}$	$9{\cdot}2\times10^{15}$	
K0	$4{\cdot}1\times10^{13}$	$3{\cdot}4\times10^{14}$	$9{\cdot}9\times10^{15}$	
K5	$2{\cdot}1\times10^{13}$	$1{\cdot}7\times10^{14}$	$11{\cdot}1\times10^{15}$	
M0	$1{\cdot}6\times10^{13}$	$1{\cdot}1\times10^{14}$	$13{\cdot}6\times10^{15}$	
M5	...	...	$3{\cdot}3\times10^{16}$	

These results show that if collisions are neglected, then Eddington's conclusion that in general accretion is quite insignificant is fully confirmed. They also suggest that, since the case where there is spherical symmetry (i.e. $c=0$) gives the maximum rate of accretion, a more exact treatment, including collision effects, would be useful for this case.

Appendix.—Collision frequencies in a rarefied gas at rest in a gravitational field. —We have seen that a gas in which collisions can be effectively neglected and which has a velocity distribution function at infinity of the form

$$\rho_0 h^3(2\pi)^{-3/2}\exp\{-\tfrac{1}{2}h^2(X^2+Y^2+Z^2)\},$$

will have a distribution function of the form

$$\rho_0 h^3(2\pi)^{-3/2}\exp\{-\tfrac{1}{2}h^2(X^2+Y^2+Z^2-2\mu/r)\},\quad (X^2+Y^2+Z^2-2\mu/r)\geqslant 0, \quad (12)$$

at a distance r from the centre of attraction. This result has been obtained on the assumption that collisions never occur. However, if the molecules are of finite size, there will be collisions, though, for low densities, they may be very infrequent. We shall therefore examine the collision frequencies when the velocity-distribution is given by (12). The methods used are standard ones (**11**), but of course the velocity-distribution is not Maxwellian.

We seek both the total number of collisions per unit volume per unit time, and also the total number per unit volume per unit time of those collisions in which the speed of one particle is reduced to a value less than $(2\lambda\mu/r)^{1/2}$, $\lambda\leqslant 1$.

Let us specify two particles, A and B, of speeds W and W', which collide in such a way that their line of centres lies in a certain small solid angle $\delta\omega$. The line of centres is directed in such a way that the direction of motion of A is inclined to it at an angle α, $0\leqslant\alpha\leqslant\pi/2$. The direction of motion of B is inclined at β to the line of centres, where $0\leqslant\beta\leqslant\pi$. Then if σ is the diameter of the particles, the number of particles such as B which collide with A in the chosen solid angle in time δt is $\sigma^2\delta\omega\,|W\cos\alpha - W'\cos\beta|\,\delta t\,.f(W')$, where

$$f(W')=\rho_0 h^3(2\pi)^{-1/2}\exp\{-\tfrac{1}{2}h^2(W'^2-2\mu/r)\}W'^2\,dW'\sin\beta\,d\beta,$$

and $W'^2\geqslant 2\mu/r$. This expression is integrated over $\delta\omega$, β and W to give the probable number of collisions in which A is involved in a time interval δt. The integrations are not difficult, but cases such as $W'\gtrless W\cos\alpha$ have to be treated separately. We find that the probable number of collisions is

$$(8\pi)^{1/2}\sigma^2\delta t\rho_0 h\left\{W'^2\cos^2\alpha+\frac{2\mu}{r}+\frac{2}{h^2}\right\},$$

for $W\cos\alpha\leqslant(2\mu/r)^{1/2}$, and

$$(8\pi)^{1/2}\sigma^2\delta t\rho_0 h\left\{2W\cos\alpha\left(\frac{2\mu}{r}\right)^{1/2}+2h^{-2}\exp[-\tfrac{1}{2}h^2(W^2\cos^2\alpha-2\mu/r)]\right.$$
$$\left.+2W\cos\alpha\int_{(2\mu/r)^{1/2}}^{W\cos\alpha}\exp[-\tfrac{1}{2}h^2(W'^2-2\mu/r)]\,dW'\right\},$$

for $W\cos\alpha>(2\mu/r)^{1/2}$. To obtain the total number of collisions per unit volume per unit time, we multiply these expressions by the number of particles per unit volume such as A (namely $\rho_0 h^3(2\pi)^{-1/2}\exp\{-\tfrac{1}{2}h^2(W^2-2\mu/r)\}W^2\,dW\sin\alpha\,d\alpha$, $W^2\geqslant 2\mu/r$) and integrate over α and W. In so doing, of course, every collision is counted twice. Again the integrations are tedious, but we finally obtain for the total number of collisions per unit volume per unit time the quantity

$$4\rho_0{}^2\sigma^2h^{-1}\left\{\frac{1}{3}q^3+q+\int_q^\infty\exp(q^2-x^2)\,dx\right\}, \quad (13)$$

where $q^2 = 2\mu h^2/r$. As $r \to \infty$, $q \to 0$, and the expression tends to the Maxwellian value of $2\pi^{1/2}\sigma^2\rho_0{}^2h^{-1}$.

In very similar fashion we can calculate the number of collisions per unit volume per unit time in which the speed of one particle is reduced to a value less than $(2\lambda\mu/r)^{1/2}$, $\lambda \leqslant 1$. In a perfectly elastic collision between A and B the components of velocity perpendicular to the line of centres are unaltered, and the components along the line of centres are interchanged. It follows that if A is to lose kinetic energy of amount $\frac{1}{2}U^2$ per unit mass, then

$$W^2\cos^2\alpha - W'^2\cos^2\beta = U^2. \tag{14}$$

Thus the probability that A will be involved in a collision in unit time in which it loses energy of amount between $\frac{1}{2}U^2$ and $\frac{1}{2}U^2 + U\delta U$ per unit mass is

$$\sigma^2\delta\omega \int \rho_0 h^2(2\pi)^{-1/2} \exp\{-\tfrac{1}{2}h^2(W'^2 - 2\mu/r)\}|W\cos\alpha - W'\cos\beta|W'^2\,dW'\sin\beta\,\delta\beta,$$

where β is given by (14), and

$$W'^2\sin\beta\cos\beta\,\delta\beta = U\,\delta U.$$

This leads to probabilities

$$\sigma^2\delta\omega U\,\delta U\rho_0 h^3(2\pi)^{-1/2} \times \int \exp\{-\tfrac{1}{2}h^2(W'^2 - 2\mu/r)\}\frac{W\cos\alpha - (W^2\cos^2\alpha - U^2)^{1/2}}{(W^2\cos^2\alpha - U^2)^{1/2}}W'\,dW',$$

for particles which A overtakes, and

$$\sigma^2\delta\omega U\,\delta U\rho_0 h^3(2\pi)^{-1/2} \times \int \exp\{-\tfrac{1}{2}h^2(W'^2 - 2\mu/r)\}\frac{W\cos\alpha + (W^2\cos^2\alpha - U^2)^{1/2}}{(W^2\cos^2\alpha - U^2)^{1/2}}W'\,dW',$$

for particles which A meets. Thus the total probability is

$$2\sigma^2\delta\omega U\,\delta U\rho_0 h^3(2\pi)^{-1/2}\frac{W\cos\alpha}{(W^2\cos^2\alpha - U^2)^{1/2}}\int \exp\{-\tfrac{1}{2}h^2(W'^2 - 2\mu/r)\}W'\,dW'.$$

In both integrals we require

$$W'^2 \geqslant W^2\cos^2\alpha - U^2, \quad \text{and} \quad W'^2 \geqslant 2\mu/r.$$

Thus the probability is

$$2\sigma^2\delta\omega U\,\delta U\rho_0 h(2\pi)^{-1/2}\frac{W\cos\alpha}{(W^2\cos^2\alpha - U^2)^{1/2}},$$

if $W^2\cos^2\alpha \leqslant U^2 + 2\mu/r$, or

$$2\sigma^2\delta\omega U\,\delta U\rho_0 h(2\pi)^{-1/2}\frac{W\cos\alpha}{(W^2\cos^2\alpha - U^2)^{1/2}}\exp\{-\tfrac{1}{2}h^2(W^2\cos^2\alpha - U^2 - 2\mu/r\},$$

if $W^2\cos^2\alpha > U^2 + 2\mu/r$. The integration over all elements of solid angle $\delta\omega$ is trivial. Next we multiply by

$$\rho_0 h^3(2\pi)^{-1/2}\exp\{-\tfrac{1}{2}h^2(W^2 - 2\mu/r)\}W^2\,\delta W\sin\alpha\,\delta\alpha,$$

which is the number of particles per unit volume with speed W inclined to the selected direction at an angle α. Integrating over α, we obtain the total number of collisions per unit volume per unit time in which particles of speed W are reduced in speed to $(W^2 - U^2)^{1/2}$. The answer will depend on whether $W^2 >$ or $< U^2 + 2\mu/r$; however, we are going to apply these results to the case in which a capture is effected, so that $W^2 \leqslant U^2 + 2\mu/r$. It follows that for all α in $0 \leqslant \alpha \leqslant \pi/2$

$$W^2\cos^2\alpha \leqslant U^2 + 2\mu/r.$$

The number of collisions of the kind described is therefore

$$4\sigma^2 U\,\delta U \rho_0{}^2 h^4 \exp\{-\tfrac{1}{2}h^2(W^2-2\mu/r)\}W^2\,\delta W \int_{\alpha=0}^{\cos^{-1}(U/W)} \frac{W\cos\alpha}{(W^2\cos^2\alpha - U^2)^{1/2}}\sin\alpha\, d\alpha,$$

or

$$4\sigma^2 U\,\delta U \rho_0{}^2 h^4 \exp\{-\tfrac{1}{2}h^2(W^2-2\mu/r)\}W\,\delta W\,[-(W^2\cos^2\alpha - U^2)^{1/2}]_{\alpha=0}^{\cos^{-1}(U/W)}$$

or

$$4\sigma^2 U\,\delta U \rho_0{}^2 h^4 \exp\{-\tfrac{1}{2}h^2/(W^2-2\mu/r)\}W(W^2-U^2)^{1/2}\,\delta W.$$

To find the number of collisions per unit volume and per unit time in which particles of speed W are reduced in speed to a value less than $(2\lambda\mu/r)^{1/2}$, we integrate with regard to U, for values of U lying between $(W^2-2\lambda\mu/r)^{1/2}$ and W. This gives

$$\tfrac{4}{3}\sigma^2\rho_0{}^2 h^4 \exp\{-\tfrac{1}{2}h^2(W^2-2\mu/r)\}W(2\lambda\mu/r)^{3/2}\,\delta W.$$

Finally we integrate over all values of W, to get the total number of collisions per unit volume and per unit time in which the energy of one of the particles is reduced to $\lambda\mu/r$ per unit mass, or less. The number is found to be $\frac{4}{3}\sigma^2\rho_0{}^2 h^2(2\lambda\mu/r)^{3/2}$, or, in terms of the parameter q,

$$\tfrac{4}{3}\sigma^2\rho_0{}^2 h^{-1}\lambda^{3/2}q^3. \qquad (15)$$

A comparison between (13) and (15) shows that the first term in (13) gives the number of collisions which lead to captures ($\lambda=1$), and the remaining terms give the number of collisions which do not lead to captures. Only for $q=2$ and larger values is the proportion of collisions leading to captures significant. Even then, as is clear from (15), the distribution with regard to kinetic energy amongst those particles which are captured favours energies just below the energy of escape rather than small values.

Department of Mathematics,
The University,
Manchester, 13:
1956 *October* 5.

References

(1) C. W. Allen, *Astrophysical Quantities*, p. 185, London, 1955.
(2) H. Bondi and F. Hoyle, *M.N.*, **104**, 273, 1944.
(3) H. Bondi, *M.N.*, **112**, 195, 1952.
(4) S. Chandrasekhar, *Principles of Stellar Dynamics*, p. 75, Chicago, 1947.
(5) K. N. Dodd, *M.N.*, **112**, 374, 1952.
(6) K. N. Dodd, *Proc. Camb. Phil. Soc.*, **49**, 486, 1953.
(7) W. C. H. Eakin and W. H. McCrea, *Proc. Roy. Irish Acad.*, **46 A**, 91, 1940.
(8) A. S. Eddington, *The Internal Constitution of the Stars*, p. 391, Cambridge, 1926.
(9) F. Hoyle and R. A. Lyttleton, *Proc. Camb. Phil. Soc.*, **35**, 405, 1939.
(10) F. Hoyle and R. A. Lyttleton, *Proc. Camb. Phil. Soc.*, **36**, 325 and 424, 1940. (See also R. d'E Atkinson, *Proc. Camb. Phil. Soc.*, **36**, 314, 1940; F. Hoyle and R. A. Lyttleton, *Proc. Camb. Phil. Soc.*, **36**, 323, 1940.)
(11) J. H. Jeans, *The Dynamical Theory of Gases*, 2nd ed., p. 18, Cambridge, 1916.
(12) W. H. McCrea and K. N. Dodd, *M.N.*, **112**, 204, 1952.
(13) L. Spitzer, *Problems of Cosmical Aerodynamics* (Symposium), p. 36, 1951.
(14) B. Strömgren, *Ap. J.*, **89**, 526, 1939.
(15) H. C. van de Hulst, C. A. Muller and J. H. Oort, *B.A.N.*, **12**, No. 452, 1954.

A STATISTICAL STUDY OF PULSATING STARS

E. A. Kreiken and Dilhan Ege

(Received 1956 December 15)

Summary

In a series of papers which are now being issued by the Astronomical Institute of the Ankara University (**18**) the autocorrelation and subsequent power analysis is applied to large numbers of RR Lyrae and cepheid variables in the Milky Way cloud, globular clusters, etc. The present paper contains a brief outline of the method which was used in these papers and also a brief discussion of the significance of the intensities of the overtones obtained in that way. For statistical purposes only the relative intensities $A(1)$ of the first overtone are important. The values $A(1)$ are plotted against the logarithms of the period. With periods $P<10^{d}$ there is a general decrease of $A(1)$ with increasing period, while with periods $P>10^{d}$ $A(1)$ increases with the period. There is a tendency of the points $A(1)$ to concentrate along certain lines, but it is difficult to say whether these lines indicate certain levels or correspond to the limits of fairly broad belts in which there is a concentration of the points $A(1)$. With the shorter periods there is a discontinuity near log $P=-0{\cdot}30$, where a sudden increase of the values $A(1)$ occurs. This discontinuity could be related with a transition from Bailey's subtype c to a–b or vice versa. The points $A(1)$ corresponding to the RW Draconis variables are confined to a narrow vertical belt around log $P=-0{\cdot}30$. Some systematic differences seem to occur between the distribution of the points $A(1)$ in the different galactic star clouds and the Magellanic Clouds.

---

1. *Outline of method.*—The discussions in this article are based on the results of an autocorrelation analysis of the light curves of different groups of cluster variables and of cepheids. The autocorrelation method for analysing time series has been developed by Kendall (**16**). For a time series with equidistant terms $u_1, u_2, \ldots, u_n$ for which $\Sigma u_i=0$, the autocorrelation coefficient r_k is defined by

$$r_k=\frac{\Sigma u_i u_{i+k}}{\{\Sigma u_i^2 . \Sigma u_{i+k}^2\}^{1/2}} \tag{1.1}$$

where all summations are from 0 to $N-k$. Here we use the notation introduced by Ashbrook, Duncombe and van Woerkom (**2**) who give the convenient approximation

$$r_k=(\Sigma u_i u_{i+k})/\{\Sigma u_i^2-k\overline{u_i^2}\} \tag{1.2}$$

which is adequate if $N \gg k$. The disadvantage of the correlogram is to mask a secondary periodicity. To overcome this disability the correlogram can be transformed into the corresponding power spectrum. By Kintchine's theorem (**6**) the power spectrum is the Fourier transform of the correlation function. It is computed from the relation

$$\pi(f)=\frac{2}{N}\Sigma r_k \cos 2\pi f k, \tag{1.3}$$

where f is the reciprocal of the trial period and $\pi(f)$ indicates the mean squared amplitude of each frequency.

As a rule the requirements of extent, continuity and reasonable homogeneity of the light curve to be analysed are difficult to meet. With the RR Lyrae stars and the cepheids the light curve remains almost unchanged, period after period. So it was supposed that the light curve continually repeats itself and as a consequence the time series can be considered to be infinite. The period of the correlogram is the period of the variable. Obviously the introduction of a constant period and light curve imposes some restrictions. The power series is converted in something very much like a Fourier series. A consequence of our assumption is that for any value of f which is not commensurate with the fundamental period we have $\pi(f) \equiv 0$. From the relation (1.3) we obtain the squares of the intensities of the frequencies ν, 2ν, 3ν, ..., that is, of the fundamental and its overtones. These correspond to $\pi(0)$, $\pi(1)$, $\pi(2)$, etc. In this paper we use the relative intensities of the overtones, e.g. the values

$$A(f) = \left\{\frac{\pi(f)}{\pi(0)}\right\}^{1/2}.$$

With all light curves which were analysed the series $A(0)$, $A(1)$, $A(2)$, ..., is represented by a sequence of numbers with rapidly decreasing values. The only term which is of interest for a general statistical study is the term $A(1)$. The terms of higher order were found to be of the same order of magnitude as the probable error in their determination. By this method the amplitudes of all light curves are reduced to a uniform scale, while the shape of the light curve is described in terms of the numerical values of a few parameters. Starting from the assumption that the atmosphere of a star is affected by strictly periodic disturbances, while each disturbance sets up a damped oscillation (**23**), it is not difficult to construct artificial light curves which closely resemble that of a cepheid. With such an artificial light curve only one period is present but in the analysis several terms $A(f)$ of non-zero value will turn up. The description of a light curve in terms of the numerical values of $A(f)$ therefore is a purely formal one. It is not necessary that the overtones have any physical importance. Finally the following remarks should be made:

(i) On the one hand it is an advantage that in this method all light curves are reduced to a uniform scale. On the other hand the amplitude of a light curve is a valuable part of the observational evidence and this part is suppressed.

(ii) The light curve was supposed indefinitely to repeat itself so that small variations in the period and in the shape of the light curve are suppressed. Especially with the variables of the RW Draconis type this is a disadvantage. Several authors consider these stars to be affected by two vibrations of almost equal periods resulting in the occurrence of a beat period. Within each beat period the shape of the light curve varies considerably. When possible the light curves corresponding to different phases of the beat period were analysed and the range of the values $A(f)$ was determined. The periods of the RW Draconis variables are around $\frac{1}{2}$ day and only a few have been observed sufficiently to allow of a complete analysis. For some additional variables light curves for two different epochs are available, so that part of the range in $A(1)$ is known. For the majority of the RW Draconis variables only certain mean values $A(f)$ could be obtained.

(iii) While the light curve completely determines the correlogram, the correlogram does not uniquely determine the light curve.

2. *A survey of data.*—Using the method described in the preceding section, large numbers of variables were analysed. Here only a short survey is given of the different groups of variables which were analysed with a reference to the sources from which the light curves were obtained.

(*a*) *Variables in globular clusters.*—A large number of variables in ω Cen, for which the light curves were taken from the work of Martin (**20**(*a*)), was investigated. First, a number of variables was selected at random but in such a way that all periods are represented. In addition, a number of variables was analysed which either have:

(i) a very short period;

(ii) a comparatively long period; or

(iii) a period near the transition from the Baily subtype *c* to *a*–*b*.

All stars with $P>1^d$ have been included. In the same way a number of variables in M5 were analysed for which the light curves were determined by Oosterhoff (**22**(*a*)). In M3 forty variables were analysed for which the light curves given by Hett (**14**) or by Greenstein (**11**) were used, except for those variables for which Martin (**20**(*b*)) has given improved light curves. Next, all in M53 were analysed. As a rule the light curves given by Grosse (**12**) were used, but for some the improved ones as determined by Oosterhoff (**22**(*c*)). Of the 86 variables which Wright (**33**) has studied in NGC 3201, thirty-eight were used and also all variables which this same author has studied in NGC 4833. For the clusters M9, M22, NGC 6218, NGC 6254, M13, M80, NGC 5053, NGC 5466 and M2, the light curves given by Sawyer (**26**) were analysed. The curves which Sawyer indicates as uncertain were excluded.

(*b*) *Variables in the Magellanic Clouds.*—For the Small Magellanic Cloud Shapley, Carlston and Nail (**28**) have given a sequence of light curves for different periods which they consider as being representative for this Cloud. For the Large Cloud a similar sequence is given by Shapley and Nail (**29**). All variables contained in these two sequences were analysed except those for which the authors indicate that there was a faint companion in contact with the variable or a doubling which distorted the image and decreased the range. A few variables were included of which for special reasons Shapley (**27**) has separately published the light curves.

(*c*) *Variables in galactic star clouds.*—In the Sagittarius cloud the values $A(f)$ were derived for 70 RR Lyrae stars and cepheids. The light curves were taken from the publications by Uitterdijk (**32**), Martin (**20**), Swope (**31**) and Ferwerda (**7**). From the light curve given by van Gent (**9**) for the variables in or near the constellation Corona Australis fifty were analysed. For a large number of variables in or near the constellation Carina, the light curves were determined by Plaut (**24**), Gaposchkin (**8**) and Payne-Gaposchkin (**24**). For fifty-five of these variables the values $A(f)$ were determined.

(*d*) *Galactic cepheids.*—The analysis was applied to the variables in lists collected by Hertzsprung (**13**) and Joy (**15**). All thirty-eight variables contained in the list of Hertzsprung were used. From the list of Joy fifty-five systems were selected in such a way that all periods are represented. In addition to these the light curves based on "mean coordinates" were considered. These "mean coordinates" given by Payne-Gaposchkin (**24**) for different periods represent the mean of light curves which previously had all been reduced to a uniform amplitude.

(*e*) *RW Draconis variables.*—An analysis of the light curve at all phases ψ of the beat period was possible only for AR Her, which variable has been extensively observed by Balasz and Detre (**3**). For the RW Draconis variables in ω Cen Martin (**20**) gives the light curves at two or three epochs. All of these were analysed. Consequently for these variables part of the range over which $A(f)$ varies is known. Moreover all stars were analysed which in the lists mentioned under (*a*), (*b*), (*c*) and (*d*) are indicated to be or are suspected to be of the RW Draconis type.

In some cases one and the same variable occurs in several of the lists mentioned in (*a*), (*b*), (*c*), etc. So we have several systems for which the light curve has been determined by at least two different authors. This makes it possible to evaluate the probable error in the determination of $A(f)$. Here only the probable error in the numerical value of $A(1)$ is given, viz. $p = \pm 0{\cdot}040$. With recent light curves the value of p may be smaller, but as our lists contain many older light curves here the value $p = \pm 0{\cdot}040$ must be used. This value includes influences which arise from the differences between visual and photographic curves, from instrumental differences and from the way in which the mean light curve was drawn through the observed points. With the majority of the variables the numerical values of $A(2)$, $A(3)$ were found to be of the same order of magnitude as p. Therefore in the following only the values $A(1)$ are used. In the *Communications of the Astronomical Institute of Ankara* the values $A(1)$ have been tabulated for several hundreds of variables (**18**). There is no reason to repeat this tabulation, and for the numerical values of $A(1)$ the reader is referred to the original lists.

3. *The relation between $A(1)$ and log P.*—Fig. 1 gives a plot of the values $A(1)$ against log P. All variables contained in the lists mentioned in Section 2 were used with the exception of:

(*a*) the irregular and RW Draconis stars;

(*b*) two stars with period around 100 days which fall outside the limits of the figure (one in the Magellanic Clouds, one in M5);

(*c*) the values $A(1)$ based on "mean coordinates".

In Fig. 2 the open circles correspond to the values $A(1)$ derived from the mean coordinates given by Payne-Gaposchkin (**24**). Black dots are cepheids with a distance over 250 parsecs from the galactic plane which according to Payne-Gaposchkin (*loc. cit.*) must be considered as Population II stars. Triangles correspond to cepheids in globular clusters. If the shape of the light curve is well determined, black triangles were used. If the shape of the light curve was uncertain an open triangle was used. From Figs. 1 and 2 it is apparent that the distribution of the points $A(1)$ in the correlation plane is not an haphazard one. The points $A(1)$ seem to be concentrated along certain levels. These different levels are poorly defined and it is dubious whether they must be considered as being levels in a strict sense or merely as the limits of fairly wide belts of preference. It would not be difficult to draw another set of lines a little higher or lower in the figure, or with a slightly different inclination, which are equally probable. However, provided that their relative value is kept in mind, these levels are convenient for discussing the main features of Figs. 1 and 2 and later on will enable us to compare the distribution of the points $A(1)$ within the different groups of stars. From Fig. 1 it appears that, for periods $P < 10^d$, $A(1)$ decreases along all levels with increasing period. For evident reason there is an upper limit for the values $A(1)$

which in our diagram is around $+0^{m}60$. Near $P=10^{d}$ small values of $A(1)$ prevail. In other words here the light curves resemble a pure sine curve.

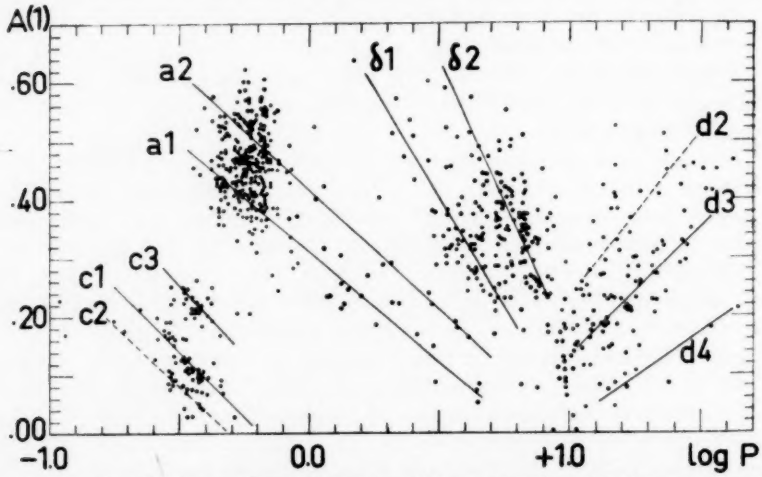

FIG. 1.—*In this diagram all available values $A(1)$ are plotted against their corresponding value log P. The variables seem to be arranged along a number of levels which do not all have physical significance. The period $P=10$ indicates a reversal. Before this $A(1)$ decreases with increasing P. Beyond $P=10$ the value $A(1)$ increases with increasing P. Except the levels c, all levels to the left of $P=10$ start in the upper left part of the diagram and can be traced up to $P=10$. There are no discontinuities except near log $P=-0^{m}3$.*

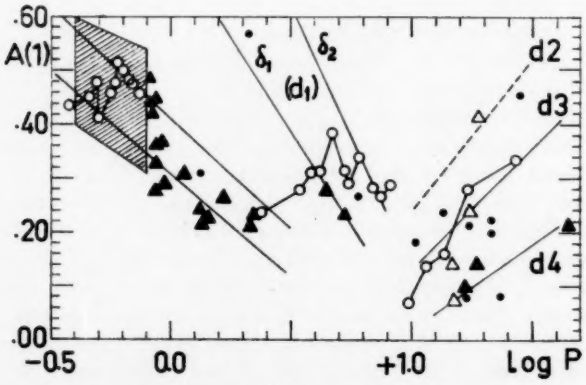

FIG. 2.—*In this diagram the large open circles indicate the values $A(1)$ derived from the mean coordinates of light curves. Black triangles correspond to cluster cepheids with well determined light curves, open triangles to those with poorly determined curves. Black dots are cepheids with distance over 250 parsecs from galactic plane. The shaded area corresponds to the region occupied by the RR Lyrae stars.*

With the periods $P>10^{d}$ there is a general tendency of the values $A(1)$ to increase with period. With the periods $P<10^{d}$ a discontinuity occurs around log $P=-0^{m}30$. The majority of the stars for which log $P<-0^{m}30$ are arranged along the levels *c*, while those for which log $P>0^{m}30$ are along the levels *a*. The

stars on levels *c* belong to Bailey's subtype *c*, those on a_1 and a_2 to the Bailey subtypes *a* and *b*.

These irregularities in the distribution of the points $A(1)$ correspond to the period intervals detected by Ludendorff (**19**) and Hertzsprung (**13**). As appears from the set of curves collected by Campbell and Jacchia (**5**), each interval sets in with asymmetrical light curves (high value of $A(1)$) and ends with symmetrical light curves. From our diagram it would appear that this trend is reversed with the longer periods. In Fig. 1 the final interval sets in around $\log P = 1{\cdot}0$ with low values of $A(1)$, while the asymmetry increases with increasing period.

Fig. 2 leads to identical conclusions. In this figure the variables of Bailey's subtype *c* have not been included. The cross-hatched area in the upper left part of the diagram indicates the area which is densely crowded by variables of the subtypes *a* and *b*. From Fig. 2 it appears that the levels a_1 and a_2 (the belt a_1–a_2) are typical for variables of the Population II type, but some P II variables also occur along δ_1 and δ_2. Conversely the majority of the variables on the levels δ_1 and δ_2 (belt d_1) is of Population I type.

For periods $P > 10^d$ the situation is not clear. The levels d_2, d_3 and d_4 are very indistinct. In Fig. 1 the majority of the stars are along d_3 and in Fig. 2 the points corresponding to the "mean coordinates" are also along d_3.

From a Fourier analysis of the light curves of δ Cepheid stars Payne-Gaposchkin (**24**(*b*)) finds that up to periods 16^d there is a difference between the variables of Population I and those of Population II. From Fig. 2 it would appear that in the mean with $P > 10^d$ values $A(1)$ for Population II variables are smaller than those of Population I variables, but the evidence is not conclusive. All variables along d_4 are of type II. But along d_2 and d_3 the distribution of the values $A(1)$ seems to be the same for the two population types. This may be due partly to the fact that we have included some dubious values in our material (the open triangles).

4. *The RW Draconis stars and the irregular variables.*—The values $A(1)$ corresponding to the irregular variables and RW Draconis stars are plotted in Fig. 3. The levels c_3, a_1 and a_2 are borrowed from Fig. 1. From Fig. 3 it is evident that the RW Draconis stars are confined to a vertical belt which is roughly limited by the values $\log P = -0{\cdot}40$ and $-0{\cdot}20$. This vertical belt therefore also roughly coincides with the discontinuity in the distribution of the values $A(1)$ around $\log P = -0{\cdot}30$. It might therefore tentatively be suggested that the RW Draconis stars are variables in a state of transition between the mode of vibration corresponding to the levels *c* and the one corresponding to the levels *a*. Temporarily both vibrations are present. From the work of Schwarzschild (**30**) and Kluyver (**17**) we know that the simultaneous occurrence of two vibrations is possible. Also, in their study of the light curve of AR Her, Balasz and Detre (**3**) have shown that its complicated variations can be explained if it is accepted that simultaneously two vibrations are present. The RW Draconis stars and the irregular variables are not evenly distributed over the whole interval between the levels *c* and *a*. This may be a question of selection, the amplitude of the variables on or near the *c* levels being much smaller than of those near the levels *a* so that the latter ones are more easily discovered.

Further evidence that with the RW Draconis stars and the irregular stars we may have to deal with variables in a state of transition is given by Fig. 4. In this latter figure we have indicated the intervals in $\log P$ which with the various

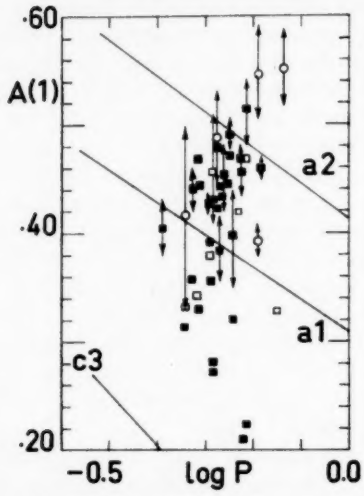

FIG. 3.—*The irregular variables of the RW Draconis type. The arrows indicate the range of the values A(1) through the secondary cycle. The irregular variables are confined to a narrow interval of log P and may represent a group which is transitional between c and a.*

groups of stars are occupied by the variables on the levels *c* and those on the levels *a*. For the first the intervals are indicated by dotted rectangles and for the second by black rectangles. The cross-hatched vertical belt indicates the interval in which the RW Draconis and irregular variables occur. From the figure it is evident that with all groups of stars the end of the levels *c* and the starting point of the levels *a* is in or at least very near the interval occupied by the irregular variables. With the Carina cloud we have not been able to find any variables which could be identified with the levels *c*.

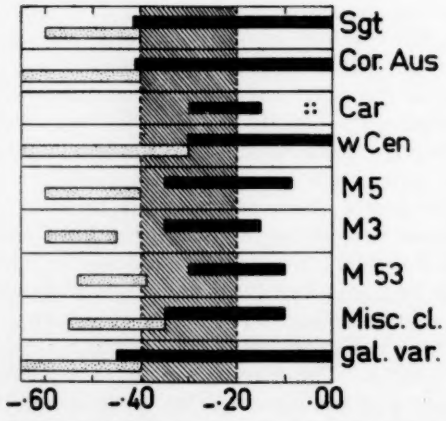

FIG. 4.—*The black rectangles indicate the range in period of the levels a, the spotted rectangles that of the levels c. The cross-hatched strip indicates the period range of the RW Draconis stars. For Carina the results are uncertain. It is noticed that in the Milky Way clouds the a levels extend to far shorter periods than in the clusters. All levels a and c start or end near the interval occupied by the irregular variables.*

5. *The distribution of the points $A(1)$ in Carina, Sagittarius and the Magellanic Clouds.*—When plotted separately some typical differences appear between the distributions of the values $A(1)$ in the Carina cloud, the Sagittarius cloud and the Magellanic Clouds.

For the Sagittarius cloud the distribution of the values $A(1)$ is given in Fig. 5 and that for the Carina cloud and the Magellanic Clouds in Figs. 6 and 7 respectively. In this case only the variables with $P>1^d$ are used. From the figures it would appear that in the Sagittarius cloud the relative frequency of the cepheids with $P>10^d$ is slightly larger than in the Carina and the Magellanic Clouds.

In Sagittarius the levels δ_1 and δ_2 (the belt d_1) end abruptly towards the left, but in Carina they extend to much shorter periods. This is even more so with the cepheids in the Magellanic Clouds. The large extension of the cepheids towards short periods, especially in the Small Cloud, has been discussed by Shapley (**28**). This abrupt end of the levels δ_1, δ_2 in Sagittarius may explain why the frequency of cepheids with $P<10^d$ is relatively small in this cloud. Between the distributions prevailing in Sagittarius and those in Carina and the Magellanic Clouds there is a second difference. In Sagittarius several variables are on the level d_4. On the other hand, in the Carina cloud and in the Magellanic Clouds no variables occur which can be identified with the level d_4. It is evident that the differences mentioned before are in the nature of small shifts. But it is interesting to notice that the stars in Sagittarius are considered to represent Population II and those in Carina and the Magellanic Clouds Population I stars.

From Fig. 2 it appeared that the variables corresponding to Population II have a preference for the levels a and d_4 (see Section 3). This might explain why the level d_4 occurs in Sagittarius but is absent both in the Carina and in the Magellanic Clouds. Payne-Gaposchkin (**24**) has pointed out that there is a much closer resemblance between the cepheids in Carina and those in the Magellanic Clouds than between the cepheids in Carina and those around Sagittarius.

This conclusion is confirmed by the distribution of the points $A(1)$ in Figs. 5, 6 and 7. There are some differences between the distributions in Carina and the Magellanic Clouds. When we consider the cepheids with $P<10^d$, it is evident that with the Magellanic Cloud variables the values $A(1)$ in the mean are slightly larger than with those in Carina.

6. *The different levels.*—When considering Fig. 1 it was remarked that the different levels are badly determined and that it is doubtful whether we have to deal with real levels or simply with certain regions or belts of preference. In the subsequent figures the levels were convenient for discussing the general distribution of the values $A(1)$ but in these additional diagrams also the levels are poorly determined. We must therefore consider the question whether or not any real value can be attached to them.

We first consider the levels c. These are the only levels along which the variables of Bailey's subtype c occur. From Fig. 1 it might appear that there is a faint preference for three different sublevels c_1, c_2 and c_3, but c_3 is especially badly determined.

In view of the large probable error in the determination of the values $A(1)$ it is dangerous to attach much importance to these three levels. But, according

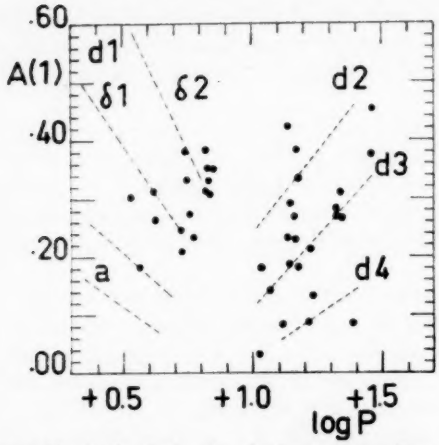

FIG. 5.—*The variables in the Sagittarius cloud and surroundings are plotted. The levels* δ_1 *and* δ_2 *are separated but poorly developed. The presence of* d_4 *should be noticed. The galactic longitude is from* $l = 310°–350°$.

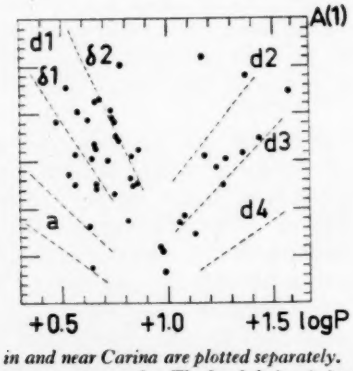

FIG. 6.—*The variables in and near Carina are plotted separately. The levels* δ_1 *and* δ_2 *are more pronounced but are not separated. The level* d_4 *is missing and perhaps also* d_2.

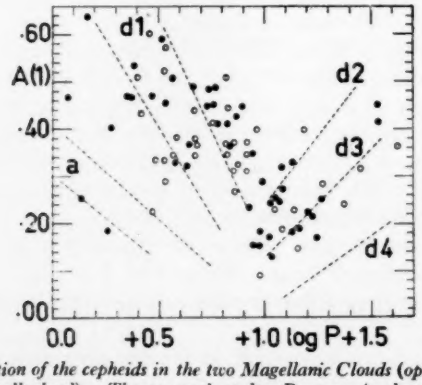

FIG. 7.—*Distribution of the cepheids in the two Magellanic Clouds (open circles = large cloud, dots = small cloud). The reversal at log* $P = 1{\cdot}00$ *is clearly indicated.*

to Martin, the c-type variables in ω Cen fall apart into two different classes which he indicates as the classes c and c'. It appears that all variables to which he assigns the class c' are on the level c_1. Of the variables which he indicates as being of type c only a few are on the level c_2, the majority being along c_1 and c_3.

The variables along the levels a are mainly those belonging to the Bailey subclasses a and b and the cepheids occurring in globular clusters. The levels a are clearly distinct from the levels c. Only in some globular clusters do these variables seem to fall apart into two different groups. Of this no trace remains in the composite diagram (Fig. 2).

The variables of the Bailey subtype a are found along both levels a_1 and a_2 and this is also the case with the variables of the subtype b. So it is improbable that the levels a_1 and a_2 are real. From a study of the period–amplitude relation in the outer regions of the globular clusters ω Cen, M3 and M5, Belserene (**4**) concludes that the period-amplitude diagram suggests that there are two groups of stars, each represented in the different clusters but with a relative population that differs markedly from cluster to cluster.

From our study of the distribution of the values $A(1)$ in the different clusters a similar result was obtained. The paper from Belserene does not indicate the individual variables which belong to the one group or the other and a direct comparison is not possible.

Consequently we will consider the variables along a_1 and a_2 as members of one and the same group, but will admit the possibility that further research may reveal the existence of two different levels. From Figs. 1 and 2 it is evident that this group can be traced almost up to the period of reversal at $P = 10^d$. Apparently this group is typical for stars of Population type II. However, a few stars also of the Carina cloud and the Magellanic Clouds seem to belong to that group. This suggests that close relation may exist between these stars and the cluster variables. The levels δ_1 and δ_2 (the belt d_1) are well developed with the stars in the Carina cloud and the Magellanic Clouds (type I stars). In Sagittarius the levels δ_1 and δ_2 are short, but it is only in this cloud that there is a separation between δ_1 and δ_2. In the other clouds δ_1 and δ_2 overlap each other. The stars along δ_1 and δ_2 are to be taken together as a group which is indicated by the belt d_1. The belt d_1 seems to be typical for Population I stars. For the periods $P > 10^d$ the level d_4 is typical for the variables of Population II. Only cepheids in globular clusters and some cepheids in Sagittarius fall along d_4 and not one variable from the other groups which we have considered. So it seems possible that d_4 represents a separate level.

Along d_2 and d_3 the scatter of the individual values $A(1)$ is so large and the separation of d_2 and d_3 in the different diagrams so unsatisfactory, that these variables must be considered as one group. The group (d_2, d_3) contains variables from both population types and there are no indications that within this group the distributions of the two types are different.

It has been suggested that whole groups of variables may vibrate in an overtone rather than in the fundamental. Of this Schwarzschild (**30**) thinks the variables in M3 to be a notable example.

Also Arp, Baum and Sandage (**1**) conclude that there is no unique period–luminosity relationship for the type II cepheids as exists for the classical cepheids. The points indicating the absolute magnitudes of type II cepheids fall along a number of lines which are more or less parallel to that

indicating the period–luminosity relation for classical cepheids. They can be made to coincide with the curve for classical cepheids by a horizontal shift over a distance $\log 2$, $2 \log 2$ or $3 \log 2$, suggesting that the variables vibrate in the first, second or third overtone. We have considered the possibility that the apparent arrangement of the points $A(1)$ along different levels is due to a similar effect.

If this were the case the period–luminosity relations corresponding to the different levels would not be identical. This possibility is tested in Fig. 8 where, for all cepheids in the Magellanic Clouds for which values $A(1)$ are available, the apparent magnitude is plotted against the logarithm of the period.

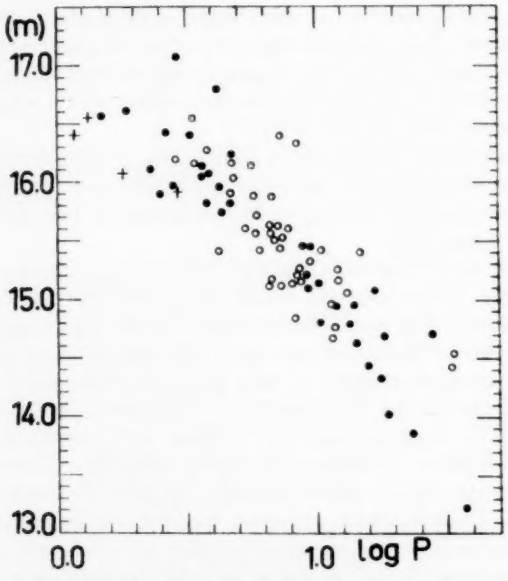

FIG. 8.—*Period–luminosity diagram in the Magellanic Clouds. The variables on different levels are indicated by different symbols. There is no evidence of several separate period–luminosity relations.*

Different symbols were used for indicating the variables on the different levels $A(1)$. Those on the levels a are indicated by crosses, those on or near δ_1 and δ_2 by open circles and black dots respectively. The same symbols have been used for indicating the variables along d_2 and d_3. It was supposed that both clouds have the same distance modulus. The results of this test are negative. The diagram merely indicates the mean period–luminosity relation, which has been given repeatedly by Shapley, and for which he has discussed the large scatter of the individual points around the mean curve.

Between the distributions of the different groups of variables in Fig. 8 no systematic differences are apparent. This confirms that the variables along δ_1 and δ_2 must be considered as one group and also the variables along d_2 and d_3.

The variables which we have used in Fig. 8 are Population I cepheids. Consequently our negative results do not invalidate the conclusions which the aforementioned authors have obtained for the variables in globular clusters.

7. ***Final remarks and summary.***—The material upon which Figs. 1 and 2 are based is far from homogeneous. Therefore an attempt to give an explanation of the general distribution of the points $A(1)$ in the correlation plane would be premature. We therefore only give a brief summary of those results which seem rather positive.

(*a*) With the variables with $P<10^d$ the asymmetry of the light curve decreases with increasing period; with those for which $P>10^d$ the asymmetry increases with increasing period. Apparently around $P=10^d$ a point of reversal occurs.

(*b*) Around $\log P=-0{\cdot}30$ a discontinuity occurs. Here there is a sudden increase of the asymmetry. This discontinuity may be related to a transition from the variables of type *c* to the types *a* and *b*, while the RW Draconis variables may be stars in a transitional stage.

(*c*) With periods $\log P<-0{\cdot}30$ the variables are arranged along the levels *c* and there is a possibility that we have to deal with at least two different levels.

(*d*) With the periods $1>\log P>-0{\cdot}30$ the variables are arranged along the belts *a* and d_1. A division in sublevels has no physical reality. The levels *a* are mainly occupied by variables taken from groups of stars which are considered to represent the Population type II. The levels δ are mainly occupied by variables from groups of stars representing the Population type I. However, a few variables of type II also are on the levels δ while conversely a few type I variables are on the levels *a*.

(*e*) With periods $\log P>1$ the level d_4 is exclusively occupied by variables of Population type II. Thus d_4 may represent a separate level. Along d_2 and d_3 variables occur from both population types. The subdivision of these variables into the separate levels d_2 and d_3 does not seem to be real.

Astronomical Institute,
Ankara:
1956 *December.*

References

(1) Arp, H. C., Baum, W. A. and Sandage, A. R., *A.J.*, **57**, 5, 1952.
(2) Ashbrook, J., Duncombe, R. L. and van Woerkom, A. J. J., *A.J.*, **59**, 12, 1954.
(3) Balász, J. and Detre, L., *Publ. Budapest*, **8**, 1, 1939.
(4) Belserene, E. P., *A.J.*, **59**, 406, 1954.
(5) Campbell, J. and Jacchia, *The Story of Variable Stars*, **67**, 1946.
(6) Feller, W., *General Theory of Probability*, Princeton, 1951.
(7) Ferwerda, J. G., *B.A.N.*, **6**, 231, 1932.
(8) Gaposchkin, S., *H.A.*, **115**, 5, 1946.
(9) Van Gent, H., *B.A.N.*, **6**, 227, 1932.
(10) Gordon, K. G. and Kron, G., *Ap. J.*, **109**, 177, 1949.
(11) Greenstein, J. L., *A.N.*, **257**, 301, 1935.
(12) Grosse, E., *A.N.*, **246**, 398, 1932.
(13) Hertzsprung, E., *B.A.N.*, **3**, 96, 1926.
(14) Hett, J. H., *A.J.*, **50**, 77, 1942.
(15) Joy, A. H., *Ap. J.*, **86**, 409, 1937.
(16) Kendall, *The Advanced Theory of Statistics*, **2**, 402 ff, 1952.
(17) Kluyver, P., *B.A.N.*, **7**, 313, 1936.
(18) Kreiken, E. A.: *Comm. Astron. Inst. Ank.*: (*a*) **5**, 174, 1954; (*b*) **6**, 253, 1955.
(19) Ludendorff, H., *A.N.*, **209**, 217, 1919.
(20) Martin, W. C.: (*a*) *B.A.N.*, **6**, 235, 1932; (*b*) *Annalen Leiden*, **17**, 2, 1918; (*c*) *Ap. J.*, **95**, 314, 1942.
(21) Nielsen, A., *A.N.*, **242**, 422, 1937.

(22) Oosterhoff, P. T.: (*a*) *Annalen Leiden*, **17**, 4, 1941; (*b*) *B.A.N.*, **9**, 325, 1942; (*c*) *B.A.N.*, **10**, 55, 1944.
(23) Pannekoek, A., *Physica*, **12**, 761, 1946.
(24) Payne–Gaposchkin, C.: (*a*) *H.A.*, **115**, 6, 1946; (*b*) *A.J.*, **52**, 218, 1947; (*c*) *H.A.*, **113**, 3, 1954.
(25) Plaut, L., *B.A.N.*, **7**, 273, 1935.
(26) Sawyer, H. B.: (*a*) *Dom. Astrophys. Obs.*, **6**, 279, 1935; (*b*) *D. Dunlap Obs Publ.*, **1**, 24 ff, 1942–54.
(27) Shapley, H., *The Observatory*, **75**, 120, 1955.
(28) Shapley, H., Carlston A. S. and McKibben Nail, V., *H.A.*, **109**, 11, 1948.
(29) Shapley, H. and McKibben Nail, V., *H.A.*, **90**, 110, 1940.
(30) Schwarzschild, M., *H.C.*, **437**, 1940.
(31) Swope, H. H., *H.A.*, **109**, 1, 1946.
(32) Uitterdijk, J., *Annalen Leiden*, **20**, 2, 1949.
(33) Wright, F. W.: (*a*) *H.B.*, **915**, 2, 1941; (*b*) **916**, 3, 1942.

RADIUS VARIATION AND POPULATION TYPE OF CEPHEID VARIABLES

A. W. Rodgers

(Communicated by the Commonwealth Astronomer)

(Received 1956 December 4)*

Summary

The method of Wesselink for the determination of the radii of pulsating variables is applied to the southern cepheids κ Pavonis, β Doradus and l Carinae. The radius of β Doradus is found to be abnormally large for its period. The results are combined with the radii of other cepheids found by previous workers using the same method and a plot of relative radius amplitude against period is made. It is apparent that, for classical cepheids, the light variations are mainly due to changes in effective temperature, and the relative radius amplitude increases slowly with period.

However, for the type II cepheids, the relative radius amplitude increases rapidly with period until for stars of the longest period W Virginis type the variation in radius is of the order of the mean radius of the star itself.

1. *Introduction.*—A method, due in its final form to Wesselink (**1**), for the determination of absolute diameters of cepheids from a combination of photometric and radial velocity data has been applied in recent years to δ Cephei, η Aquilae and RR Lyrae by Stebbins (**2**), and to Y Ophiuchi (**3**) and W Virginis (**4**) by Abt.

Recent radial velocity determinations by Stibbs (**5**) and photometric work by Eggen and Gascoigne (**6**) have made it possible to extend this work to the three southern cepheids κ Pavonis, β Doradus and l Carinae. κ Pavonis (9·1 days) was selected because there are a number of indications that it belongs to Population type II (in which case incidentally it is easily the brightest of the type II cepheids); β Doradus because of its unusual light curve, high galactic latitude and period of 9·8 days, and l Carinae because it has a much longer period (35·5 days) than any other cepheid for which a radius has been determined.

The validity of Wesselink's method rests on the basic assumptions (*a*) that at two points on the light curve where the colours are equal the effective temperatures are also equal; and (*b*) that actual radial displacements may be obtained from the observations of radial velocity. More recently Cavanaggia and Pecker (**7**) have presented an exhaustive discussion of the photometric and radial velocity data as a test of the pulsation hypothesis. Using the results of their computations on supergiant model atmospheres they found disagreement with the radius variations found from Wesselink's method. Whitney (**8, 9**) presented a similar analysis of δ Cephei and η Aquilae and found that, when corrected for the effects of line absorption, the use of model atmospheres gave results not inconsistent with those obtained by Wesselink's method.

* Received in original form 1956 May 8.

2. *Radii Determinations.*—Following Stebbins (**2**), we may write the luminosity of the cepheid at any phase as

$$L_R = 4\pi (R_{\min} + \delta R)^2 T_e^4 \qquad (1)$$

Thus the ratio of light at any two phases of equal colour is given by:

$$L_1/L_2 = (R_{\min} + \delta R_1)^2/(R_{\min} + \delta R_2)^2 \qquad (2)$$

and if m_1, m_2 are the observed magnitudes corresponding to L_1, L_2 then the minimum radius of the star may be written

$$R_{\min} = (\delta R_1 - A\,\delta R_2)/(A - 1) \qquad (3)$$

where $A = \text{antilog}\,(m_2 - m_1)/5$.

Observations of the three Cepheids, κ Pav, β Dor and l Car were reduced according to equation (3).

The photoelectric observations of the light and colour curves on the P, V system were made by Eggen and Gascoigne (**6**). The radial velocity variations have been observed by Stibbs (**5**) at epochs overlapping the photoelectric observations. Earlier, the radial velocity curve of β Dor was determined by Applegate (**10**), and Jacobsen (**11**) published velocity curves of κ Pavonis and l Carinae. For all three stars the measures of Stibbs were consistent with the curves drawn through the earlier observations and confirmed that the form of the curves and systemic velocities were unchanged over the interval between the observations. The combined observations from both epochs were used to define the form of the velocity curves. The relative phases of the photometric and velocity data were found using Stibbs' epochs of velocity minimum and the photometric ephemerides of Eggen and Gascoigne. An accuracy exceeding $0{\cdot}05P$ was thus obtainable in relating the two sets of curves.

The radial velocities were integrated over the period to obtain the systemic velocity, and then cumulative integration at steps of $0{\cdot}05P$ was performed to obtain the radial displacements. A correction to the displacements by a factor of 24/17 (**12**) was made to allow for intermediate limb darkening and the projection effect. A summary of the data taken from the photometric and displacement curves is given in Table I and plotted in Fig. 1 against phase.

For each star twenty pairs of phases of equal colour were taken and the radius obtained in the manner described above. A mean radius was formed, weighted according to the probable errors of the radial velocity and light curves, and the probable error of the weighted mean computed.

For adjacent pairs of phases of equal colour having low weight, i.e. small light or radius differences in equation (3), systematic deviations from the final mean were noted. This effect was probably due to the fact that the light and radial displacements were read off smoothed curves drawn through the observed points. The radii and other relevant data on these stars are given in Table 2.

3. *Results.*—In this section we shall determine the absolute magnitudes of β Dor, κ Pav and l Car and compare these with the values obtained for other galactic cepheids and cepheids in the Magellanic Clouds and M31. The absolute magnitude is determined from equation (1), taking the solar radius, effective temperature and absolute magnitude as standard. The radii we have obtained in the previous section; the effective temperatures we obtain from the observed spectral type for each star.

TABLE I

Light, colour and radius variations in κ Pav, β Dor and l Car

Phase	κ Pav			β Dor			l Car		
	V	P–V	Radius $\times 10^6$ km	V	P–V	Radius $\times 10^6$ km	V	P–V	Radius $\times 10^6$ km
0·00	3·97	+0·39	15·03	3·44	+0·55	72·61	3·40	+0·95	84·00
0·05	4·05	0·44	15·68	3·53	0·60	73·41	3·28	0·87	85·73
0·10	4·15	0·50	16·22	3·56	0·63	74·20	3·30	0·91	89·51
0·15	4·27	0·56	16·66	3·63	0·67	74·83	3·38	1·00	93·67
0·20	4·36	0·66	17·00	3·69	0·71	75·32	3·44	1·08	97·65
0·25	4·42	0·71	17·22	3·77	0·76	75·51	3·52	1·15	101·04
0·30	4·52	0·75	17·31	3·84	0·80	75·35	3·59	1·22	103·77
0·35	4·62	0·78	17·27	3·92	0·85	74·85	3·65	1·29	105·89
0·40	4·69	0·80	17·12	3·98	0·87	74·15	3·72	1·32	107·41
0·45	4·73	0·80	16·83	4·04	0·89	73·23	3·79	1·35	108·23
0·50	4·74	0·76	16·40	4·04	0·88	72·12	3·84	1·36	108·36
0·55	4·74	0·71	15·85	3·98	0·83	70·93	2·91	1·37	107·84
0·60	4·70	0·64	15·16	3·92	0·75	70·13	3·95	1·37	106·67
0·65	4·63	0·57	14·38	3·85	0·69	69·80	3·98	1·36	104·81
0·70	4·54	0·51	13·59	3·76	0·66	69·80	4·00	1·35	102·34
0·75	4·42	0·45	12·88	3·68	0·65	70·25	4·01	1·33	99·39
0·80	4·22	0·37	12·50	3·60	0·65	70·67	4·01	1·31	96·01
0·85	4·04	0·32	12·84	3·57	0·60	71·11	3·98	1·27	92·37
0·90	3·98	0·32	13·57	3·53	0·49	71·54	3·87	1·16	88·64
0·95	3·94	0·35	14·29	3·39	0·46	72·03	3·64	1·05	85·17
0·00	3·97	+0·39	15·03	3·44	+0·55	72·61	3·40	+0·95	84·00

TABLE II

Dimensions, luminosity and galactic data for κ Pav, β Dor and l Car

Star	κ Pav	β Dor	l Car
R.A. (1900)	$18^h\ 46^m{\cdot}6$	$5^h\ 32^m{\cdot}7$	$9^h\ 42^m{\cdot}5$
Dec. (1900)	$-67°\ 22'$	$-62°\ 33'$	$-62°\ 03'$
Galactic longitude	296°	239°	251°
Galactic latitude	−26·3°	−32·7°	−7·2°
Period	$9^d{\cdot}0730$	$9^d{\cdot}842603$	$35^d{\cdot}5323$
Systemic radial velocity	+38 km/sec	+8 km/sec	+3 km/sec
Spectral range	F4–G5	F6–G2	F8–G9
Light range V	3·94–4·74	3·39–4·05	3·28–4·00
Colour range, P–V	+0·31–0·80	+0·45–0·89	+0·89–1·38
Median radius	$14{\cdot}5 \times 10^6$ km	73×10^6 km	96×10^6 km
Median absolute photographic magnitude	−1·63	−4·52	−4·03
Distance	116 pc	295–468 pc	179 pc
Population type	II	I	I

(*a*) *β Doradus.*—The mean minimum radius of β Dor was found to be $(70 \pm 5) \times 10^6$ km. The radius at maximum light is $72{\cdot}1 \times 10^6$ km, at which phase the star has a visual magnitude of 3·39 and a colour of +0·46 on the P, V system.

Miss Applegate gave the spectral type, at light maximum, as F5 and Gratton (**13**) gives F6–7. Recent classification of spectra by Mme. A. de Vaucouleurs from plates obtained by Dr S. Gaposchkin at Mount Stromlo give the spectral type variation to be from F6Ia at light maximum to G2Ia,b at minimum on the revised Yerkes system. Of note is the very loose correlation found between the observed colour and spectral type variation throughout the period.

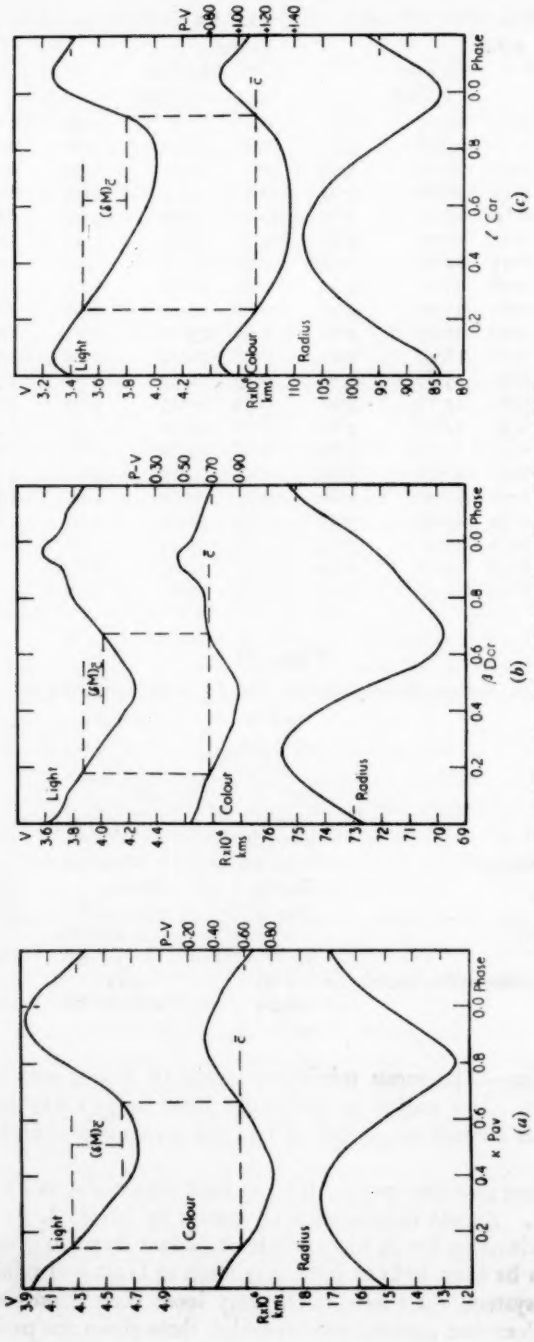

FIG. 1.—*Light, colour and radius variations for* κ *Pav,* β *Dor and l Car.*

For the spectral type at light maximum, then, we adopt F6Ia, giving from Keenan and Morgan's table (**14**) an effective temperature of 5800 deg. K, assuming the Ia and Ib temperatures to be the same. Taking the standard values of absolute bolometric magnitude, effective temperature and radius from Allen's book (**15**), we obtain a maximum absolute bolometric magnitude for β Dor of $-5{\cdot}47$. Applying a bolometric correction of $0^{m}{\cdot}17$, again from Allen, we finally find the median absolute photographic magnitude to be $-4{\cdot}52$.

(*b*) κ *Pavonis*.—The reductions gave the mean minimum radius of κ Pav as $(12{\cdot}5 \pm 0{\cdot}8) \times 10^{6}$ km. Its radius at light maximum is then $14{\cdot}5 \times 10^{6}$ km. The magnitude at light maximum is $V = 3{\cdot}95$, and colour $P - V = +0{\cdot}35$. Jacobsen's estimate of the spectral type at light maximum is F5, agreeing with the relation between spectral type and period found by Code and given in Aller's book (**16**). We adopt therefore F5Ib as the spectral type, which gives an effective temperature of 6200 deg. K from Keenan and Morgan's table. The resulting maximum absolute bolometric magnitude of κ Pav is $-2{\cdot}28$. Applying a bolometric correction of $0^{m}{\cdot}08$ from Allen's tables, we find a median absolute photographic magnitude of $-1{\cdot}63$.

(*c*) *l Carinae*.—The mean minimum radius of *l* Carinae was found to be $(84 \pm 6) \times 10^{6}$ km. Its radius at light maximum is then 87×10^{6} km at which phase the magnitude is 3·26 and the colour $+0{\cdot}87$ on the *P*, *V* system. The spectral type at maximum is given as F8 by Jacobsen. The spectral type at maximum corresponding to a period of 35·5 days is given by Code's relation also as F8. The effective temperature for a spectral type of F8Ib is 5300 deg. F and the median absolute photographic magnitude of *l* Car is then $-4{\cdot}03$.

In order to compare the absolute magnitudes derived above with those of other cepheids, we must allot the three stars to either of Baade's two population types. The criteria of population type membership can be divided into two main kinds, (*a*) spatial, i.e. whether the star is situated in or apart from the outer disk of the galaxy, whether or not it is associated with systems such as globular clusters, the galactic nucleus, spiral arms or galactic clusters and (*b*) kinematic, dependent on the velocity of the star with respect to the local standard of rest in the solar neighbourhood. These criteria are correlated in some instances with the intrinsic properties of the stars themselves, e.g. the blue supergiants of the young Population I or the metallic line deficiences of some high velocity Population II stars. The cepheids form two parallel groups belonging to each population type and the differences between them has been well summarized by Aller (**16**). However as we shall see, these purely spatial and kinematic criteria may be ambiguous. β Doradus has a small systemic velocity relative to the Sun; but it is at a distance of about 200 parsecs from the central plane of the galaxy, a distance large for the general class of type I cepheids. Its period of 9·8 days places it at a minimum of the period distribution function for classical cepheids and this may be noted when consideration is given to the star's peculiarities. The period is remarkably constant, this constancy being a feature of the classical cepheids as opposed to the type II cepheids, which exhibit much more marked irregular fluctuations in the length of the period of oscillation. In view of the above we will regard β Dor as an anomalous type I cepheid. Eggen (**17**) has asserted that κ Pavonis is a cepheid of Population type II because of the remarkable similarity of its light and colour curves to those of AL Virginis, a star definitely belonging to the high velocity group. κ Pav has a systemic velocity of $+38$ km/sec

and a distance from the plane of the galaxy of approximately 50 parsecs. The spatial and kinematic criteria are again ambiguous. However, on the basis of Eggen's photometry and because κ Pav shows the variations in period more commonly observed in the Population type II variables, we will take it to be a type II cepheid. l Carinae is at a small distance from the galactic plane, has a small systemic velocity with respect to the Sun and can be regarded as a classical cepheid.

Baade (**18**) has recently discussed the history of the derivation of the form of the period–luminosity relation. He had shown the need for, and others, including Blaauw and Morgan (**19**), have since given the value of, the revision of the original Shapley period–luminosity relation derived from the Magellanic cepheids for slope and the cluster variables for zero-point. The period–luminosity relation for classical cepheids with the Blaauw–Morgan revision of zero point is $M_{pg} = -1^{m}\cdot4(\pm0\cdot3) - 1^{m}\cdot74\log P$ where M_{pg} is the median absolute photographic magnitude and P is the period in days. Again, if we take the apparent magnitude period relation for the Magellanic cepheids from Shapley's work as $m_{pg} = 17\cdot04 - 1\cdot74\log P$, then from the modulus of the Magellanic clouds, given by de Vaucouleurs (**20**) from a summary of all determinations of

$$m - M = 18\cdot75 \pm 0\cdot10,$$

we find the period–luminosity law to be $M_{pg} = -1\cdot70 - 1\cdot74\log P$. The agreement of this determination with the Blaauw–Morgan zero-point revision within the errors of the individual determinations affords some evidence for the intrinsic similarity of galactic type I and Magellanic cepheids. It should, however, be kept in mind that there are notable differences both in the amplitudes of the light and colour curves and in the frequency distribution of their periods.

The zero-point of the period–luminosity law for the type II population is fixed by the cluster type variables. After Baade's suggestion of the need for revision of the zero-point of the type I period–luminosity law it was thought that the type II cepheids formed a continuous and single valued sequence of luminosity with period with a slope parallel to that found for the classical cepheids. In a study of variables in several globular clusters, Arp (**21**) proposed the existence of a multivalued period–luminosity relation for the type II cepheids, each sequence being displaced from the other by a factor of two in the period. The slope of each sequence is the same as for the type I relation. Recently Reddish (**22**) has suggested that, from consideration of the correlations between period, luminosity and radii, no such multivalued relationship exists. His form of the period–luminosity relationship has then a significantly greater slope than that found for the Magellanic cepheids. Further photometric observations of type II cepheids are required to settle this question. In Fig. 2 the absolute magnitudes of the cepheids for which the radii have been determined by Wesselink's method are plotted against the logarithm of the period. The two straight lines drawn are represented by the relations

$$M_{pg} = 0^{m}\cdot0 - 1^{m}\cdot74\log P \quad \text{and} \quad M_{pg} = -1^{m}\cdot6 - 1^{m}\cdot74\log P.$$

The stars β Dor and Y Oph lie 1·4 magnitudes from the brighter sequence on which fall the type I stars.

In order to determine the distances of the stars κ Pav, β Dor and l Car we must obtain the amount of interstellar extinction affecting the apparent magnitude of each star. The extinction is determined from the colour excess, the ratio of

absorption to reddening being assumed known. Knowledge of the colour excesses presupposes a knowledge of the intrinsic colours of these variables. Two recent determinations of the intrinsic colours of cepheids have been made. Stibbs (**23**), from considerations of a model of the galactic absorbing medium based on the colour excesses of B stars, gives the relation

$$(P\text{–}V)_{\max} = +0^{m}\cdot17 + 0^{m}\cdot18 \log P.$$

From observations of the colours of Magellanic cepheids Gascoigne (private communication) has suggested that the colours at maximum of the type I cepheids may be represented by the relation $(P\text{–}V)_{E,\max} = +0^{m}\cdot10 + 0^{m}\cdot13 \log P$. This equation represents the line which is the blue envelope of the observed colours on the colour-period diagram and thus neglects interstellar reddening within the galaxy in the direction of the clouds, but takes into account the possible reddening of the Magellanic cepheids by material in the Clouds themselves. In this paper we will take Gascoigne's relation to represent the intrinsic colours of type I cepheids.

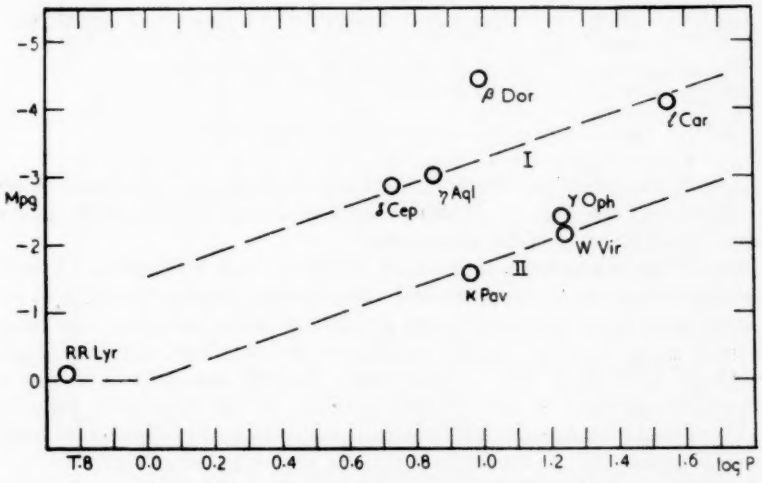

FIG. 2.—*Median absolute photographic magnitude plotted against log period.*

In determining the colour excess of β Dor we find another abnormality of this star. From Gascoigne's relation, at maximum light, the intrinsic colour of β Doradus is $+0^{m}\cdot23$ on the $(P-V)_{E}$ system. The colour excess is then $0^{m}\cdot23$ and the photographic absorption is one magnitude. However, de Vaucouleurs (**24**) has shown that β Dor is seen projected against the edge of a spiral arm and thus would appear to be in a relatively transparent region. Also it would be expected that any galactic reddening suffered by β Dor would equally affect the Magellanic cepheids; thus it would appear that the intrinsic colour is anomalous. If the colour excess is zero the distance is 468 parsecs; if the colour excess is $0^{m}\cdot23$ the distance is 295 parsecs.

Assuming type I and type II colours to be similar, κ Pav has an intrinsic colour at maximum of $+0^{m}\cdot35$ and the colour excess is then $0^{m}\cdot14$ leading to a photographic absorption of 0·6 magnitudes. The resulting distance is found to be 116 parsecs.

l Carinae has from Gascoigne's relation an intrinsic colour of $+0^{m}\cdot30$. The star is reddened by 0·47 magnitudes and the distance is found to be 179 parsecs.

4. ***Radius variations and population type.***—Using methods similar to those described above, several workers have determined radii of other cepheids. As the method demands observations pushed to the limit of their accuracy it is essential to have available good velocity curves and first-class photoelectric observations at or close to the same epoch. In Table III are listed the stars whose radii have been determined, the maximum and minimum values thereof and references.

TABLE III

Cepheid variables with known maximum and minimum radii

Star	Period	Population Type	R_{min} $\times 10^6$ km	R_{max} $\times 10^6$ km	Reference
	d				
RR Lyr	0·57	II	4·77	5·23	(2)
δ Cep	5·37	I	35·1	38·9	(1), (2), (8) (9)
η Aqu	7·18	I	44·6	49·4	(2), (8), (9)
κ Pav	9·07	II	12·5	17·3	
β Dor	9·84	I	69·8	75·5	
Y Oph	17·1	I	47·1	52·5	(3)
W Vir	17·3	II	18	40	(4)
l Car	35·5	I	84	108	

In Stebbins' paper (2) the mean radii only were given. The radii extremes were taken from his Fig. 1. Stebbins' radii gave confirmation of the new zero point of the type I period–luminosity curve.

Abt has investigated the cepheids Y Ophiuchi and W Virginis. Y Oph he found to be an anomalous type I cepheid which showed the opposite effect to β Dor of being fainter than predicted by the period–luminosity relation. His comprehensive discussion of W Virginis led him to the view that this star "expands periodically from about 18 to 40×10^6 km. At each expansion it throws off a shell which continues to rise for 35×10^6 km..." W Virginis is definitely a type II star and its behaviour has been regarded as typical of the type II variables of similar period.

From the data of Table III we can form the quantity

$$\delta R/\bar{R} = 2 \times (R_{max} - R_{min})/(R_{max} + R_{min})$$

which we shall call the ***relative radius amplitude.***

Fig. 3 shows the plot of relative radius amplitude against the logarithm of the period for the stars listed in Table III.

The stars regarded as classical cepheids show quite a slow variation of $\delta R/\bar{R}$ with period. The type II variables however show a rapidly increasing $\delta R/\bar{R}$ with period. An implication of Fig. 3 is that the mechanism of pulsation, and consequently the structure of the star, is quite different in the two population types. Of note is the convergence of the two curves for the cluster type variables. Population type criteria as applied to a single star have been in the nature of spatial or kinematic correlations with the colour luminosity arrays of a given stellar system. We see however that there are, at least for intrinsic variables in the period range considered, structural differences for an individual star dependent on the population type but largely independent of its present spatial

or kinematic situation. This is clearly portrayed by those cepheids having periods between 2 and 10 days, such as κ Pav, whose light curves do not show the characteristic hump of the W Virginis stars and which have no distinguishing spatial or kinematic property.

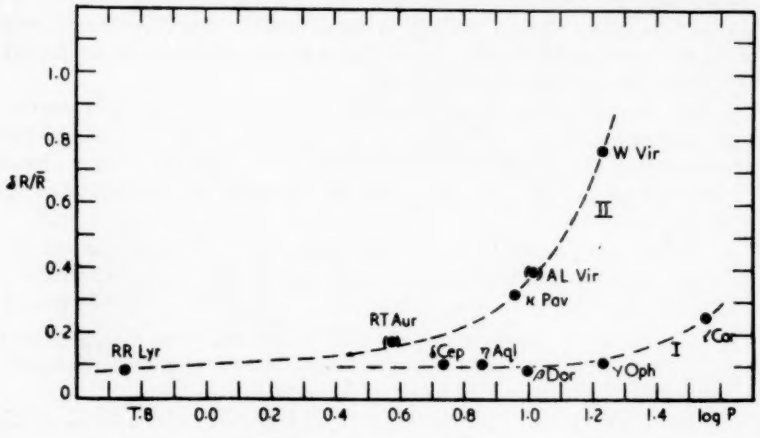

FIG. 3.—$\delta R/\bar{R}$ *against log period for the stars of Table III.*

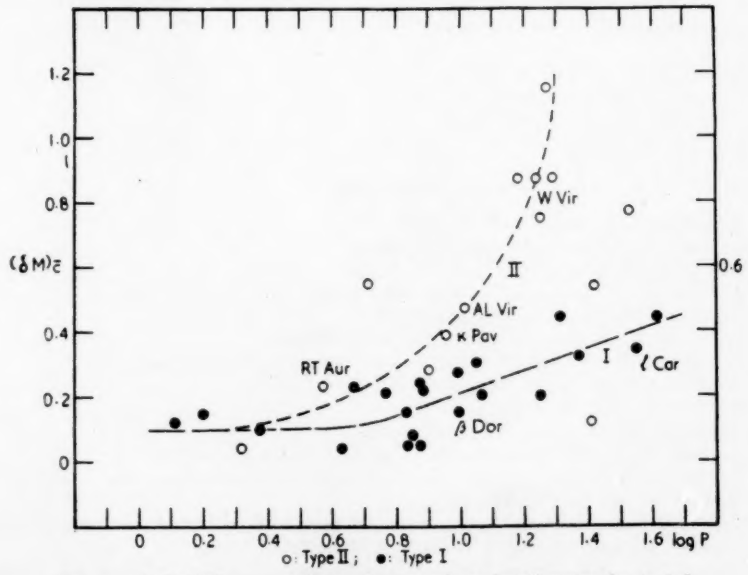

FIG. 4.—*Light difference at phases of mean colour plotted against log period.*

Determinations of absolute radius by Wesselink's method are limited to very few stars due to the stringent observational criteria mentioned above. However, a measure of $\delta R/\bar{R}$ can be obtained purely from the photometric data. If for each star listed in the paper of Eggen and Gascoigne (**6**) we find the difference in brightness from the light curve of the two phases where the star's colour equals its median colour, we are essentially determining the part played by the

variation in radius in producing the observed light curve. This difference we denote by $(\delta M)_{\bar{c}}$ and plot against the logarithm of the period in Fig. 4.

Fig. 4 shows, with more scatter, the same features as Fig. 3. The relative radius amplitude is of course a function of the form of the velocity curve as well as of $(\delta M)_{\bar{c}}$ and the increased scatter of Fig. 4 is to be expected.

AL Vir falls near κ Pav on the type II curve and the star RT Aurigae, which according to Eggen and Gascoigne has a large light amplitude for its period of 3·7 days, also falls near the type II curve.

Arp (**21**), has obtained the photographic and photovisual light curves of cepheids in globular clusters with periods greater than one day. Using the data given in his paper, $(\delta M)_{\bar{c}}$ was computed for his stars of period greater than five days. These stars are plotted along with the other type II variables as open circles in Fig. 4.

From Arp's stars plotted in Fig. 4 the following is evident. At the point corresponding to the period of the longest period stars showing the hump-backed light curve of the W Virginis type, $(\delta M)_{\bar{c}}$ ceases to increase. At this period of about twenty-five days, $\delta R/\bar{R}$ is approximately unity, i.e. $R_{\max}/R_{\min} \simeq 3$, so the possibility arises that the amplitude of oscillation becomes so large that stars of longer period having homologous structure are unstable.

5. *Acknowledgments.*—I wish to thank Drs D. W. N. Stibbs, S. C. B. Gascoigne and O. J. Eggen for the generous way in which they have provided observational data prior to publication, and the referee of this paper for much useful advice on its presentation.

Research School of Physical Sciences,
Australian National University
Mount Stromlo, A.C.T.:
1957 *November* 26.

References

(1) Wesselink, A. J., *B.A.N.*, **10**, 91, 1946.
(2) Stebbins, J., *P.A.S.P.*, **65**, 384, June, 1953.
(3) Abt, H. A., *P.A.S.P.*, **66**, 389, April, 1954.
(4) Abt, H. A., *Ap. J. Supp.*, Ser. 1, 3, April, 1954.
(5) Stibbs, D. W. N., *M.N.*, **115**, 363, 1955.
(6) Eggen, O. J. and Gascoigne, S. C. B., unpublished.
(7) Cavanaggia, R. and Pecker, J.-C., *Ann. d'Astrophys.*, **18**, 3, 1955.
(8) Whitney, C., *Ap. J.*, **121**, 682, 1955.
(9) Whitney, C., *Ap. J.*, **122**, 385, 195.
(10) Applegate, Dorothy, *L.O.B.*, **13**, 12, 1927.
(11) Jacobsen, T. S., *P.A.S.P.*, **16**, 256, 1934, *L.O.B.*, **14**, 60, 1928–30.
(12) Eddington, A. S., *Internal Constitution of the Stars*, Cambridge, 1926.
(13) Gratton, L., *Ap. J.*, **118**, 570, 1953.
(14) Keenan, P. C. and Morgan, W. W., *Astrophysics* (1st edition), Hynek, McGraw-Hill, **1951**.
(15) Allen, C. W., *Astrophysical Quantities*, Athlone Press, 1955.
(16) Aller, L. H., *Astrophysics*, Nuclear Transformations, Stellar Interiors and Nebulae, 107, Ronald Press, 1954.
(17) Eggen, O. J., *Proc. Astr. Photoelectric Conference, Flagstaff*, **31**, 1953.
(18) Baade, W., *P.A.S.P.*, **68**, 5, 1956.
(19) Blaauw, A. and Morgan, H. R., *B.A.N.*, **12**, 95, 1954.
(20) de Vaucouleurs, G. H., *P.A.S.P.*, **67**, 350, 1955.
(21) Arp, H. C., *A.J.*, **60**, 1, 1955.
(22) Reddish, V. C., *M.N.*, **115**, 480, 1955.
(23) Stibbs, D. W. N., *M.N.*, **115**, 323, 1955.
(24) de Vaucouleurs, G. H., *A.J.*, **60**, 126, 1955.

VARIATIONS IN THE LIGHT OF SIGMA SCORPII

A. R. Hogg

(Received 1956 October 19)

Summary

Photoelectric light curves of the β Canis Majoris type variable, Sigma Scorpii, were obtained nearly simultaneously with a series of radial velocity measures made by Struve and collaborators. The photoelectric results show the existence of a beat period of $8^{d}\cdot028$ superposed on the known short period variation of $0^{d}\cdot246846$.

The star is shown to be brightest and bluest when at or near minimum size.

Introduction.—Sigma Scorpii forms ADS 10009 with an $8^{m}\cdot7$ common proper motion companion 20″ distant (1). The bright star, B1 III (2), is both a single lined spectroscopic binary with a period near 34 days (3) and a β Canis Majoris type variable with a period near $0^{d}\cdot25$.

Dr O. Struve suggested that it would be of interest to re-investigate the light variations of this star (which had previously been observed at Mt Stromlo (4)) simultaneously with radial velocity measures to be carried out by him and Dr McNamara at Mt Wilson and Mt Hamilton in 1954. (The star is badly placed for precise photometry in California but passes near the Mt Stromlo zenith.) The measures could not be made exactly simultaneously because of the longitude difference at the two observatories. Photometric observations were made in 1955 as well as 1954.

Observational.—The measures were made in three colours at the Cassegrain focus of the 20-inch reflector at Mount Stromlo using an unrefrigerated EMI Type 5659 11-stage electron multiplier connected to a balanced d.c. amplifier and Brown recorder. Three filters were employed, viz.:

U, Corning 9863 (standard thickness);
B, Chance OB1 (1 mm) + Schott GG15 (2 mm);
V, Chance OY4 (2 mm).

The comparison star, τ Sco, had been used in the earlier Stromlo work and was found to be satisfactory. Although of nearly the same spectral type as σ Sco and near to it in the sky, it was distinctly bluer than the variable. Because of the relatively narrow range of each of the filters employed the effect of the difference in star colours on absorption was neglected. Small absorption corrections, generally less than $0^{m}\cdot01$, were applied, using mean values of the absorption coefficient found for other work with the filters. Measures were made through a diaphragm subtending a diameter of 27″ which was small enough to exclude the light from the 10th magnitude companion of the variable. Observations of the comparison and variable were alternated and magnitude differences between the reading for the variable and the mean of the immediately preceding and succeeding readings of the companion star were computed.

Six substantially complete light curves (i.e. curves covering the whole of one cycle with readings of the variable at average intervals of 12 minutes) were obtained during 1954 and a similar complete curve was obtained in 1955. Fragmentary curves designed to give colour at maximum were also obtained. The "complete" curves are shown in Figs. 1 *a*, 1 *b* and 1 *c* where the points are current means of three observations.

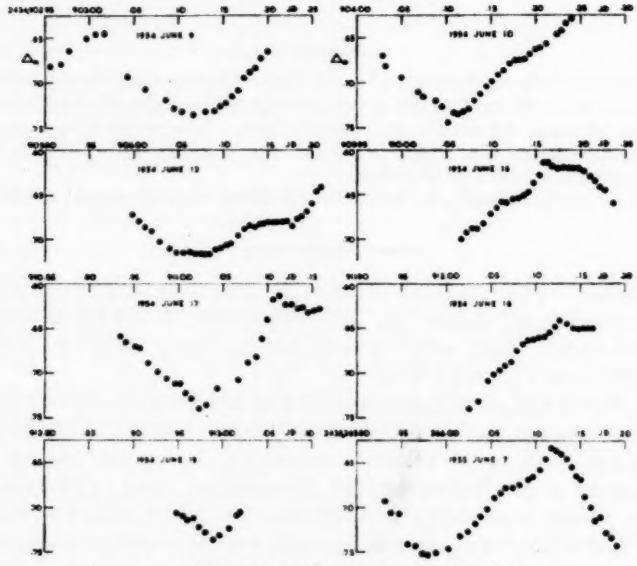

FIG. 1 *a*.—*Short period light variation of α Sco–U filter.*

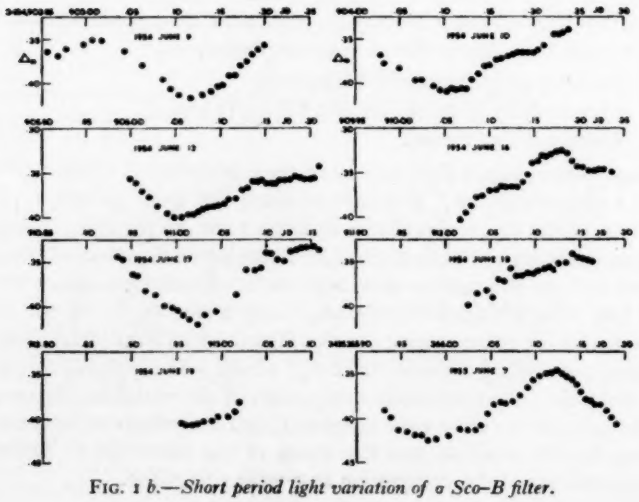

FIG. 1 *b*.—*Short period light variation of α Sco–B filter.*

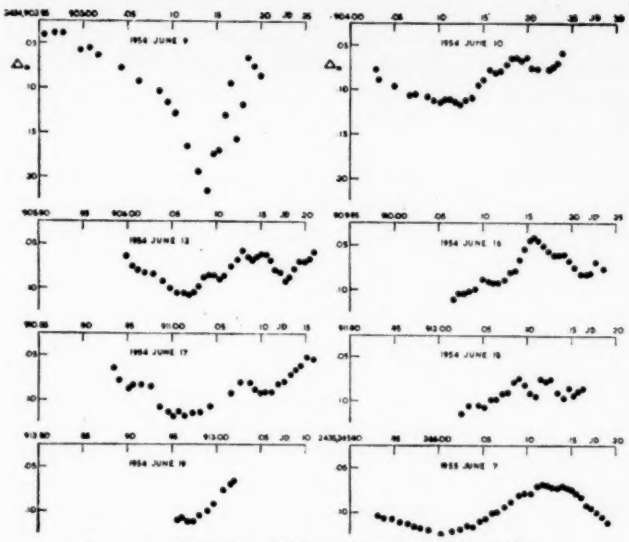

FIG. 1 c.—*Short period light variation of σ Sco–V filter.*

Periodicities.—The system is known to exhibit three periodicities, viz.:

(*a*) a periodicity of 34 days in the value of the radial velocity of the centre of mass;

(*b*) a short period variation of $0^d{\cdot}25$ in the radial velocity and also in the light output; and

(*c*) a period of 8 days in the amplitude of the radial velocity curve recently discovered by Struve *et al.* and probably the result of a beat between two interfering periods close to $0^d{\cdot}25$.

The current observations are not sufficiently numerous to detect any 34-day periodicity in the light. The $0^d{\cdot}25$ period is however clearly shown in both light and radial velocity curves. Observed heliocentric times of blue minima are shown in Table I together with their differences (O–C) from the values derived from the following expression, viz.:

$$\text{Minimum light} = \text{J.D. (Hel.)}\ 2\,432\,306{\cdot}795 + 0^d{\cdot}24\,684E.$$

TABLE I

Observed and computed minima for σ Scorpii (Blue Light)

Minimum J.D. (Hel.) $2\,432\,306{\cdot}795 + 0^d{\cdot}246\,846E$

Observed J.D. (Hel.)	O–C	Phase*	Observed J.D. (Hel.)	O–C	Phase*
		d			d
2432308·038	+0·006	6·8	2434903·121	−0·003	0·9
2313·956	0·000	4·7	4904·106	−0·006	1·8
2350·007	+0·011	0·6	4906·062	−0·024	3·8
2365,040	−0·014	7·6	4911·026	+0·003	0·7
3396·107	−0·022	3·1	4912·979	−0·019	2·7
3397·106	−0·011	4·1	5265·982	−0·006	2·5

* Computed from $T' = \text{J.D. } 2\,434\,878{\cdot}2 + 8^d{\cdot}028E.$

The standard deviation of a single O–C value in Table I is $\pm 0^{d}\cdot011$ but, as will be discussed later, systematic variations occur in the O–C values. A. D. Williams has privately communicated a result J.D. = 2 434 878·92 which agrees exactly with a value computed from the above expression. The period of $0^{d}\cdot246\,846$ agrees very well with the figure of $0^{d}\cdot246\,844$ derived from the spectroscopic results.

The results shown in Table I refer to blue light and were obtained with three different photometers (**4**). Although the time of occurrence of minimum does depend slightly on the wave-length of the light in which it is observed, the different effective wave-lengths of the three blue photometers are sufficiently close to allow the effect to be neglected.

The earlier results (**4**) gave a period of $0^{d}\cdot246\,841$, i.e. $0^{d}\cdot000\,005$ shorter than the present figure. Inspection of the O–C values in Table I does not suggest any certain systematic deceleration in the system, as the mean O–C for the first six entries is $-0^{d}\cdot005 \pm 0^{d}\cdot005$ s.d. compared with $-0^{d}\cdot009 \pm 0^{d}\cdot004$ s.d. for the second six. The rather large standard deviation could be in part due to the small amplitude, rendering difficult the exact determination of the precise time of minimum. Approaching minimum the rate of change of blue light is about $0^{m}\cdot005$ per $0^{d}\cdot01$ so that a determination of minimum even to $0^{d}\cdot005$ requires a precision of nearly $0^{m}\cdot002$ in the photometry. This of course is at or near the present practical limit.

The variation of the time of minimum of the light curves with the effective wave-length of the photometric system is shown by the results of a harmonic analysis for the curve obtained on 1954 June 17, viz.:

	U	*B*	*V*
Minimum light J.D. (Hel.) 2 434 000+	911·016	911·017	911·026
Amplitude	$\pm 0^{m}\cdot053$	$\pm 0^{m}\cdot041$	$\pm 0^{m}\cdot026$

The results refer to the first harmonic and show that as the wave-length increases the amplitude decreases and the phase becomes later.

The 8-day periodicity found by Struve *et al.* (**3**) in the values of $2K$ is also exhibited by other quantities connected with the star. The list of such periodicities is thus as follows:

(*a*) a periodicity in the magnitude reached at maximum light in successive $0^{d}\cdot25$ cycles (Δm_{max});

(*b*) a periodicity in the difference "observed minus computed" time of minimum light $(O-C)_{L}$ in the $0^{d}\cdot25$ cycle;

(*c*) a periodicity in the difference "observed minus computed" time of maximum radial velocity $(O-C)_{V}$ of the $0^{d}\cdot25$ cycle;

(*d*) a periodicity in $2K$ of the $0^{d}\cdot25$ cycle.

The periodicity in Δm_{max} is presented in the data collected in Table II where column 3 shows the phase computed from the expression

$$T' = \text{J.D. (Hel.) } 2\,434\,878\cdot2 + 8^{d}\cdot028E. \qquad (2)$$

The tabulated figures refer to magnitude differences (in the natural scale of the photometer) between σ Sco and τ Sco and are in the sense that numerically larger figures mean that σ has become fainter. The results in the individual

TABLE II

J.D. (Hel.)	Δm at max. light (σ–7)			Phase*
2430000+	*U*	*B*	*V*	
4903·008	0·642	0·346	0·058	0·76
04·244	0·625	0·333	0·050	1·99
06·218	0·640	0·330	(0·057)†	3·97
10·177	0·690	0·379	0·113	7·93
11·150	0·615	0·333	0·055	0·91
12·138	0·635	0·332	0·065	1·87
5266·120	0·634	0·344	0·069	2·58
67·115	0·655	0·355	0·076	3·61
69·085	0·672	0·368	0·077	5·53
86·121	0·656	0·342	0·072	6·53
90·076	0·647	0·336	0·057	2·47
95·018	0·677	0·364	0·080	7·41

* Computed from $T' = \text{J.D. } 2\,434\,878{\cdot}2 + 8^{d}{\cdot}028E$.
† Estimated from *U*, *B* and mean colour.

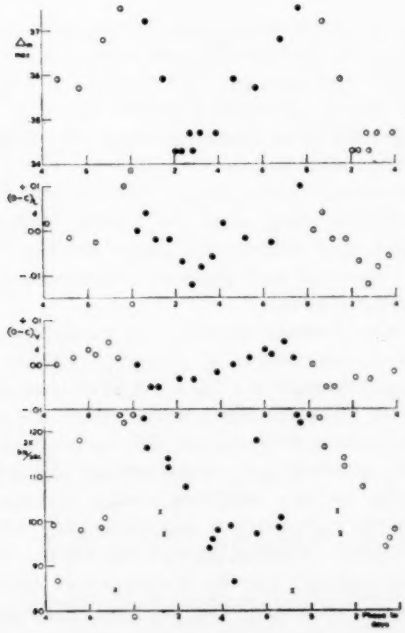

FIG. 2.—*Diagrams showing the variation of the maximum light attained in the individual* $0^{d}{\cdot}2468$ *cycles of* σ *Sco,* Δm_{max}; *and similarly the variation of the* observed *minus* computed *time of maximum light,* $(O-C)_L$; *the* observed *minus* computed *time of radial velocity,* $(O-C)_V$; *and the amplitude* $2K$ *of the radial velocity. These quantities found in individual* $0^{d}{\cdot}2468$ *cycles have been plotted against phases derived from the expression* J.D. $2\,434\,878{\cdot}2 + 8{\cdot}028$.

In the $2K$ *diagram the dots represent observations by Struve* et al. *and the crosses results obtained at Mount Stromlo (see text).*

colours are rather erratic but the periodicity is shown better if a running triple mean for the three colours is plotted as in Fig. 2.

The $(O-C)_L$ results for blue minima are presented in Table I, where column 3 gives phases computed by expression (2) above. These results, after smoothing by taking running means of three observations, are shown in Fig. 2.

The $(O-C)_V$ results were obtained by scaling off the diagrams in the paper by Struve *et al.* (3). The computed times were derived from the expression

$$T'' = \text{J.D. (Hel.) } 2\,434\,861{\cdot}980 + 0^{d}{\cdot}246\,846E.$$

The periodicity in $2K$ is illustrated by what is mainly a reproduction of Fig. 3 of Struve *et al.* but plotted with a period of $8^{d}{\cdot}028$ in place of the figure of $8^{d}{\cdot}0$ used by these authors. Three additional results obtained by courtesy of Drs Gollnow, Hagemann and Przybylski in the winter of 1955 have been included in the diagram and are indicated by crosses. These new results are:

J.D.	$2K$
2435289·02	102 Km/sec
94·93	84 ,, ,,
97·16	97 ,, ,,

The times refer to the occurrence of the maximum velocity and the ranges to the difference between it and an adjacent minimum. Actually the crosses would fall somewhat more closely amongst the dots if a period of $8^{d}{\cdot}09$ was adopted but with the use of the $8^{d}{\cdot}028$ period the three 1955 measures fit reasonably well amongst the more numerous 1954 observations and could well be part of the same series of measures.

No one of the four curves shown above, with the possible exception of the $(O-C)_V$ result, presents by itself very convincing evidence for the 8-day periodicity, but together they indicate the reality of this variation. It is not improbable that more extended and precise work would show that the 8-day cycle itself does not repeat exactly.

Change in dimensions.—Various workers, by combining light and velocity curves, have determined dimensions of pulsating systems. Because of the obvious changes from cycle to cycle in σ Sco it would be most desirable to compare light and velocity curves taken simultaneously. With the present data it was not possible to do this because of the longitude difference between the observatories at which the bulk of the spectroscopic results and the photoelectric observations were obtained. Results in two adjoining cycles however were examined, viz. J.D. 2434910·657 to 2434910·910 (spectroscopic) and 2434910·923 to 2434911·161 (photoelectric). Comparison of the above radial velocity curve with that during J.D. 2434911·740 to 2434911·900 shows no appreciable difference, so it seems fair to assume that no great changes took place in the intervening period and that the above spectroscopic and photometric results refer to essentially the same condition of the system.

The results are summarized in Fig. 3 which gives light, colour and radial velocity curves as well as a curve showing the displacement obtained by numerical integration of the velocity curve, assuming that limb darkening and projection effects ($K = 0{\cdot}6$) are accounted for by the equation $V = 24/17 V_r$ (where V = radial velocity to be used to obtain the displacement curve and V_r = the observed radial

velocity change (5)). The graph is arranged so that luminosity, temperature (represented by colour) and radius (indicated by the displacement curve) all increase upwards. For the particular cycles investigated the curves show that:

(1) at or near minimum size the star is brightest and hottest; and

(2) at or near maximum size the star is faintest and coolest.

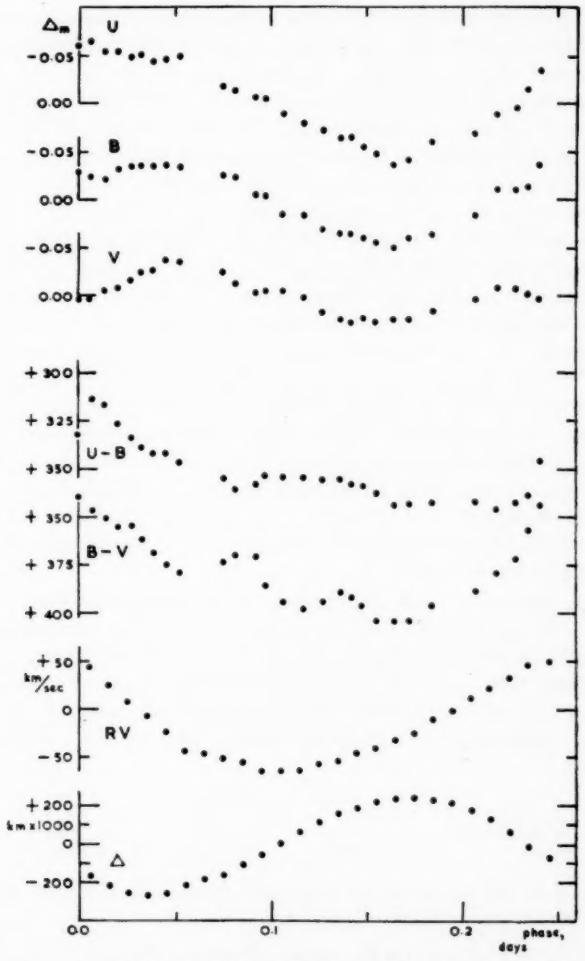

FIG. 3.—*Showing changes in light (U, B and V), short wave and long wave colours (U–B) and (B–V), radial velocity RV, and displacement during the* $0^d{\cdot}246\,846$ *day cycle of σ Sco.*

Both of these statements require elaboration. In the first place only the *B* maximum coincided with minimum size. Maximum *U* light occurred about 0·1 period (38 min) before this and maximum *V* light about 0·05 period after minimum size. The observed *U*, *B* and *V* minima were not definitely separated in time although the *V* minimum may have slightly preceded the *U* and *B* minima, and all minima may have been about 0·02 period in advance of the maximum

size. Statements about the temperature are based on the $U-B$ and $B-V$ colour differences.

To the above should be added the statements relating to changes within the 8-day period and displayed in Fig. 2, viz.:

(3) the brighter maxima occur somewhat before the predicted time and the fainter maxima occur somewhat later than the predicted time;

(4) the brighter maxima are associated with a smaller range of variation ($2K$) of velocity in the radial velocity curve, i.e. are associated with less displacement;

(5) the bigger ranges of velocity tend to occur a little later than predicted.

The data given in Fig. 3 should lead to an estimate for the radius of the star using well-known methods as exemplified in the work of Stebbins (**6**) on cepheid variables. If pairs of phases of P and P^1 be selected so that the colours at these points are respectively equal (i.e. $(U-B)=(U-B)^1$ and $(B-V)=(B-V)^1$) then it may be assumed that the surface temperature of the star is the same at the two phases and that any change in light is due solely to a change in dimensions. The fractional change in light is known (from the light curve) and the absolute change in radius can be found by integration of the radial velocity curve. These two quantities then lead to a figure for the radius. In the cycle discussed only one pair of phases of the required nature could be located. These occur at $0^d{\cdot}082$ and $0^d{\cdot}229$ in Fig. 3. Inspection of the figure at these two points shows that an increase of radius of 140 000 km at a nominally constant temperature is accompanied by an apparent 1 per cent increase of luminosity. Whether this result is to be attributed to observational inaccuracy, the use of photometric and spectroscopic results covering different cycles, or to deficiencies in theory, is an open question, but it is of interest to note that Walker (**7**) in a similar investigation of 16 Lac also found luminosity and radius to vary in a manner opposite to that to be expected.

Colour and magnitude.—Except for Fig. 3 the foregoing results have been given in the "natural system" of the photometer. This corresponds closely enough in the V magnitude to the V system of Johnson and Morgan but V and B natural systems differ somewhat from the standard U and B systems.

Comparisons of σ Sco and τ Sco against nine Johnson and Morgan standard stars on three nights gave the following results reduced to the Johnson and Morgan system:

	V	$B-V$	$U-B$
σ Sco (mean)	2·92	+0·16	−0·64
τ Sco	2·84	−0·27	−0·98

Using the relations given by Johnson and Morgan it is found that σ Sco is distinctly reddened, the intrinsic colours being

$$(B-V)_I = -0{\cdot}26 \quad \text{and} \quad (U-B)_I = -0{\cdot}94.$$

Conclusions.—There is nothing in the present observations to cause σ Sco to be regarded as other than a typical β Canis Majoris star. The intrinsic colour fits reasonably well into the colour–period relation obtained by McNamara and Williams (**8**). The results show the same phase relations between radial velocity and light curves that have come to be associated with β C Ma stars and thus confirm the work of Williams and Struve (**9**). Although it has not been possible to obtain a quantitative confirmation of the pulsating nature of the system, the light, colour and displacement curves are in agreement with the idea of pulsation

in that the star is bluest and brightest at minimum size. Also beat periods in light curves have been observed in the case of 16 Lac, 12 Lac and ν Eri (de Jager (**10**) and Walker (**7**)) and may exist in β C Ma and BW Vulpecula which show changes in their light variation.

Acknowledgments.—It is a pleasure to acknowledge the assistance received from both Mrs A. de Vaucouleurs and Mrs C. Wehner in the reduction of the observations and also to thank Drs Gollnow, Hagemann and Przybylski for making available their radial velocity measures of σ Sco in advance of publication.

Comommwealth Observatory,
Mount Stromlo,
Canberra:
1956 *October* 12.

References

(**1**) A. Wallenquist, *Uppsala Astr. Obs. Ann.*, **4**, No. 2, 55, 1954.
(**2**) M. L. Woods, *Comm. Obs. Memoir* No. 13, 1955.
(**3**) O. Struve, D. H. McNamara and V. Zebergs, *Ap. J.*, **122**, 122, 1955.
(**4**) A. R. Hogg, K. Gottlieb, G. V. Simonow and Beryl Hall, *M.N.*, **111**, 325, 1951.
(**5**) M. Schwarzschild, B. Schwarzschild and W. S. Adams, *Ap. J.*, **108**, 207, 1948.
(**6**) J. Stebbins, *P.A.S.P.*, **65**, 118, 1953.
(**7**) M. F. Walker, *Ap. J.*, **120**, 58, 1954.
(**8**) D. H. McNamara and A. O. Williams, *Ap. J.*, **121**, 51, 1955.
(**9**) A. D. Williams and O. Struve, *P.A.S.P.*, **67**, 250, 1953.
(**10**) C. de Jager, *B.A.N.*, *XII*, 88, 1953.
(**11**) C. Roger Lynds, *P.A.S.P.*, **66**, 197, 1954.

JEANS' FORMULA FOR GRAVITATIONAL INSTABILITY

W. B. Bonnor

(Communicated by J. Kershaw)

(Received 1956 November 26)

Summary

Jeans' formula gives the condition that a gravitating mass of gas shall be stable to small fluctuations in the density. It was originally obtained for a static mass of uniform density, and the proof is questionable. In this paper the formula is derived by studying small perturbations of the density and velocity in an expanding Newtonian world-model. It turns out that, given a suitable interpretation of the quantities involved, the formula is valid in all cosmologies except the steady-state theory.

Although instability occurs in the models as suggested by Jeans' formula, the condensation process is too slow to account for the formation of the nebulae—a result which has now been reached in several ways, and which may be regarded as well-established.

In the Newtonian version of the steady-state theory small perturbations of the average density die out, and so Jeans' formula does not apply. The relevance of this to the work of Sciama, who assumes the contrary, is discussed. It seems that the claim that the steady-state theory explains the formation of the nebulae requires further substantiation.

---

1. *Introduction.*—Jeans' formula (**4, 5**) gives the maximum size consistent with stability of a cloud of gas whose density ρ, and equation of state $p(\rho)$, are known. It states that a cloud with linear dimensions greater than

$$\left(\frac{\pi}{G\rho}\frac{dp}{d\rho}\right)^{1/2} \tag{1.1}$$

(where G is the constant of gravitation) is unstable to slight fluctuations in the density. This formula is often used in astrophysical work, and important deductions are made from it.

In (1.1) the density and pressure are supposed to be uniform throughout the gas. In fact, however, if gravitation is taken into account, the equation of hydrostatic equilibrium has no solution for a finite uniform mass. This is disturbing, and one's uneasiness is enhanced if one remembers that certain of the polytropic gas spheres (which *do* satisfy the hydrostatic equation) are mechanically stable, so far as is known, whatever their size. On the other hand, as I have recently shown (**3**), an isothermal gas sphere of sufficient size is unstable, and the condition for instability is similar to (1.1).

Since Jeans' work appeared, uniform distributions of matter have been studied in great detail in cosmology. For the most part, this work has been based on general relativity, in which uniform distributions are quite unobjectionable as there are rigorous solutions of the field equations referring to them. However, the Newtonian cosmological models of Milne and McCrea (**9, 10**) also use uniform distributions of matter, and these seem to be a natural vehicle for a further study of Jeans' type of gravitational instability. As a result of recent

work of McCrea (**8**), the assumptions on which these models are based are now well understood, and they can be used with confidence as a guide to the models of general relativity, and also of the steady-state theory.

My intention in this paper is to use the Newtonian models to study the gravitational instability of a uniform material filling an expanding universe. I write with full awareness of the extremely beautiful and powerful work of Lifshitz (**6**) on gravitational instability in relativistic cosmology, and my results, as far as they are comparable, agree with his. However, the extra simplicity gained by using the Newtonian models, apart from giving formulae which are more tractable and readily comprehensible, enables one to extend the investigation to a wider class of models—namely, those with cosmological constant, and that representing the steady-state universe.

The result of my work, very briefly, is that something very like Jeans' instability occurs in all the cosmologies, *except* the steady-state theory. This latter conclusion is unfortunate because the steady-state theory is the only one which has at present an explanation of the formation of the nebulae (**11**), and it now seems that this explanation is made doubtful by an unjustified use of Jeans' formula. However, it may be possible to retrieve the situation, as will be explained later.

The plan of the paper is as follows: in Section 2, I obtain Jeans' formula in its original form, and I follow this in Section 3 by a derivation of the corresponding results in the expanding universe; this is followed in Sections 4–6 by a discussion of the results for certain special models, and in Section 7 by the application of the theory to the steady-state universe; in the Conclusion, Section 8, I give a brief summary and general discussion of the results of the earlier sections.

2. *Jeans' formula.*—To derive Jeans' formula we use the theory of sound in a large mass of gas, taking gravitation into account. Let us suppose that the gas satisfies an equation of state $p = g(\rho)$, and is at rest except for a small velocity $\boldsymbol{u}(\boldsymbol{r}, t)$ due to the wave motion. Let $\rho(\boldsymbol{r}, t)$ and $p(\boldsymbol{r}, t)$ be the density and pressure; the space derivatives of p and ρ are not at the moment supposed to be small, but we shall assume that the deviations of p and ρ from their equilibrium values are of the same order of smallness as $\boldsymbol{u}$. Squares and products of small quantities (and of their derivatives) are to be neglected.

On these assumptions the hydrodynamical equations

$$\frac{\partial \boldsymbol{u}}{\partial t} + (\boldsymbol{u} \cdot \nabla)\boldsymbol{u} = \boldsymbol{F} - \frac{1}{\rho} \nabla p, \tag{2.1}$$

$$\frac{\partial \rho}{\partial t} + \nabla \cdot (\rho \boldsymbol{u}) = 0, \tag{2.2}$$

become

$$\frac{\partial \boldsymbol{u}}{\partial t} = \boldsymbol{F} - \frac{1}{\rho} \nabla p, \tag{2.3}$$

$$\frac{\partial \rho}{\partial t} + \nabla \cdot (\rho \boldsymbol{u}) = 0, \tag{2.4}$$

where $\boldsymbol{F}$ is the body force per unit mass, consisting solely of gravitation. Since the gas is in equilibrium except for the small perturbations, we have

$$\boldsymbol{F}_0 = \frac{1}{\rho_0} \nabla p_0, \tag{2.5}$$

where a suffix 0 refers to the equilibrium value. Put

$$\boldsymbol{F} = \boldsymbol{F}_0 + \boldsymbol{F}_1, \qquad \rho = \rho_0 + \omega,$$

where $\boldsymbol{F}_1$ and ω are small; then Poisson's equation gives

$$\nabla \cdot \boldsymbol{F}_0 = -4\pi G\rho_0, \qquad \nabla \cdot \boldsymbol{F}_1 = -4\pi G\omega. \tag{2.6}$$

Equations (2.3) and (2.5) give

$$\frac{\partial \boldsymbol{u}}{\partial t} = \boldsymbol{F}_1 - \nabla\left\{\frac{\omega}{\rho_0}\frac{dp}{d\rho}\right\}, \tag{2.7}$$

where the equilibrium value of $dp/d\rho$ is to be taken. From (2.6) and (2.7) we have

$$\begin{aligned}\frac{\partial}{\partial t}\nabla \cdot \boldsymbol{u} &= \nabla \cdot \boldsymbol{F}_1 - \nabla^2\left\{\frac{\omega}{\rho_0}\frac{dp}{d\rho}\right\} \\ &= -4\pi G\omega - \nabla^2\left\{\frac{\omega}{\rho_0}\frac{dp}{d\rho}\right\}.\end{aligned} \tag{2.8}$$

Equation (2.4) may be written, after differentiation and neglect of second order terms,

$$\frac{\partial^2\omega}{\partial t^2} + \rho_0\frac{\partial}{\partial t}(\nabla \cdot \boldsymbol{u}) + (\nabla\rho_0)\cdot\frac{\partial \boldsymbol{u}}{\partial t} = 0. \tag{2.9}$$

From (2.8) and (2.9) we find

$$\frac{\partial^2 s}{\partial t^2} + \frac{(\nabla\rho_0)}{\rho_0}\cdot\frac{\partial \boldsymbol{u}}{\partial t} = 4\pi G s\rho_0 + \nabla^2\left(s\frac{dp}{d\rho}\right), \tag{2.10}$$

where we have introduced the condensation s defined by

$$s = \omega/\rho_0.$$

If now we suppose that ρ_0 is constant, (2.10) reduces to the formula given by Jeans'

$$\frac{\partial^2 s}{\partial t^2} = 4\pi G\rho_0 s + \nabla^2\left(s\frac{dp}{d\rho}\right). \tag{2.11}$$

Jeans (**4**) is not quite explicit on this point, and his method is somewhat different, but careful study of his work shows that in order to get (2.11) he also is required to take ρ_0 as constant. If ρ_0 (and therefore p_0) is constant, (2.5) gives $\boldsymbol{F}_0$ zero throughout the gas, and one is at first inclined to think that the gravitation has been removed from the problem. However, one can retrieve the situation, after a fashion, by supposing that one has an infinite mass of gas so that, as there can be no preferred direction for $\boldsymbol{F}_0$ it must be zero. (Strictly, $\boldsymbol{F}_0$ is in this case not zero, but undefined.) As, however, Jeans goes on to apply the investigation to a finite mass of gas, the argument is, to say the least, precarious.

The deduction of Jeans' formula from (2.11) is simple. Consider a wave of length λ propagated along Ox and suppose a solution of the form

$$s = h(t)\cos 2\pi x/\lambda.$$

Since $dp/d\rho$ is constant, we find

$$\frac{d^2h}{dt^2} = \left[4\pi G\rho_0 - \frac{4\pi^2}{\lambda^2}\frac{dp}{d\rho}\right]h. \tag{2.12}$$

Hence the disturbance increases exponentially with time if

$$\lambda > \left(\frac{\pi}{G\rho_0}\frac{dp}{d\rho}\right)^{1/2}. \tag{2.13}$$

A mass of gas with linear dimensions greater than this will allow such disturbances, and will therefore be unstable.

As it will be convenient in the following sections to study spherical waves, I shall show that (2.13) holds also for such waves. If we suppose that the disturbance has spherical symmetry, we may write

$$s = h(t)r^{-1} \sin 2\pi r/\lambda.$$

Equation (2.11) then gives (2.12), and (2.13) follows as before.

3. *Gravitational stability of Newtonian world-models.*—Let us consider small perturbations in a Newtonian world-model. Suppose that a definite observer O sees the motion of the world-fluid as purely radial, and that the velocity, density and pressure have spherical symmetry about O. The imposition of this symmetry on the perturbations is not essential to the analysis, which can be followed through in a similar way if small non-radial motion and deviations from spherical symmetry are allowed. These latter perturbations make little difference to the final result, and are not important from the point of view of stability, so for simplicity I confine the argument to the use of radial perturbations with spherical symmetry.

The hydrodynamical equations (2.1) and (2.2) give

$$\frac{\partial u}{\partial t} + u\frac{\partial u}{\partial r} = F - \frac{1}{\rho}\frac{\partial p}{\partial r}, \tag{3.1}$$

$$\frac{\partial \rho}{\partial t} + u\frac{\partial \rho}{\partial r} + \rho\left(\frac{\partial u}{\partial r} + \frac{2u}{r}\right) = 0, \tag{3.2}$$

where u is the radial velocity measured by O, and p, ρ and F are the pressure, density and radial force per unit mass. As the motion is supposed to be that of a slightly perturbed Newtonian world-model, we may write

$$\left.\begin{aligned} u &= rf(t) + v(r, t), \\ \rho &= \rho_0(t) + \omega(r, t), \\ p &= p_0(t) + q(r, t), \end{aligned}\right\} \tag{3.3}$$

where v, ω and q are small functions whose squares and products (and those of their derivatives) may be neglected, and where $f(t)$, $\rho_0(t)$, $p_0(t)$ are the functions which occur in the unperturbed model. The body force per unit mass $\boldsymbol{F}$ satisfies

$$\nabla . \boldsymbol{F} \equiv \frac{\partial F}{\partial r} + \frac{2F}{r} = -4\pi G\rho + \Lambda, \tag{3.4}$$

where Λ is the cosmological constant. In the homogeneous model v, ω and q are zero, and the functions ρ_0 and f satisfy

$$\dot{\rho}_0/\rho_0 = -3f, \qquad 3\dot{f} + 3f^2 = -4\pi G\rho_0 + \Lambda, \tag{3.5}$$

where $\cdot$ denotes $\partial/\partial t$. Later we shall need the function $R(t)$ given in terms of f by

$$f = \dot{R}/R. \tag{3.6}$$

From (3.5) and (3.6) we find

$$\rho_0 = \alpha R^{-3},$$

where α is an arbitrary constant. Equations (3.5) follow from (3.1)–(3.4) if v, ω and q are zero. The pressure does not appear in the theory of the homogeneous model since it enters (3.1) only through its gradient. We shall suppose that there is an equation of state of the form

$$p = g(\rho)$$

so that

$$q(r, t) = \omega(r, t)\frac{dg}{d\rho}. \tag{3.7}$$

Here and elsewhere it is to be understood that $dg/d\rho$ is to be calculated at $\rho=\rho_0$.

If we substitute (3.3) and (3.7) into (3.1) and (3.2), and neglect small quantities of the second order, we find

$$\dot{rf}+\dot{v}+rf^2+rfv'+fv=F-\frac{\omega'}{\rho_0}\frac{dg}{d\rho}, \tag{3.8}$$

$$\dot{\rho}_0+\dot{\omega}+rf\omega'+3\rho_0 f+2\rho_0 vr^{-1}+\rho_0 v'+3\omega f=0, \tag{3.9}$$

where $'$ means $\partial/\partial r$. If from (3.8) we form $\partial F/\partial r+2F/r$, and use (3.4) and (3.5), we have

$$\dot{v}'+rfv''+4fv'+2\frac{\dot{v}}{r}+\frac{2fv}{r}=-4\pi G\omega-\frac{1}{\rho_0}\frac{dg}{d\rho}\left(\omega''+\frac{2\omega'}{r}\right), \tag{3.10}$$

where once again products of small quantities have been neglected. Equations (3.9) and (3.5) together give

$$\dot{\omega}+rf\omega'+2\rho_0 vr^{-1}+\rho_0 v'+3\omega f=0,$$

which may be written

$$\frac{\partial}{\partial r}(r^2v)=-\frac{r^2}{\rho_0}(\dot{\omega}+rf\omega'+3\omega f)\equiv X, \text{ say.} \tag{3.11}$$

Equation (3.10) may be written

$$\frac{1}{r^2}\frac{\partial^2}{\partial r\partial t}(r^2v)+\frac{f}{r}\frac{\partial^2}{\partial r^2}(r^2v)=-4\pi G\omega-\frac{1}{\rho_0}\frac{dg}{d\rho}\left(\omega''+\frac{2\omega'}{r}\right); \tag{3.12}$$

then (3.11) and (3.12) together give

$$\dot{X}+rfX'=-4\pi G\omega r^2-\frac{r^2}{\rho_0}\frac{dg}{d\rho}\left(\omega''+\frac{2\omega'}{r}\right).$$

Introducing for X its value in (3.11), we find, after a rather long calculation in which use is made of (3.5),

$$\ddot{\omega}+2rf\dot{\omega}'+r^2f^2\omega''+8f\dot{\omega}+r\omega'(9f^2+\dot{f})+\omega(18f^2+6\dot{f}-\Lambda)=\frac{dg}{d\rho}\left(\omega''+\frac{2\omega'}{r}\right). \tag{3.13}$$

This is a differential equation for the perturbation in the density, ω, in terms of the functions f and $dg/d\rho$, supposed given.

To simplify (3.13) we change to a new independent variable x by the transformation

$$r=xR(t)$$

where R is the function introduced in (3.6). A long calculation shows that (3.13) becomes

$$\frac{\partial^2\omega}{\partial x^2}+\frac{2}{x}\frac{\partial\omega}{\partial x}=\left(\frac{dg}{d\rho}\right)^{-1}R^2\left[\frac{\partial^2\omega}{\partial t^2}+8\frac{\dot{R}}{R}\frac{\partial\omega}{\partial t}+\omega\left(12\frac{\dot{R}^2}{R^2}+6\frac{\ddot{R}}{R}-\Lambda\right)\right]. \tag{3.14}$$

Finally, we introduce the condensation s by

$$s=\omega/\rho_0=\varkappa^{-1}\omega R^3,$$

which reduces (3.14) to

$$\frac{\partial^2 s}{\partial x^2}+\frac{2}{x}\frac{\partial s}{\partial x}=\left(\frac{dg}{d\rho}\right)^{-1}R^2\left[\ddot{s}+\frac{2\dot{R}}{R}\dot{s}+s\left(3\frac{\ddot{R}}{R}-\Lambda\right)\right]. \tag{3.15}$$

Equation (3.14) or (3.15) is the equation representing the propagation of spherically symmetric sound waves through the Newtonian world-model. Let us study solutions of the form

$$s=\frac{\sin kx}{kx}h(t), \tag{3.16}$$

where k is a real constant and where $h(t)$ is a function to be determined which will show how the amplitude of the wave changes with time. Substituting (3.16) into (3.15) we find

$$\ddot{h}+2\frac{\dot{R}}{R}\dot{h}+h\left(\frac{3\ddot{R}}{R}-\Lambda+k^2R^{-2}\frac{dg}{d\rho}\right)=0,$$

which with the help of (3.5) and (3.6) gives

$$\ddot{h}+2\frac{\dot{R}}{R}\dot{h}+h\left(k^2R^{-2}\frac{dg}{d\rho}-4\pi G\rho_0\right)=0. \tag{3.17}$$

In (3.16) $\sin kx/kx$ is a bounded oscillating function of r with order of magnitude 1 near the origin for all time, so the growth of the condensation is measured by $h(t)$. Thus $h(t)$ is strictly comparable with the function h in Section 2, and formula (3.17) corresponds to equation (2.12). The similarity between the two equations is obviously close, but in (3.17) there is a secular change in the coefficients owing to the expansion.

It can be shown from (3.17) that condensations can begin to form in favourable circumstances. Suppose that there is a perturbation at time t_1 such that

$$h=h_1>0, \quad \frac{dh}{dt}=\dot{h}_1>0 \quad \text{at} \quad t=t_1, \tag{3.18}$$

where h_1, $\dot{h}_1$ are assumed given; suppose also that

$$k^2R^{-2}\frac{dg}{d\rho}-4\pi G\rho_0<0 \quad \text{for} \quad t_1\leqslant t\leqslant t_2. \tag{3.19}$$

Immediately after t_1, $\dot{h}$ is positive so that h increases; and h will stop increasing only if it reaches a maximum, for which the conditions are

$$\dot{h}=0, \quad \ddot{h}<0.$$

Now from (3.17) and (3.19) it follows that, when $\dot{h}=0$ and $h>0$, $\ddot{h}>0$ so that h does not achieve a maximum in $t_1\leqslant t\leqslant t_2$, and it must go on increasing. Hence, given the initial conditions (3.18) and also the condition (3.19), a condensation begins to form.

We may express (3.19) in a form closer to Jeans' formula if we introduce the wave-length λ of the disturbance by

$$\lambda=2\pi R/k. \tag{3.20}$$

Substituting (3.20) into (3.19) we find

$$\lambda^2>\frac{\pi}{G\rho_0}\frac{dg}{d\rho}. \tag{3.21}$$

Here λ is a function of the time as expressed by (3.20), and so are ρ_0 and $dg/d\rho$. The condensation process continues so long as (3.21) is satisfied. Equation (3.21) is formally the same as (2.13), so, *with the appropriate interpretation of the quantities involved, Jeans' formula is true in the expanding universe.* In terms of the initial wave-length λ_1, (3.21) may be written

$$\lambda_1^2>\frac{\pi}{G\rho_0}\frac{dg}{d\rho}\frac{R_1^2}{R^2}, \tag{3.22}$$

where R_1 is the value of R at time t_1. Supposing this inequality satisfied at $t=t_1$, the condensation process will continue until such time t_2 as it ceases to hold.

Let us consider the special case in which the equation of state is

$$p \equiv g(\rho) = \kappa\rho^{4/3}. \tag{3.23}$$

The formulae (3.21) and (3.22) then simplify, and give as condition for instability

$$\lambda_1^2 > \frac{4\pi\kappa}{3G\rho_1^{2/3}}, \tag{3.24}$$

where ρ_1 means the unperturbed density at time t_1; if this condition is satisfied at t_1, condensation will proceed indefinitely. *Equation* (3.24) *is precisely Jeans' condition for a gas with equation of state* (3.23). The equation of state for diatomic hydrogen ($p = \kappa\rho^{7/5}$) is not very different from (3.23), and in Section 5 I shall use the latter equation to obtain an estimate of the behaviour of an expanding model filled with hydrogen.

If we had not confined attention to spherically symmetric perturbations we should have found an equation similar to (3.15) but containing angular terms on the left-hand side, making up the full Laplacian. The solution (3.16) would have contained a surface harmonic, and a spherical Bessel function would have replaced sin kx/kx. The results of this and the subsequent sections would not have been basically different.

The foregoing results will now be applied to certain special models.

4. *The Einstein universe.*—In the Einstein universe we have

$$R = \text{const.} \qquad \Lambda = 4\pi G\rho_0,$$

so that (3.17) becomes

$$\ddot{h} + h\left(\frac{4\pi^2}{\lambda^2}\frac{dg}{d\rho} - 4\pi G\rho_0\right) = 0,$$

where

$$\lambda = 2\pi R/k.$$

Thus h depends exponentially on the time if

$$\lambda > \left(\frac{\pi}{G\rho_0}\frac{dg}{d\rho}\right)^{1/2}.$$

This is exactly the same as (2.13) and gives the maximum size of a stable sphere. It follows that *Jeans' formula is true without modification for the Einstein universe.* It should be noted, however, that the constant density of the unstable gas cloud must be that appropriate to the Einstein universe, i.e. $\Lambda/4\pi G$. The theory would not apply to a uniform mass of gas of different density.

5. *The expanding world-models with* $\Lambda = 0$.—The main interest in the present theory is in what it predicts about the formation of the nebulae in an initially homogeneous universe. Except for the steady-state theory, which will be dealt with later, most of the plausible models start from a singular state of infinite density. For some time after the singular state the pressure would be large, and for this period the Newtonian models do not give a satisfactory representation because Newtonian theory does not allow for the gravitational effects of the pressure. The theory constructed here will therefore apply only to the later stages in the history of the universe when the pressure is small. From Lifshitz's work it seems that the later period is the most favourable for the formation of the nebulae, so the inapplicability of the theory to the earlier stages is not very serious.

Equations (3.5) and (3.6) for the unperturbed model may be integrated to give

$$\rho_0 = \frac{\alpha}{R^3}, \quad \dot{R}^2 = \frac{8\pi G\alpha}{3R} + \frac{1}{3}\Lambda R^2 + \epsilon, \tag{5.1}$$

where α and ϵ are constants of integration. Let us now consider a definite model, obtained by taking

$$\Lambda = 0, \qquad \epsilon = -\beta^2,$$

where β is a real constant. This model corresponds to one of general relativity which is spatially closed, and has zero cosmological constant and zero pressure. Of the pressure-free models with zero cosmological constant, it seems that this one is the most favourable to the formation of condensation (**2**). We can see from the Newtonian analogue why this should be so. It is easily shown (**9**) that the total energy of any one of the fundamental particles of the Newtonian model has the sign of ϵ, so if ϵ is negative all these particles have velocities less than that required to escape from the matter within the spheres on whose boundaries they lie. This makes the model more favourable to the growth of condensations.

The second of equations (5.1) gives on integration

$$R = \frac{8\pi G\alpha}{3\beta^2} \sin^2 \tfrac{1}{2}\theta, \tag{5.2}$$

$$t + t_0 = \frac{4\pi G\alpha}{3\beta^3} (\theta - \sin \theta), \tag{5.3}$$

where t_0 is a constant of integration which we may take to be zero by choosing the origin of θ at $t = 0$. The observations which the model is required to fit are the present values of Hubble's constant, $\dot{R}/R$, and the average density. Taking these as

$$\rho = 2 \times 10^{-28} \text{ g/cm}^3, \qquad \dot{R}/R = 2{\cdot}8 \times 10^{-10} \text{ (yrs.)}^{-1},$$

we find (**2**)

$$K \equiv \frac{4\pi G\alpha}{3\beta^3} = 9{\cdot}3 \times 10^9 \text{ yrs.},$$

and the value of θ referring to the present time is

$$\theta = 1{\cdot}15 \text{ rad.}$$

We may now return to (3·17) which governs the growth of a condensation. If we transform the independent variable from t to θ by (5.3) and express ρ_0 as a function of θ we find, using (5.1) and (5.2), that (3.17) becomes

$$\frac{d^2h}{d\theta^2} + \cot \tfrac{1}{2}\theta \frac{dh}{d\theta} - h\left[\frac{3}{2} \operatorname{cosec}^2 \tfrac{1}{2}\theta - \frac{k^2}{\beta^2} \frac{dg}{d\rho}\right] = 0. \tag{5.4}$$

To proceed further we must make some assumptions about the equation of state. For the reasons explained at the end of Section 3, let us suppose that

$$p \equiv g(\rho) = \kappa\rho^{4/3};$$

then proceeding as in Section 3 we find that (5.4) becomes

$$\frac{d^2h}{d\theta^2} + \cot \tfrac{1}{2}\theta \frac{dh}{d\theta} - h \operatorname{cosec}^2 \tfrac{1}{2}\theta \left[\frac{3}{2} - \frac{2\pi\kappa}{G\rho_1^{2/3}\lambda_1^2}\right] = 0, \tag{5.5}$$

where a perturbation of wave-length λ_1 originated the disturbance when the density was ρ_1. Suppose that this was at time $t = t_1$ when $\theta = \theta_1$. As in Section 3, it follows that the disturbance can continue to grow if (3.24) is satisfied.

Let us get an idea of the behaviour of the solution of (5.5) by using the approximations

$$\cos \theta \sim 1, \qquad \sin \theta \sim \theta.$$

The equation then becomes

$$\theta^2 \frac{d^2h}{d\theta^2} + 2\theta \frac{dh}{d\theta} - 4n^2 h = 0, \tag{5.6}$$

where

$$n^2 = \frac{3}{2} - \frac{2\pi\kappa}{G\rho_1^{\,2/3}\lambda_1^{\,2}}.$$

The solution of (5.6) is

$$h = A\theta^{m_1} + B\theta^{m_2},$$

where A and B are arbitrary constants, and where

$$m_1,\ m_2 = -\tfrac{1}{2} \pm \tfrac{1}{2}\sqrt{1+16n^2}.$$

As expected, the disturbance will grow if $n^2 > 0$.

From this approximate solution it seems that the most favourable case for condensation is that when n^2 has its maximum value, i.e. $3/2$. This is obtained by taking $p = 0$, and supposing the model filled with dust. Condensations will then form for perturbations of any wave-length. If $n^2 = 3/2$, (5.5) can be solved exactly in terms of elementary functions. A particular solution is

$$h = \operatorname{cosec}^2 \tfrac{1}{2}\theta \cot \tfrac{1}{2}\theta,$$

and the general one can be found by substituting in (5.5)

$$h = v(\theta) \operatorname{cosec}^2 \tfrac{1}{2}\theta \cot \tfrac{1}{2}\theta.$$

This eventually leads to the solution

$$h = -\tfrac{3}{2}A\theta \operatorname{cosec}^2 \tfrac{1}{2}\theta \cot \tfrac{1}{2}\theta + A(2 + 3\cot^2 \tfrac{1}{2}\theta) + B \operatorname{cosec}^2 \tfrac{1}{2}\theta \cot \tfrac{1}{2}\theta, \tag{5.7}$$

where A and B are arbitrary constants.

We now wish to find out how quickly a small perturbation can grow. Suppose that the time t_1 is early enough for us to put

$$\cos\theta_1 \sim 1, \qquad \sin\theta_1 \sim \theta_1.$$

Then (5.7) gives

$$h_1 \sim 8B\theta_1^{-3} + \tfrac{1}{10}A\theta_1^{\,2}. \tag{5.8}$$

If we assume that h_1 is initially small, we must have B very small since θ_1 is small; however, A need not be as small as h_1.* At the present time, say when $\theta \sim 1$, we have from (5.7)

$$h \sim A;$$

therefore from (5.8)

$$h \sim 10 h_1 \theta_1^{-2}. \tag{5.9}$$

It is now easy to see that the condensation process does not take place quickly enough to account for the formation of the nebulae. For a collection of N molecules of an ideal gas the fluctuation in the density is

$$\frac{\delta\rho}{\rho} = N^{-1/2},$$

and for a nebula of hydrogen $N \sim 3 \times 10^{67}$. Hence we may take

$$h_1 \sim 10^{-34}.$$

Supposing the perturbation to have occurred, say, 1000 years after the singular state, we have

$$\theta_1 \sim 10^{-2},$$

and from (5.9)

$$h \sim 10^{-29}.$$

Thus although the disturbance has grown in magnitude, it is still quite negligible,

* One might at first think that, since A and B are independent constants, one could satisfy (5.8) with h_1 small and yet have A and B large. However, it must be remembered that dh/dt must also be small at time t_1, and this leads to the conclusion given.

and there seems no hope whatever of accounting for the formation of the nebulae by this mechanism if one assumes fluctuations of the values to be expected on ordinary statistical theory. The difficulty cannot be overcome by taking a sufficiently small value for θ_1 because at such times the gravitational effect of the pressure could not be ignored and the model (5.2)–(5.3) would not apply. (For a fuller discussion, see (**2**)).

The foregoing analysis applies to the "closed" model with $\Lambda=0$. The "open" models with $\Lambda=0$, obtained by putting $\epsilon\geqslant 0$ in (5.1), give similar results; that is to say, small perturbations cannot grow into nebulae in the time available.*

6. *Models with* $\Lambda\neq 0$.—The foregoing analysis is not easy to apply to models with non-zero cosmological constant, because, in general, elliptic functions are needed to integrate the second of equations (5.1). I shall not deal with this problem in detail here. I have previously discussed the formation of condensations in Lemaître's model (**2**), and shown that this model seems hardly more favourable to the condensation process than those with $\Lambda=0$. Considered in the light of equation (3.17), the main difference between Lemaître's model and those with $\Lambda=0$ is that in the former $\dot{R}/R$ is nearly zero for a certain period, and at this time the model resembles the Einstein universe. If this period were long enough it would certainly allow the formation of the nebulae provided $dg/d\rho$ were small. However, if one supposes, as Lemaître did, that the model started about 5×10^9 years ago, this state of affairs cannot go on for very long. It might be worth while to investigate this problem further, but I have little doubt that detailed calculations would show that the condensations form too slowly to account for the formation of the nebulae.

It is clear that if one allows Λ to be non-zero, models exist in which the nebulae could have formed. If the pressure is small enough to be neglected, and if $\dot{R}/R$ is small for a long period, (3.17) shows that h will increase very rapidly provided the density is not too small. A model with these characteristics is the one investigated by Eddington and Lemaître which expands from the Einstein state, though this is not the only one.

7. *Condensations in the steady-state theory.*—The only plausible cosmology which has a theory of the formation of nebulae is the steady-state theory of Bondi, Gold and Hoyle. Sciama (**11**) has worked out the mechanism in some detail, and in his work Jeans' formula plays a fundamental part. It is therefore important to see whether the use of Jeans' formula in the steady-state theory can be justified.

Here, however, one meets a difficulty. The steady-state theory, though an interesting and imaginative cosmology, has not yet developed either a dynamics or a gravitation theory which carries any conviction. There is, though, a Newtonian model of the theory, developed with much ingenuity by McCrea (**7**). I shall try to adapt McCrea's work to the problem in hand.

According to McCrea, the Newtonian world models will accommodate the steady-state universe if one adds two postulates: (*a*) that mass and energy are convertible; (*b*) that the density of gravitational mass, instead of being ρ, is

$$\sigma=\rho+3p/c^2, \qquad (7.1)$$

* Attempts have been made to overcome the difficulty by postulating turbulence in the primordial medium; this gives rise to large fluctuations from which the nebulae could have formed. However, this proposal can hardly be regarded as a satisfactory solution of the problem unless it can be shown first how the turbulence might have arisen, and secondly that it would have survived the period of high pressure. Neither of these questions has yet been answered.

c being the velocity of light. The equations of the unperturbed model, after allowing for McCrea's two extra assumptions, are

$$3\dot{f}+3f^2=-4\pi G(\rho_0+3p_0c^{-2}), \tag{7.2}$$

$$\dot{\rho}_0+3\rho_0 f+3p_0fc^{-2}=0. \tag{7.3}$$

These differ from the equation (3.5) of the standard theory in the presence of the terms involving p_0. The solution of (7.2) and (7.3) which gives the Newtonian analogue of the steady-state theory is

$$f=\dot{R}/R, \qquad R=Ae^{t/a}, \tag{7.4}$$

$$\rho_0=3c^2/8\pi Ga^2, \qquad p_0=-3c^4/3\pi Ga^2, \tag{7.5}$$

where A and a are arbitrary constants.

To extend this work to the perturbed Newtonian model considered in Section 2, let us make two further assumptions:

(c) equation (7.1) holds even in the non-uniform model;

(d) the rate of creation of matter is independent of the density, and is

$$9c^3/8\pi Ga^3 \quad \text{g/cm}^3 \text{ sec}.$$

The latter is the rate in the model (7.4) and (7.5). Although the theory is not quite explicit about the dependence of the creation rate on the local density, postulate (d) seems a reasonable interpretation of the authors' intentions (1). The last term on the left in (7.3) represents the creation of matter, which, of course, causes an alteration in the equation of continuity.

With these assumptions the equations for the model subject to spherically symmetric perturbations are

$$\frac{\partial u}{\partial t}+u\frac{\partial u}{\partial r}=F-\frac{1}{\rho}\frac{\partial p}{\partial r}, \tag{7.6}$$

$$\frac{\partial \rho}{\partial t}+u\frac{\partial \rho}{\partial r}+\rho\frac{\partial u}{\partial r}+\frac{2\rho u}{r}+\frac{3p_0}{c^2}f=0, \tag{7.7}$$

$$\nabla\,.\,\boldsymbol{F}\equiv\frac{\partial F}{\partial r}+\frac{2F}{r}=-4\pi G\left(\rho+\frac{3p}{c^2}\right). \tag{7.8}$$

These correspond to (3.1), (3.2) and (3.4), and in the unperturbed model are equivalent to (7.2)–(7.5).*

If, following McCrea, we regard the negative pressure p_0 of the homogeneous model as a "zero-point" pressure, we may suppose that the equation of state of the gas of the model takes the form

$$p=p_0+g(\rho),$$

where $g(\rho_0)=0$. Using the notation of (3.3), we find that for small perturbations

$$p=p_0+\omega\frac{dg}{d\rho}, \tag{7.9}$$

$$\frac{\partial p}{\partial r}=\omega'\frac{dg}{d\rho}, \tag{7.10}$$

where, as usual, $dg/d\rho$ is to be calculated at $\rho=\rho_0$.

* A difficulty should be pointed out here. In (7.6) F is the force per unit inertial mass, whereas in (7.8) F is the force on unit "passive" gravitational mass (i.e. mass on which gravitation acts). One cannot be sure that these F's are really the same, especially as we are taking the density of "active" (gravitation-producing) mass as $\rho+3pc^{-2}$, whereas the density of inertial mass is ρ. My justification for equating the two F's lies in McCrea's demonstration of the self-consistency of his use of gravitational mass, which is similar to that here.

We may now treat (7.6)–(7.8) as we treated the corresponding equations in Section 3, using (7.2), (7.3), (7.9) and (7.10) where necessary. The result, corresponding to (3.13) is

$$\ddot{\omega}+2rf\dot{\omega}'+r^2f^2\omega''+\dot{\omega}f(8+3p_0c^{-2}\rho_0^{-1})$$
$$+r\omega'f^2\left(9+\frac{\dot{f}}{f^2}+\frac{3p_0}{c^2\rho_0}\right)+\omega f^2\left(18+\frac{6\dot{f}}{f^2}+\frac{9p_0}{c^2\rho_0}+\frac{12\pi Gp_0}{c^2f^2}\right)$$
$$=\frac{dg}{d\rho}\left(\omega''+\frac{2\omega'}{r}\right)-\frac{\omega}{c^2}\frac{dg}{d\rho}\left(9f^2+9\dot{f}+\frac{36\pi Gp_0}{c^2}\right).$$

We can simplify this by using (7.4) and (7.5), which reduces it to

$$\ddot{\omega}+2r\frac{c}{a}\dot{\omega}'+r^2\frac{c^2}{a^2}\omega''+\frac{5c}{a}\dot{\omega}+6r\frac{c^2}{a^2}\omega'+\frac{9c^2}{2a^2}\omega\left(1-\frac{1}{c^2}\frac{dg}{d\rho}\right)$$
$$=\frac{dg}{d\rho}\left(\omega''+\frac{2\omega'}{r}\right). \qquad (7.11)$$

Now change to a new variable x by the transformation

$$r=xR(t);$$

this changes (7.11) to

$$\frac{\partial^2\omega}{\partial t^2}+\frac{5c}{a}\frac{\partial\omega}{\partial t}+\frac{9c^2}{2a^2}\omega\left(1-\frac{1}{c^2}\frac{dg}{d\rho}\right)=\frac{dg}{d\rho}R^{-2}\left(\frac{\partial^2\omega}{\partial x^2}+\frac{2}{x}\frac{\partial\omega}{\partial x}\right).$$

If we assume a solution of the form

$$\omega=\frac{\sin kx}{kx}h(t),$$

we find the following equation for h:

$$\ddot{h}+\frac{5c}{a}\dot{h}+\frac{9c^2}{2a^2}h\left(1-\frac{1}{c^2}\frac{dg}{d\rho}+\frac{k^2}{R^2}\frac{dg}{d\rho}\right)=0. \qquad (7.12)$$

Evidently we may ignore the term $c^{-2}dg/d\rho$ in the bracket, which in the case of a gas at ordinary temperatures will be small compared with unity, and it is then clear that h cannot increase with time. In the most favourable case, in which $dg/d\rho=0$, the solution of the equation (7.12) then is

$$h=Ae^{m_1t}+Be^{m_2t},$$

where

$$m_1,\ m_2=\frac{1}{2}\frac{c}{a}[-5\pm\sqrt{7}].$$

Since the condensation $\delta\rho/\rho_0$ is proportional to ω (because ρ_0 is constant) it follows that *in the steady-state theory condensations cannot form as a result of small perturbations in the average density.*

In Sciama's work the density ρ of the condensing gas-cloud is taken to be equal to the average density ρ_0, and from the foregoing analysis it seems that no condensation would in fact take place if ρ and ρ_0 were equal, or differed by a small quantity. Strictly, therefore, Sciama's theory of the formation of the nebulae is not valid. However, in the steady-state theory, large perturbations—of the order of several times the average density—are possible as a result of clouds of gas breaking away from the accretions of already-existing nebulae. It may be that with such large perturbations new nebulae can form in the time allowed; but this is not obvious, and until it has been proved one cannot say with any confidence that the steady-state theory explains the formation of the nebulae.

8. *Conclusion.*—In this paper I have been studying the applicability of Jeans' formula to the expanding universe. Only small perturbations of the average cosmic density ρ_0 have been investigated: this is the only case to which Jeans' work strictly applies because in no other circumstances is one allowed to treat the unperturbed gas as uniform.

The result of this work is that, with a suitable interpretation of the quantities involved, Jeans' formula applies in the present phase of the expansion (except in the steady-state theory). Thus disturbances of sufficiently large wave-lengths result in instability of the cosmic gas, which causes it to start condensing. If one supposes that independent perturbations take place in different regions of the universe, then matter will condense into separate conglomerations. The size and mass of the condensing regions are connected by (3.21), in which the epoch of the perturbation implicitly enters through ρ_0, which, of course, depends on the epoch.

Where Jeans' original work is misleading (though through no fault of Jeans) is in the suggestion (from the solution of (2.12)) that the condensations begin to form at an exponential rate. It is only in the Einstein universe that this actually happens. When the expansion is taken into account one finds that the condensation process takes place very slowly—too slowly to account for the formation of the nebulae unless one supposes either that the perturbations are much larger than those to be expected on ordinary statistical theory, or that the universe has a longer time-scale than that provided by the point-source models.

Since so much of the matter in the universe is now condensed into nebulae, clouds of gas with density very nearly equal to the average density ρ_0 must be rare at the present time. Thus Jeans' formula as originally derived and as studied in this paper, though it may prove to be important in explaining the growth of the nebulae, has little practical application to contemporary astrophysics.

Naturally one would like to know whether Jeans' type of instability operates for clouds of gas with densities larger than ρ_0. This represents an unsolved problem, even in the spherically-symmetric case, but the stability will presumably depend markedly on the equation of state; this follows from the fact, mentioned in the introduction, that an isothermal gas sphere of sufficient size is unstable whereas adiabatic spheres with $\gamma > 4/3$ are stable so far as is known. I hope to deal with this question in another paper.

The University,
Liverpool, 3:
1956 *December.*

References

(1) Bondi, H., *Cosmology*, Cambridge, p. 143, 1952.
(2) Bonnor, W. B., *Zeits. f. Astrophys.*, **39**, 143, 1956.
(3) Bonnor, W. B., *M.N.*, **116**, 351, 1956.
(4) Jeans, J. H., *Astronomy and Cosmology*, Cambridge, p. 345, 1929.
(5) Jeans, J. H., *Philosophical Transactions*, Series A, **199**, 1.
(6) Lifshitz, E., *Journal of Physics*, (*U.S.S.R.*), X, 116, 1946.
(7) McCrea, W. H., *Proc. Roy. Soc.* A, **206**, 562, 1951.
(8) McCrea, W. H., *Astronomical Journal*, **60**, 271, 1955.
(9) McCrea, W. H. and Milne, E. A., *Quarterly Journal of Mathematics*, **5**, 73, 1934.
(10) Milne, E. A., *Quarterly Journal of Mathematics*, **5**, 64, 1934.
(11) Sciama, D. W., *M.N.*, **115**, 3, 1955.

Note added by D. W. Sciama on "Jeans' Formula for Gravitational Instability". —Bonnor's paper demonstrates in a very clear way what has been generally believed for some time, namely that infinitesimal density fluctuations will not give rise to galaxies in the times available. This difficulty led Gamow to suggest that large density fluctuations would be produced by the high Mach number ($\sim$10) compressible turbulence that he invoked. Unfortunately the analogue of the Jeans' criterion is not known for this type of motion.

At first sight the situation is even worse for the steady-state theory. For the material density must increase by a factor three in order that self-gravitation should exactly compensate the cosmical repulsive forces that the steady-state theory must invoke. However, the situation is saved by the fact that these large density fluctuations do not have to form in an initially homogeneous universe. Indeed, all we have to show is that galaxies are self-propagating. We can hence use the fact that a galaxy will produce a large density fluctuation in its wake in a *systematic* way, so that the region of large density will not be highly turbulent, and Jeans' criterion can be applied to it.

In my paper I gave some sketchy calculations of the process of galaxy formation in a steady-state universe. Further details are given in my thesis (*On the Origin of Inertia*, Chapter V, Cambridge University 1953). In my paper I glossed over the cosmological aspects of the problem in order to concentrate on the astrophysical ones. That is why I assumed that the system was Newtonian in the region of interest. In fact one must consider only that part of the wake in which the density exceeds 3ρ. If we go further and require the density to exceed 4ρ, then the net gravitating density to be used in the Jeans formula is of order ρ (because of the cosmical repulsion). From the formula for ρ_p given on page 5 of my paper we see that $\rho_p \geqslant 4\rho$ when

$$r_p \sin\theta_p \leqslant \frac{1}{16}\left(\frac{3M_1}{8\pi\rho}\right)^{1/3}$$

where ρ_p is the density at the point p, r_p is the distance of p from the parent galaxy P, θ_p is the angle Pp makes with the peculiar velocity vector of P, and M_1 is the mass of P. Gravitational instability only occurs in the part of the wake which satisfies this equation. This restriction does not alter the order of magnitude estimates made in my paper.

I should add that various other points are considered in the thesis, e.g. the effect of the Hubble velocities initially present in the inter-galactic gas, and the stress produced by newly-created matter which is presumably under the gravitational influence of the parent galaxy only after it appears. Again these effects do not alter the order of magnitude estimates. I conclude then that Bonnor's calculations do not affect my theory of galaxy formation.

8. *Conclusion.*—In this paper I have been studying the applicability of Jeans' formula to the expanding universe. Only small perturbations of the average cosmic density ρ_0 have been investigated: this is the only case to which Jeans' work strictly applies because in no other circumstances is one allowed to treat the unperturbed gas as uniform.

The result of this work is that, with a suitable interpretation of the quantities involved, Jeans' formula applies in the present phase of the expansion (except in the steady-state theory). Thus disturbances of sufficiently large wave-lengths result in instability of the cosmic gas, which causes it to start condensing. If one supposes that independent perturbations take place in different regions of the universe, then matter will condense into separate conglomerations. The size and mass of the condensing regions are connected by (3.21), in which the epoch of the perturbation implicitly enters through ρ_0, which, of course, depends on the epoch.

Where Jeans' original work is misleading (though through no fault of Jeans) is in the suggestion (from the solution of (2.12)) that the condensations begin to form at an exponential rate. It is only in the Einstein universe that this actually happens. When the expansion is taken into account one finds that the condensation process takes place very slowly—too slowly to account for the formation of the nebulae unless one supposes either that the perturbations are much larger than those to be expected on ordinary statistical theory, or that the universe has a longer time-scale than that provided by the point-source models.

Since so much of the matter in the universe is now condensed into nebulae, clouds of gas with density very nearly equal to the average density ρ_0 must be rare at the present time. Thus Jeans' formula as originally derived and as studied in this paper, though it may prove to be important in explaining the growth of the nebulae, has little practical application to contemporary astrophysics.

Naturally one would like to know whether Jeans' type of instability operates for clouds of gas with densities larger than ρ_0. This represents an unsolved problem, even in the spherically-symmetric case, but the stability will presumably depend markedly on the equation of state; this follows from the fact, mentioned in the introduction, that an isothermal gas sphere of sufficient size is unstable whereas adiabatic spheres with $\gamma > 4/3$ are stable so far as is known. I hope to deal with this question in another paper.

The University,
Liverpool, 3:
1956 *December.*

References

(1) Bondi, H., *Cosmology*, Cambridge, p. 143, 1952.
(2) Bonnor, W. B., *Zeits. f. Astrophys.*, **39**, 143, 1956.
(3) Bonnor, W. B., *M.N.*, **116**, 351, 1956.
(4) Jeans, J. H., *Astronomy and Cosmology*, Cambridge, p. 345, 1929.
(5) Jeans, J. H., *Philosophical Transactions*, Series A, **199**, 1.
(6) Lifshitz, E., *Journal of Physics*, (*U.S.S.R.*), X, 116, 1946.
(7) McCrea, W. H., *Proc. Roy. Soc.* A, **206**, 562, 1951.
(8) McCrea, W. H., *Astronomical Journal*, **60**, 271, 1955.
(9) McCrea, W. H. and Milne, E. A., *Quarterly Journal of Mathematics*, **5**, 73, 1934.
(10) Milne, E. A., *Quarterly Journal of Mathematics*, **5**, 64, 1934.
(11) Sciama, D. W., *M.N.*, **115**, 3, 1955.

Note added by D. W. Sciama on "Jeans' Formula for Gravitational Instability". —Bonnor's paper demonstrates in a very clear way what has been generally believed for some time, namely that infinitesimal density fluctuations will not give rise to galaxies in the times available. This difficulty led Gamow to suggest that large density fluctuations would be produced by the high Mach number ($\sim$10) compressible turbulence that he invoked. Unfortunately the analogue of the Jeans' criterion is not known for this type of motion.

At first sight the situation is even worse for the steady-state theory. For the material density must increase by a factor three in order that self-gravitation should exactly compensate the cosmical repulsive forces that the steady-state theory must invoke. However, the situation is saved by the fact that these large density fluctuations do not have to form in an initially homogeneous universe. Indeed, all we have to show is that galaxies are self-propagating. We can hence use the fact that a galaxy will produce a large density fluctuation in its wake in a *systematic* way, so that the region of large density will not be highly turbulent, and Jeans' criterion can be applied to it.

In my paper I gave some sketchy calculations of the process of galaxy formation in a steady-state universe. Further details are given in my thesis (*On the Origin of Inertia*, Chapter V, Cambridge University 1953). In my paper I glossed over the cosmological aspects of the problem in order to concentrate on the astrophysical ones. That is why I assumed that the system was Newtonian in the region of interest. In fact one must consider only that part of the wake in which the density exceeds 3ρ. If we go further and require the density to exceed 4ρ, then the net gravitating density to be used in the Jeans formula is of order ρ (because of the cosmical repulsion). From the formula for ρ_p given on page 5 of my paper we see that $\rho_p \geqslant 4\rho$ when

$$r_p \sin\theta_p \leqslant \frac{1}{16}\left(\frac{3M_1}{8\pi\rho}\right)^{1/3}$$

where ρ_p is the density at the point p, r_p is the distance of p from the parent galaxy P, θ_p is the angle Pp makes with the peculiar velocity vector of P, and M_1 is the mass of P. Gravitational instability only occurs in the part of the wake which satisfies this equation. This restriction does not alter the order of magnitude estimates made in my paper.

I should add that various other points are considered in the thesis, e.g. the effect of the Hubble velocities initially present in the inter-galactic gas, and the stress produced by newly-created matter which is presumably under the gravitational influence of the parent galaxy only after it appears. Again these effects do not alter the order of magnitude estimates. I conclude then that Bonnor's calculations do not affect my theory of galaxy formation.

NOTICE TO AUTHORS

1. *Communications.*—Papers must be communicated to the Society by a Fellow. They should be accompanied by a summary at the *beginning* of the paper conveying briefly the content of the paper, and drawing attention to important new information and to the main conclusions. The summary should be intelligible in itself, without reference to the paper, to a reader with some knowledge of the subject; it should not normally exceed 200 words in length. **Authors are requested to submit MSS. in duplicate. These should be typed using double spacing and leaving a margin of not less than one inch on the left-hand side. Corrections to the MSS. should be made in the text and not in the margin.** Unless a paper reaches the Secretaries more than seven days before a Council meeting it will not normally be considered at that meeting. By Council decision, MSS. of accepted papers are retained by the Society for one year after publication; unless their return is then requested by the author, they are destroyed.

2. *Presentation.*—Authors are allowed considerable latitude, but they are requested to follow the general style and arrangement of *Monthly Notices*. References to literature should be given in the standard form, including a date, for printing either as footnotes or in a numbered list at the end of the paper. Each reference should give the **name and initials** of the author cited, irrespective of the occurrence of the name in the text (some latitude being permissible, however, in the case of an author referring to his own work). The following examples indicate the style of reference appropriate for a paper and a book, respectively :—

A. Corlin, *Zs. f. Astrophys.*, **15**, 239, 1938.
H. Jeffreys, *Theory of Probability*, 2nd edn., section 5.45, p. 258, Oxford, 1948.

Alternatively, the Harvard reference system may be used.

3. *Notation.*—For technical astronomical terms, authors should conform closely to the recommendations of Commission 3 of the International Astronomical Union (*Trans. I.A.U.*, Vol. VI, p. 345, 1938). Council has decided to adopt the I.A.U. 3-letter abbreviations for constellations where contraction is desirable (Vol. IV, p. 221, 1932). In general matters, authors should follow the recommendations in *Symbols, Signs and Abbreviations* (London : Royal Society, 1951) except where these conflict with I.A.U. practice.

4. *Diagrams.*—**These should be designed to appear upright on the page, drawn about twice the size required in print and prepared for direct photographic reproduction except for the lettering, which should be inserted in pencil. Legends should be given in the manuscript indicating where in the text the figure should appear.** Blocks are retained by the Society for 10 years; unless the author requires them before the end of this period they are then destroyed.

5. *Tables.*—**These should be arranged so that they can be printed upright on the page.**

6. *Proofs.*—Costs of alteration exceeding 5 per cent of composition must be borne by the author. Fellows are warned that such costs have risen sharply in recent years, and it is in their own and the Society's interests to seek the maximum conciseness and simplification of symbols and equations consistent with clarity.

7. *Revised Manuscripts.*—When papers are submitted in revised form it is especially requested that they be accompanied by the original MSS.

Reading of Papers at Meetings

8. When submitting papers authors are requested to indicate whether they will be willing and able to read the paper at the next or some subsequent meeting, and approximately how long they would like to be allotted for speaking.

9. Postcards giving the programme of each meeting are issued some days before the meeting concerned. Fellows wishing to receive such cards whether for Ordinary Meetings or for the Geophysical Discussions or both should notify the Assistant Secretary.

CONTENTS

Meeting of 1957 January 11 : PAGE

Award of the Gold Medal to Professor Albrecht Unsöld... 1

Award of the Jackson-Gwilt Medal and Gift to Mr R. P. de Kock 1

Fellows and Junior Members elected 1

Presents announced... 1

Z. Suemoto, Interferometric study of profiles of faint Fraunhofer lines 2

P. J. Treanor, Chromospheric interferometry... 22

C. W. Allen and A. S. Asaad, Oscillator strengths from arc spectra of diluted copper alloys 36

J. M. A. Danby and G. L. Camm, Statistical dynamics and accretion 50

E. A. Kreiken and Dilhan Ege, A statistical study of pulsating stars 72

A. W. Rodgers, Radius variation and population type of cepheid variables... ... 85

A. R. Hogg, Variations in the light of Sigma Scorpii 95

W. B. Bonnor, Jeans' formula for gravitational instability 104

Printed in London by Taylor & Francis, Ltd., 1957 June